



**HAL**  
open science

## Magmatic-hydrothermal evolution of rare metal pegmatites from the Mesoproterozoic Orange River pegmatite belt (Namaqualand, South Africa)

Christophe Ballouard, Marlina A Elburg, Sebastian Tappe, Christian Reinke, Henriette Ueckermann, Shane Doggart

### ► To cite this version:

Christophe Ballouard, Marlina A Elburg, Sebastian Tappe, Christian Reinke, Henriette Ueckermann, et al.. Magmatic-hydrothermal evolution of rare metal pegmatites from the Mesoproterozoic Orange River pegmatite belt (Namaqualand, South Africa). *Ore Geology Reviews*, 2020, 116, pp.103252. 10.1016/j.oregeorev.2019.103252 . hal-04627194

**HAL Id: hal-04627194**

**<https://cnrs.hal.science/hal-04627194v1>**

Submitted on 28 Jun 2024

**HAL** is a multi-disciplinary open access archive for the deposit and dissemination of scientific research documents, whether they are published or not. The documents may come from teaching and research institutions in France or abroad, or from public or private research centers.

L'archive ouverte pluridisciplinaire **HAL**, est destinée au dépôt et à la diffusion de documents scientifiques de niveau recherche, publiés ou non, émanant des établissements d'enseignement et de recherche français ou étrangers, des laboratoires publics ou privés.

## Journal Pre-proofs

Magmatic-hydrothermal evolution of rare metal pegmatites from the Mesoproterozoic Orange River pegmatite belt (Namaqualand, South Africa)

Christophe Ballouard, Marlina A. Elburg, Sebastian Tappe, Christian Reinke, Henriette Ueckermann, Shane Doggart

PII: S0169-1368(19)30774-7

DOI: <https://doi.org/10.1016/j.oregeorev.2019.103252>

Reference: OREGEO 103252

To appear in: *Ore Geology Reviews*

Received Date: 19 August 2019

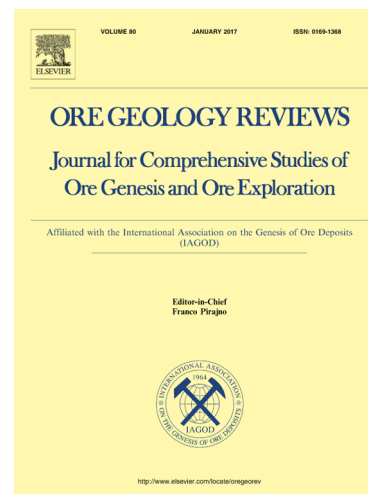
Revised Date: 10 November 2019

Accepted Date: 22 November 2019

Please cite this article as: C. Ballouard, M.A. Elburg, S. Tappe, C. Reinke, H. Ueckermann, S. Doggart, Magmatic-hydrothermal evolution of rare metal pegmatites from the Mesoproterozoic Orange River pegmatite belt (Namaqualand, South Africa), *Ore Geology Reviews* (2019), doi: <https://doi.org/10.1016/j.oregeorev.2019.103252>

This is a PDF file of an article that has undergone enhancements after acceptance, such as the addition of a cover page and metadata, and formatting for readability, but it is not yet the definitive version of record. This version will undergo additional copyediting, typesetting and review before it is published in its final form, but we are providing this version to give early visibility of the article. Please note that, during the production process, errors may be discovered which could affect the content, and all legal disclaimers that apply to the journal pertain.

© 2019 Published by Elsevier B.V.



## **Magmatic-hydrothermal evolution of rare metal pegmatites from the Mesoproterozoic Orange River pegmatite belt (Namaqualand, South Africa)**

**Authors:** Christophe Ballouard<sup>1\*</sup>, Marlina A. Elburg<sup>1</sup>, Sebastian Tappe<sup>1</sup>, Christian Reinke<sup>2</sup>, Henriette Ueckermann<sup>1</sup>, Shane Doggart<sup>3</sup>

<sup>1</sup>Department of Geology, University of Johannesburg, P.O. Box 524, Auckland Park 2006, South Africa

<sup>2</sup>Spectrum Analytical Facility, University of Johannesburg, P.O. Box 524, Auckland Park, 2006, South Africa

<sup>3</sup>Council for Geoscience, P.O. Box 775, Uppington, South Africa, 8800

\*Corresponding author: christopheballouard@outlook.com; christopheb@uj.ac.za

**Keywords:** LCT pegmatites; melt-melt-fluid immiscibility; metasomatism; Nb-Ta fractionation; mineral compositions; U/Pb geochronology

### **Abstract**

The 450 km long Orange River pegmatite belt intruded the Namaqua Sector of the Mesoproterozoic Namaqua-Natal Province, Southern Africa, at ca. 1 Ga. The western part of the belt is characterized by the occurrence of LCT pegmatites locally mineralized in Li, Ta, Nb, Be and Bi. Most of these mineralized pegmatites display zonation with a quartz-feldspar-muscovite-garnet-beryl-bearing aplite border and wall zone, a quartz-feldspar-spodumene-lepidolite-bearing intermediate zone, and a quartz-K-feldspar core. The pegmatites and their granodioritic country rocks commonly show evidence of albitization and greisenization (i.e. secondary muscovitization). In this study, detailed petrographic observations and the compositions of mica, feldspar, spodumene and Nb-Ta oxide minerals are reported. This information is combined with bulk country rock compositions and new U-Pb zircon and monazite ages plus Sm-Nd isotope compositions of monazite to constrain the origin and magmatic-hydrothermal evolution of weakly and strongly mineralized LCT pegmatites.

The Li-Ta-Be Kokerboomrand I pegmatite emplaced at ca. 985 Ma during the main stage of pegmatite emplacement in the Orange River belt and regional strike-slip deformation. It has  $\epsilon\text{Nd}(t)_{\text{monazite}} = -14 \pm 3$  and formed by partial melting of Paleoproterozoic rocks from the Richtersveld magmatic arc. Alternatively, Mesoproterozoic sediments of the Bushmanland Subprovince may also provide a suitable magma source for the Kokerboomrand I pegmatite.

The rare metal contents of muscovite and columbite group minerals (CGM) increase from the weakly mineralized to strongly mineralized pegmatites, suggesting early-stage fractional crystallization or variable partial melting conditions. Mica Nb/Ta values of  $<14$  and K/Rb ratios of  $<40$  can be used as geochemical tools for Li-Ta-(Nb)-Be exploration in the region, and possibly in other pegmatite belts worldwide.

Rare metal-bearing minerals crystallized throughout the magmatic-hydrothermal evolution of mineralized pegmatites. During the magmatic-dominated stage I, constitutional zone refining likely induced a decrease of spodumene Fe contents and increase of CGM Ta contents toward the pegmatite core. Stage II marks the pervasive circulation of an immiscible hydrosaline melt. This stage is characterized by the replacement of the primary mineral assemblage by lamellar albite (cleavelandite), (fluor)calciomicrolite and Cs-Ta-rich Li-muscovite and zinnwaldite. Stage III represents the progressive transition from a magmatic-hydrothermal system dominated by a Li-Cs-Ta-rich hydrosaline melt toward a system mainly involving (Li)-Cs-(Ta)-Bi-rich aqueous fluids. This stage is characterized by the crystallization of lepidolite and zero-valence-dominant pyrochlore as well as strong localized greisenization and Bi mineralization.

Magmatic-hydrothermal alteration of the immediate country rock of the mineralized pegmatites is marked by the crystallization of albite, Li-Ta-Cs-rich mica, various Nb-Ta oxide

minerals, and led to a strong decrease of the whole-rock Nb/Ta ratio plus significant rare metal enrichment.

Our findings from the Orange River belt demonstrate that an important role can be ascribed to melt-melt and melt-fluid immiscibility and metasomatism in the formation of pegmatite-related rare metal deposits. Greisens and albitites associated with pegmatites and their immediate country rocks can be considered as favorable targets for Li-Ta mineral exploration. Strong and pervasive metasomatism across the mineralized pegmatites and their country rocks suggests involvement of a parental medium that was highly enriched in water.

## 1. Introduction

Highly peraluminous rare metal granites (PRMG, Černý et al., 2005; Linnen and Cuney, 2005) and pegmatites of the LCT family, enriched in Li-Cs-Ta (Černý and Ercit, 2005), host a disseminated magmatic mineralization type that contrasts with common muscovite-bearing peraluminous granites (MPG, Barbarin, 1996), in which saturation of rare metals is not achieved at the magmatic stage. Both PRMG and LCT pegmatites represent a major source of rare metals (e.g., Li, Ta, Nb, Be, Sn, W), many of which are strategic for the high-tech industry and transition to sustainable energy sources (Linnen and Cuney, 2005; Linnen et al., 2012; Gunn, 2014). Despite a significant economic potential, the reasons for rare metal enrichments of these highly peraluminous intrusions remain unclear.

LCT pegmatites and PRMG are commonly interpreted as residual melts formed by extreme degrees of fractional crystallization of a large peraluminous granitic body (e.g. Norton, 1973; Raimbault et al., 1995; Černý and Ercit, 2005; Černý et al., 2005; Buick et al., 2008; Hulsbosch et al., 2014; London, 2014; Roda-Robles et al., 2018; Knoll et al., 2018). However, due to the

lack of spatial, compositional and temporal relationships between several pegmatite fields and granite intrusions worldwide, a second model based on the partial melting of rare metal- and fluxing element-rich sediments or igneous rocks along shear zones was proposed (e.g. Norton, 1973; Zasedatelev, 1974, 1977; Stewart, 1978; Shmakin, 1983; Matheis, 1987; Kontak et al., 2005; Melleton et al., 2012; Deveaud et al., 2013, 2015; Shaw et al., 2016; Müller et al., 2017; Fuchsloch et al., 2018; Konzett et al., 2018a, 2018b; Gourcerol et al., 2019). Formation of rare metal-enriched granitic magmas may result from a weathering-related increase of these metals in sediments prior to partial melting of such source rocks (Romer and Kroner, 2016) while the fluxing components such as B and Li may be provided by partial melting of evaporite-rich sedimentary sequences (Simmons and Webber, 2008). Alternatively, during granulite facies metamorphism, regional shear zones may channel fluids that are enriched in rare metals and fluxing elements. Such fluids may enhance partial melting of the deep crust, resulting in the formation of rare metal-enriched melts (Cuney and Barbey, 2014).

Following partial melting, further metal enrichment can take place by fractional crystallization either during magma ascent in dykes (Yamato et al., 2015) or in magma chambers (Dufek and Bachmann, 2010). The parental magmas of these pegmatites and granites can be highly enriched in fluxing components, such as B, P, F, water and Li, which has the effect to reduce the viscosity and solidus of the magma and, thus, enhance mineral-melt segregation (e.g. Černý et al., 2005; Linnen and Cuney, 2005; Thomas and Davidson, 2012). At the site of magma emplacement, undercooling- and supersaturation-induced processes, such as isothermal fractional crystallization and migration of a boundary layer liquid enriched in fluxing elements, can also lead to metal enrichment in the internal zones of pegmatites (e.g. London, 2014, 2018; Van Lichtenvelde et al., 2018).

On the other hand, the parental magmas of highly evolved granites and pegmatites may contain up to 30 wt.% water, and melt and fluid inclusion studies have demonstrated that at least three phases can coexist during crystallization of these intrusions in the upper crust: (i) a high viscosity, water-poor, silicate-rich melt (type A), (ii) a low viscosity, water ( $\pm$  carbonate)-rich, silicate-poor melt (type B), and (iii) a lower salinity aqueous ( $\pm$  carbonate-rich) fluid (e.g. Thomas et al., 2005, 2012; Thomas and Davidson, 2012). Hydrosaline melts and hydrothermal fluids may cause important element mobilities in and around granitic intrusions via exsolution and metasomatism and, therefore, contribute to the formation of granite- and pegmatite-related rare metal deposits (e.g. Thomas et al., 2009, 2011; Badanina et al., 2010, 2015; Dostal et al., 2015; Ballouard et al., 2016a; Kaeter et al., 2018; Wu et al., 2018).

The Namaqua sector of the Mesoproterozoic Namaqua-Natal metamorphic province, southern Africa, which was deformed and metamorphosed from 1.2 to 1.0 Ga, hosts an E-W oriented 500 by 50 km belt containing more than 30,000 individual pegmatites (Fig. 1) (Hugo, 1970; Schutte, 1972; Thomas et al., 1994; Minnaar and Theart, 2006). Recent studies indicate that the pegmatites were emplaced in relationship with strike-slip tectonics between ca. 1040 and 960 Ma, after the peak of metamorphism and granitic magmatism in the region (Lambert, 2013; Doggart, 2019). This so-called Orange River pegmatite belt is zoned: the western and eastern extremities contain mostly Li-Ta-Be-Bi-Sn-rich pegmatites showing an affinity to the LCT family (Černý and Ercit, 2005), whereas Nb-F-REE-Y-Be-rich pegmatites with NYF (Nb-Y-F) characteristics (Černý and Ercit, 2005) dominate the central part (Fig. 1). Pegmatites of the Orange River belt were mined sporadically since the beginning of the 1900's for Bi, Be, Li, Ta and Nb as well as industrial minerals such as feldspar and mica (Hugo, 1970; Schutte, 1972; Minnaar and Theart, 2006). The pegmatites with the most significant economic potential are located in the western

part of the belt (this study), and some pegmatite bodies of the region (Noumas I, Blesberg mine and Kokerboomrand I) are currently re-evaluated for their Li and Ta mineralization.

Despite several decades of exploration, mining and geological research, the nature of the source(s) as well as magmatic and magmatic-hydrothermal processes involved in the rare metal enrichment of pegmatites from the Orange River belt remain poorly understood. To tackle these issues, we carried out a detailed petrological, geochemical and geochronological study of selected barren and Li-Ta-Nb-Be-(Bi) mineralized LCT pegmatites from the western part of the belt including metasomatized country rocks. We present compositional data for mica (major, minor and trace elements), feldspar, spodumene and Nb-Ta oxide minerals (major and minor elements) from the pegmatites along with mineral composition and whole-rock major and trace element analyses of their immediate country rocks. U-Pb zircon and monazite ages, as well as Sm-Nd isotopic compositions of monazite were also obtained for mineralized pegmatites. These results show that, in addition to fractional crystallization and supersaturation processes, melt and fluid immiscibility and metasomatism have a major control on the distribution of rare metals in the pegmatites and their country rocks and are therefore considered critical to the formation of pegmatite-related Li-Ta-Bi deposits. Finally, we provide new constraints on the sources of these pegmatites and discuss their tectonic context.

## **2. Geological context**

### **2.1. The Namaqua Sector of the Namaqua-Natal belt**

The Namaqua Sector (Fig. 1), located in the north-western part of South Africa and southern part of Namibia, represents the western portion of the Mesoproterozoic Namaqua-Natal mobile belt, which was accreted to the Archean Kaapvaal Craton between ca. 1.2 and 1 Ga during formation of the supercontinent Rodinia (Thomas et al., 1994; Cornell et al., 2006). The

Namaqua Sector comprises a number of tectonostratigraphic domains and subprovinces bound by thrust and shear zones, which were juxtaposed and reworked during the Namaqua-Natal orogeny (Figs. 1 and 2):

- The Bushmanland Subprovince forms the structurally lowermost domain of the Namaqua Sector. It is mostly composed of a ca. 1.8 Ga old orthogneissic basement (the Gladkop Suite) overlain by ca. 1.6 to 1.1 Ga old metamorphosed supracrustal rocks (the Bushmanland and Kamiesberg groups) that were intruded by granitoids (the Little Namaqualand Suite, Concordia granite and Spektakel Suite) and mafic rocks (the Koperberg Suite) from ca. 1230 to 1030 Ma (Robb et al., 1999; Clifford et al., 2004; Cornell et al., 2009; Macey et al., 2018). Northern and eastern parts of the Bushmanland Subprovince record amphibolite facies conditions whereas other areas were affected by granulite facies metamorphism with peak ultra-high temperature conditions of 850-900 °C at 4-6 kbar (Robb et al., 1999).
- The Richtersveld magmatic arc, structurally overlying the Bushmanland Subprovince, comprises volcano-sedimentary rocks (the Orange River Group) and intrusions (i.e. the Vioolsdrif Suite) formed in an island arc-related setting between ca. 1.91 and 1.87 Ga (Macey et al., 2017). The Richtersveld magmatic arc was variably affected by the Namaqua orogeny and two tectono-metamorphic domains are distinguished. In the Vioolsdrif Domain, deformation was limited and metamorphism did not surpass greenschist facies conditions, whereas the Pella Domain experienced significant deformation under amphibolite facies conditions with peak conditions of ~600°C at 5-6 kbar (Macey et al., 2017).

- The Kakamas Domain, overthrusting the Bushmanland Subprovince, is separated from the Richtersveld magmatic arc by a wide thrust mélange: the Lower Fish-River Onseepkans thrust (LFROT) zone (Macey et al., 2018). The Kakamas Domain is interpreted as a mega-nappe stack of granulite facies metasedimentary rocks that record peak P-T conditions of 800-900°C at 4-5 kbar and were intruded at ca. 1200-1080 Ma by granitoids (Cornell and Pettersson, 2007a; Bial et al., 2015a, 2015b, 2016; Bailie et al., 2017).
- The granulitic Aus Domain, located to the NW of the Kakamas Domain in Namibia (not shown on Fig. 1), is made of granitoids emplaced between ca. 1120 and 1085 Ma and metasediments that reached peak P-T conditions of 825°C at 5.5 kbar (Diener et al., 2013).
- The lower granulite to amphibolite-grade Areachap Domain, with peak conditions of 600-700°C at 6-8 kbar and ~730°C at 4.1 kbar, consists of supracrustal rocks deposited at ca. 1250-1300 Ma in an arc-related setting and intruded at ca. 1200-1100 Ma by granitoids (Cornell et al., 1992; Cornell and Pettersson, 2007a; Bachmann et al., 2015; Bailie et al., 2017).
- The Kaaien Domain forms a tectonic transition between the Kaapvaal craton, Kheis belt and Namaqua Sector and is mostly composed of variably deformed greenschist facies supracrustal rocks deposited between ca. 1.9 and 1.1 Ga and ca. 1.4 to 1.1 Ga old granitoids (Van Niekerk, 2006; Pettersson et al., 2007; Moen and Armstrong, 2008; Van Schijndel et al., in press). Some metasediments record eclogite-facies peak metamorphic conditions of ~650 °C at ~10 kbar (Van Schijndel et al., in press). The Kaaien Domain

has recently been proposed to be part of the newly defined Kheis Terrane (Van Niekerk and Beukes, 2019).

Most domains of the Namaqua Sector experienced at least two low-pressure, high temperature tectono-metamorphic events (Fig. 2): an older one at ca. 1200-1100 Ma (D2) related to the development of a penetrative foliation and domain juxtaposition, and a younger one between ca. 1100 and 1000 Ma (D3) associated with large scale folding (Diener et al., 2013; Bial et al. 2015a, 2016; Macey et al., 2018). The end of the Namaqua Orogeny is marked between ca. 1005 and 960 Ma by dextral deformation along NW-SE vertical faults (D4), such as the Pofadder Shear Zone. Transcurrent deformation was synchronous with the emplacement of pegmatites from ca. 1040 to 960 Ma (Lambert, 2013; Doggart, 2019) and scarce granitic magmatism or fluid influx at ca. 1 Ga, as represented by the Warmbad Suite in the Pella Domain (Macey et al., 2015), dykes in the Aus Domain (Diener et al., 2013), and pronounced fluid-related metasomatism in the Kakamas Domain (Bial et al., 2015b). Cooling of most domains below 350°C occurred at ca. 960 Ma (Pettersson, 2008).

Despite significant thrust tectonics, no evidence of high-pressure metamorphism and therefore important crustal thickening exists in the Namaqua Sector except for the marginal Kaaien Domain, representing the Namaqua front. This led Van Schijndel et al. (in press) to suggest that D2 high-pressure metamorphism was overprinted in the core of the Namaqua Sector by D3 thermal events, and these authors invoke collisional-type tectonics. In contrast, Bial et al. (2015a, 2015b, 2016) and Macey et al. (2018) argued that the polyphase near-isobaric high-temperature and low-pressure history of several domains of the Namaqua Sector is not compatible with classic tectonic models involving continental break-up, subduction and continental collision. These authors propose a continental back-arc mobile belt setting where

episodic heat transfer from the convecting mantle into a thinned lithosphere may have occurred over a period of 200 Myr. Dewey et al. (2006) also proposed that mafic underplating, ultra-high temperature metamorphism and granitic magmatism at ca. 1030 Ma occurred during transtension and lithospheric thinning.

## **2.2. The Orange River pegmatite belt**

Pegmatites from the Orange River belt are ca. 960 to 1040 Ma old (Lambert, 2013, Doggart, 2019). Dykes and lenses with a thickness and length up to ~40 m and 500 m, respectively, strike either parallel to or crosscut the main foliation of their country rocks with a main NW-SE direction (Hugo, 1970; Schutte, 1972; Minnaar and Theart, 2006) (Fig. 3). In the Pofadder Shear Zone area (Fig. 1), pegmatite emplacement is mainly controlled by D4-related subvertical foliation, parasitic fold axial planes, Riedel shears and dextral dilatant jogs as well as late D4 extensional fractures (Lambert, 2013). The internal structure of the pegmatites varies from homogeneous to heterogeneous and their mineralogy is variable across the belt. In the central part of the belt (western and central parts of the Kakamas Domain, Fig. 1), homogeneous pegmatites generally contain quartz, feldspar, biotite, muscovite with zircon, monazite, titanite, magnetite and tourmaline as accessory minerals. The heterogeneous pegmatites display complex zoning and commonly contain topaz, fluorite, beryl, allanite, gadolinite, euxenite, columbite group minerals (CGM) and pyrochlore in addition to the mineral assemblage of the homogeneous pegmatites (Hugo, 1970). According to the classification scheme of Černý and Ercit (2005), these pegmatites belong to the REE subclass of the NYF family. In the Richtersveld magmatic arc (Schutte, 1972; Baldwin, 1989; MacDonald, 2013) and eastern part of the Kakamas Domain (Hugo, 1970), homogeneous pegmatites commonly contain quartz, feldspar, muscovite and garnet, with apatite, zircon, monazite and rare tourmaline, CGM and beryl as accessory minerals. Heterogeneous

pegmatites are generally characterized by an aplite border, wall zone, intermediate zone and a quartz-K-feldspar core (Fig. 4). These intrusions commonly contain, in addition to the homogeneous pegmatite mineral assemblage, Li-bearing minerals (e.g., spodumene, lepidolite and Li-tourmaline), beryl, CGM, microlite, cassiterite and Bi-minerals that tend to concentrate in the intermediate zones. These pegmatites belong to the Li subclass of the LCT family (Černý and Ercit, 2005).

### **3. Field and sample descriptions**

The study area is located in the western part of the Orange River belt at the transition between the amphibolite facies Pella Domain and greenschist facies Vioolsdrif Domain of the Richtersveld magmatic arc (Figs. 1 and 3). In this area, Schutte (1972) identified three main types of pegmatites referred to as: 1. non- or weakly mineralized, unzoned, homogeneous, 2. mineralized, weakly zoned, homogeneous, 3. mineralized, zoned, heterogeneous (Fig. 3). We sampled and studied five heterogeneous and mineralized pegmatites, namely, from west to east: the Li-Ta-Be-Bi Noumas I pegmatite, Nb-Ta-Be Kokerboomrand II pegmatite, Li-Ta-Be Kokerboomrand I pegmatite (Fig. 4), Li-Ta-Be Norabees I pegmatite and Nb-Ta-Be Witkop pegmatite. Three homogeneous and weakly mineralized pegmatites were also sampled including two (KOK-17-13 and 14) from the area of Kokerboomrand and one (NORA-17-6) located to the south of the Norabees I pegmatite. A description of the sampled pegmatites and their country rocks, including GPS coordinates, texture, mineralogy, thickness, strike and dip angle as well as their position in the CMS classification scheme of pegmatitic and aplitic rocks (Dill, 2015a, 2015b) is provided in Supplementary Files 1 and 2 and summarized below. Representative field and sample photographs are shown in Figures 5, 6 and 7.

#### **3.1. Weakly mineralized pegmatites**

In the area of Kokerboomrand, the two NW-SE to N-S striking and subvertical homogeneous pegmatite dykes or lenses crosscut the foliation of a micaschist (KOK-17-13) and a metagranodiorite (KOK-17-14). They have thicknesses of ~2 m and 10 m, respectively. Graphic intergrowth between quartz and microcline was observed in KOK-17-14. Both pegmatites contain microcline, quartz, muscovite, garnet and rare Nb-Ta oxide minerals, but plagioclase was only observed in KOK-17-13. In the Norabees area, the N-S striking subvertical homogeneous pegmatite dyke crosscuts the foliation of a pink granitic gneiss and has a thickness of ~2 m. The pegmatite contains microcline, plagioclase, quartz, muscovite as well as zircon and monazite as accessory phases.

### **3.2. Li-Ta-Be-Bi Noumas I pegmatite (Blesberg mine)**

The Noumas I pegmatite is the largest known heterogeneous and mineralized pegmatite of the Orange River belt with a length of ~500 m, a width between 10 and 40 m and a height of exposure of ~140 m. Its exploitation began in 1925 for Bi, and subsequently the body was mined for beryl and CGM as well as spodumene, feldspar and mica. The dyke-like body is discordant to the foliation of the Gaarseep granodiorite (Macey et al., 2017) and strikes NW-SE with a dip angle between 50 and 80° (Schutte, 1972).

The Noumas I pegmatite mainly consists of an aplite border (Fig. 5a), wall zone (Figs. 5a and 5b), intermediate zone and quartz-K-feldspar core. The aplite border contains sugary plagioclase, quartz, microcline, muscovite and subordinate amounts of Nb-Ta oxide minerals and zircon. Accessory garnet and apatite locally form layers parallel to the contact of the pegmatite. In addition to the mineral assemblage found in the aplite border, the wall zone hosts beryl and lamellar plagioclase (cleavelandite variety, Fisher, 1968). Muscovite and beryl (Fig. 5b) locally have a skeletal shape and microcline is commonly found as relics inside cleavelandite (Fig. 8a).

The intermediate zone consists of green, pink or white spodumene, plagioclase, quartz and accessory microcline, beryl and Nb-Ta oxide minerals. Veinlets or patches (~100  $\mu\text{m}$ ) of plagioclase are locally found within spodumene.

Replacement bodies occur as fracture-filling lenses close to the contact between the wall zone and intermediate zone (Fig. 5c). They consist of garnet and muscovite with subordinate amounts of smoky quartz, Bi-minerals and U ( $\pm$  Th, Pb, Cu)-rich phosphates, such as torbernite and plumbogummite.

Meter-sized rafts of variably metasomatized granodiorite are found inside the wall zone of the pegmatite (Figs. 7a and 7b). The degree of greisenization, i.e. high-temperature metasomatic breakdown of biotite and feldspar and replacement by muscovite or Li-mica and quartz (e.g. Štemprok, 1987; Schwartz and Surjono, 1990; Launay et al., 2019), increases toward the contact with the pegmatite. Two types of greisens, separated by a millimeter-thick apatite-rich zone, were identified (Fig. 7c). At the contact with the pegmatite, the Green greisen, consisting of muscovite with accessory apatite, Nb-Ta-Ti oxide minerals and zircon is followed by the Black greisen constituted by muscovite with subordinate amounts of weakly chloritized biotite, quartz, plagioclase, ilmenite, zircon, apatite, rutile with monazite inclusions and Mn ( $\pm$  Ba) oxide minerals. The less metasomatized (meta)granodioritic country rock consists of plagioclase, K-feldspar, quartz, locally chloritized biotite, zircon and oxide minerals.

### **3.3. Nb-Ta-Be Kokerboomrand II pegmatite**

The Kokerboomrand II pegmatite is exposed in a 2-3 m deep extraction pit. It forms a lens ~40 m in length and 5-15 m in thickness, striking subvertically at ~150°, either discordant or sub-concordant to the foliation of the metagranodioritic country rock (Gaarseep granodiorite). The

pegmatite is constituted by a wall zone made of microcline, lamellar plagioclase, quartz, muscovite, garnet, apatite, beryl and Nb-Ta oxide minerals, and a quartz core. Microcline is commonly found as anhedral relics between or within lamellar plagioclase and graphic texture was observed close to the contact with the metagranodiorite.

### **3.4. Li-Ta-Be Kokerboomrand I pegmatite**

The Kokerboomrand I pegmatite was mined to a depth of ~11 m and is exposed over a surface area of 45 by 10 m (Fig. 4). The lens-like body intrudes the Gaarseep metagranodiorite and strikes NW-SE with a dip angle of ~75° toward the SW and plunges northward (Schutte, 1972).

The pegmatite consists of an aplite border, wall zone, intermediate zone and quartz-K-feldspar core. The aplite border contains sugary plagioclase, quartz, muscovite, garnet and accessory apatite, zircon, monazite and Nb-Ta(-Ti) oxide minerals. Rare microcline is also found as anhedral grains between plagioclase. The wall zone consists of a similar mineral assemblage as the aplite border but contains beryl, and plagioclase is generally prismatic. The intermediate zone consists of lamellar plagioclase, quartz, Li-mica, pink spodumene and accessory apatite. In this zone, pink spodumene is replaced by purple Li-mica, and lamellar plagioclase may also be corroded by Li-mica (Figs. 6a and 8b).

A meter-scale replacement body is here referred to as albitized intermediate zone (Fig. 6b). It consists of plagioclase, pink spodumene as well as accessory microcline and Nb-Ta oxide minerals. Both spodumene and microcline are partially replaced by plagioclase (Fig. 8c). A second type of meter-sized replacement body occurs in the intermediate zone, close to the contact with the wall zone, and is hereafter referred to as greisenized intermediate zone (Figs. 5d and 6c).

It is made of green mica, plagioclase with a cleavelandite habit, quartz, white and green spodumene, microcline, garnet and various oxide minerals. Plagioclase replaces spodumene (Fig. 6c), and both these minerals are partially replaced by green mica (Fig. 8d).

A ~1 m thick zone of partially assimilated and strongly metasomatized granodioritic country-rock was sampled at the contact with the pegmatite (Fig. 7e). This zone has a heterogeneous crystal size and consists of fine- (0.1-0.3 cm) and coarse-grained (0.5-2 cm) subzones corresponding to the strongly metasomatized granodiorite and pegmatite, respectively. The fine-grained subzone comprises biotite, muscovite, plagioclase and quartz along with garnet, zircon, monazite and various Nb-Ta-Ti oxide minerals. The coarse-grained subzone consists of quartz, plagioclase, tourmaline, muscovite with accessory garnet and apatite. A moderately metasomatized granodiorite, sampled 50-100 cm away from the contact of the pegmatite consists of plagioclase, biotite, muscovite and rare quartz along with accessory monazite, zircon and apatite. The high abundance of plagioclase in this sample may have resulted from albitization (Fig. 7d).

### **3.5. Li-Ta-Be Norabees I pegmatite**

The Norabees I pegmatite is exposed in a ~55 by 25 m quarry that is at maximum 30 m deep. Approximately 1100 t of spodumene and ~36 t of beryl were extracted since the 1960's (Schutte, 1972). The contact strikes N-S, dips at ~60° W and is discordant to the foliation of the Gaarseep metagranodiorite.

The pegmatite comprises a wall zone, intermediate zone and quartz-K-feldspar core. The wall zone consists of plagioclase (locally lamellar), quartz, muscovite, green spodumene, tourmaline, garnet, beryl and accessory Nb-Ta-(Ti) oxide minerals, zircon, monazite, pollucite and fluorite

(Fig. 5e). The intermediate zone consists of lamellar plagioclase, quartz, purple Li-mica, pink spodumene, watermelon tourmaline, characterized by a pink core and black rim, along with accessory Nb-Ta oxide minerals and apatite (Fig. 5f). Li-mica is locally observed as millimeter-thick veinlets in plagioclase.

Meter-scale rafts of metasomatized metagranodiorite comprise quartz, biotite, muscovite, tourmaline and rare plagioclase as well as accessory magnetite, rutile, fluorite, zircon, titanite, epidote, Bi and Mn oxide minerals, apatite, monazite and garnet (Fig. 7f). A less metasomatized granodioritic country-rock was sampled ~2-3 m below the contact with the footwall of the pegmatite. It consists of plagioclase, quartz, biotite, apatite, titanite, apatite and oxide minerals.

### **3.6. Nb-Ta-Be Witkop pegmatite**

The Witkop pegmatite is exposed on a hill over a surface area of ~75 by 105 m (Schutte, 1972). The body is ~25-30 m thick, strikes E-W, dips at a low angle toward the south and crosscuts the foliation of metagranitoid country rock. The wall zone of the pegmatite, commonly showing graphic texture, consists of plagioclase, microcline, quartz, muscovite, garnet along with accessory zircon, monazite and Nb-Ta oxide minerals. The intermediate zone was mined for CGM and beryl and contains also plagioclase, quartz, muscovite, tourmaline, garnet, zircon and monazite. A greisen (Fig. 6d), consisting of muscovite, plagioclase, garnet, microcline, and subordinate Nb-Ta oxide minerals and zircon, was sampled at the transition between the wall zone and the quartz-microcline core. In the greisenized intermediate zone, microcline is partially replaced by lamellar plagioclase (cleavelandite) and both minerals are partially replaced by muscovite (Fig. 8e).

## **4. Results**

Sample preparation, mineral imaging as well as elemental and isotopic analyses were carried out at the Spectrum analytical facility of the University of Johannesburg. Detailed analytical protocols are provided in Supplementary File 3.

#### **4.1. Feldspar and spodumene mineral compositions**

The major and minor element composition of feldspar and spodumene from the LCT pegmatites and their country rocks, obtained by electron microprobe analyses (EPMA), is provided in Supplementary File 4.

##### **4.1.1. Feldspar**

The albite (Ab) content of plagioclase from weakly mineralized pegmatites ranges from 94 to 98 mol.% and most grains have an Ab concentration between 96 and 98 mol.% (Fig. 9). The lamellar plagioclase from the Nb-Ta-Be Kokerboomrand II pegmatite shows limited compositional variation and has slightly higher Ab content ranging from 98 to 99 mol.%. In the Nb-Ta-Be Witkop pegmatite, the composition is more variable and the Na content increases from prismatic plagioclase in the wall zone (Ab<sub>85-95</sub>) and intermediate zone (Ab<sub>94-98</sub>) to lamellar plagioclase (Ab<sub>98-99</sub>) replacing microcline in the greisenized intermediate zone. Sugary plagioclase from the aplite border and lamellar crystals from the wall zone of the Li-Ta-Be-Bi Noumas I pegmatite have a comparable Ab content, mostly ranging from 97 to 100 mol.% whereas plagioclase that occurs as veinlets in spodumene from the intermediate zone has an almost pure albite composition (Ab<sub>99-100</sub>). In the weakly metasomatized granodiorite, plagioclase has an andesine composition (Ab<sub>58-61</sub>). In the Li-Ta-Be Kokerboomrand I pegmatite, the Ab content increases from sugary plagioclase in the aplite border (Ab<sub>90-93</sub>), prismatic crystals in the wall zone (Ab<sub>91-98</sub>) toward lamellar plagioclase in the intermediate zone (Ab<sub>98-100</sub>). Lamellar

plagioclase from the greisenized intermediate zone has similar Ab content as in the less metasomatized portion with most values around 99 mol.% Ab. In the moderately metasomatized granodiorite, the plagioclase has an oligoclase composition (Ab<sub>73-82</sub>). However, in the strongly metasomatized granodiorite, plagioclase has an Ab content ranging from 91 to 93 mol.%, comparable to that in the aplite border. Regarding the Li-Ta-Be Norabees I pegmatite, the Ab content of pristine to lamellar plagioclase in the wall zone is variable (Ab<sub>92-99</sub>) and generally lower than lamellar plagioclase in the intermediate zone (Ab<sub>98-99</sub>).

Although our dataset for K-feldspar is smaller compared to plagioclase, the orthoclase (Or) content and K/Rb ratio of microcline from weakly mineralized pegmatites (Or<sub>91-97</sub>; K/Rb ~ 160-530) are comparable with that of microcline found in the Nb-Ta-Be pegmatites (Or<sub>92-98</sub>; K/Rb ~ 150-630). The K/Rb values of microcline from Li-Ta-Be-(Bi) mineralized pegmatites are mostly similar to those of other pegmatites (K/Rb ~1000-180); however, the Or content of microcline is restricted to high values between 95 and 98 mol.% (Supplementary File 5, Fig. S5.1).

#### **4.1.2. Spodumene**

White, green and pink spodumene crystals from Li-Ta-Be-(Bi) pegmatites follow a well-defined anticorrelation, with a slope around -1 in an Al versus Fe diagram, likely reflecting the substitution between Fe<sup>3+</sup> and Al<sup>3+</sup> in the M1 site of the pyroxene structure (Fig. 10). In the Norabees I pegmatite, pink spodumene from the intermediate zone is devoid of Fe (0.00 apfu) and has high Al (0.99-1.00 apfu) compared to green spodumene (Fe = 0.01-0.07 apfu; Al = 0.93-0.99 apfu) from the wall zone. The rims of the pink spodumene from this pegmatite fall outside the trend defined by other spodumene crystals; they are slightly enriched in Fe (0.01-0.02 apfu) and have high Al (~1.10-1.13 apfu). They have relatively low Li contents (average of ~0.57 apfu based on stoichiometry). Their K (average ~0.4 apfu) and Cs (0.02 apfu) contents are elevated

compared to spodumene from the other studied pegmatites (Li calc<sub>average</sub> ~0.99 apfu; K<sub>average</sub> ~0.00 apfu; Cs<sub>average</sub> ~0.00 apfu). White spodumene from the Kokerboomrand I (Fe = 0.01-0.08 apfu; Al = 0.91-0.98 apfu) and Noumas I pegmatites (Fe = 0.02-0.03 apfu; Al = 0.95-0.98 apfu) overlap in composition with green spodumene from the Norabees I pegmatite.

#### 4.2. Mica petrography, classification and composition

Representative images and  $Fe_{tot} + Mn + Ti - Al^{VI}$  versus Mg - Li classification diagrams (feal vs. mgli diagram; Tischendorf et al., 1997, 2001) for mica from the pegmatites and their country rocks are shown in Figures 11 and 12, respectively. Major and minor element compositions, mainly determined by EPMA, are provided in Supplementary File 6. The Li content was either measured by LA-Q-ICP-MS or extrapolated based on a correlation between the Li content measured by LA-Q-ICP-MS and F content measured by EPMA (Supplementary File 3, Figure S3.2) following Van Lichtervelde et al. (2008). The reasons for using our own equations instead of the more commonly used equations of Tischendorf et al. (1997) are detailed in Supplementary File 3. All mineral formulae have been calculated based on 22 oxygen atoms per unit. Rare metal and other trace element contents of mica from the LCT pegmatites and their country rocks were analyzed by LA-Q-ICP-MS (Figs. 13 and 14; Supplementary File 7). A detailed petro-geochemical description of mica is given in Supplementary File 8 and summarized below.

##### 4.2.1. Weakly mineralized pegmatites

For homogeneous and weakly mineralized pegmatites, the cores of > 1 mm large mica crystals fall at the transition between the fields of muscovite and Fe-muscovite in the feal vs. mgli diagram and late crystals rims are generally Fe-muscovite (Fig. 12a). Large mica cores from weakly mineralized pegmatites are generally depleted in Ta, Li, Cs and characterized by high Nb

contents and Nb/Ta values (14-30) compared to the aplite borders and wall zones of strongly mineralized pegmatites (Fig. 13). Mica crystals from the aplite borders and wall zones of Li-Ta-Be-(Bi) pegmatites show lower K/Rb values (10-40) than mica from weakly mineralized pegmatites (40-130) and the wall zones of Nb-Ta-Be pegmatites (20-80) (Supplementary File 5, Fig. S5.2).

#### **4.2.2. *Witkop and Kokerboomrand II Nb-Ta-Be pegmatites***

The cores of >1 mm large mica crystals in Nb-Ta-Be pegmatites fall at the transition between the fields of muscovite and Fe-muscovite in the  $\text{Fe}^{2+}$  vs.  $\text{mgli}$  diagram (Fig. 12a). The mica cores from the greisenized intermediate zone of the Witkop pegmatite have a purer muscovite composition. In the Kokerboomrand II and Witkop pegmatites, the rims of large crystals (Fig. 11a) and small crystals found inside feldspar (<1 mm) can be either depleted or enriched in Fe and Mg compared to large mica cores. Their compositions are also transitional between muscovite and Fe-muscovite.

In the Witkop pegmatite, the Li content and Nb/Ta value of the large mica cores decrease while the Ta and Cs contents increase from the wall zone through the intermediate zone toward the greisenized intermediate zone of the intrusion (Fig. 14a). Large mica crystals from the wall zone of the Nb-Ta-Be Kokerboomrand II pegmatite are depleted in Cs and characterized by higher Nb/Ta values as well as Li and Ta contents compared to small crystals (Fig. 14a).

#### **4.2.3. *Li-Ta-Be-Bi Noumas I pegmatite***

In the Li-Ta-Be-Bi Noumas I pegmatite, the composition of large mica cores (>1 mm) from the aplite border, wall zone and garnet-mica-rich replacement bodies fall at the transition between the field of muscovite and Fe-muscovite (Fig. 12b). Small crystals (< 1mm) and rims of relatively

large crystals from these zones fall in the field of muscovite. In the less metasomatized granodiorite, mica falls at the transition between the field of Mg- and Fe-biotite. Together, the mica analyses from the metasomatized granodiorite display a positive evolutionary trend in the  $\text{Fe}^{2+}/\text{Mg}^{2+}$  vs.  $\text{Mg}^{2+}/\text{Al}^{3+}$  diagram. At the contact with the pegmatite (i.e. Green greisen), the composition of mica is similar to that of mica from the pegmatite; i.e., transitional between muscovite and Fe-muscovite. In contrast, mica flakes from the Black greisen, more distant to the contact, are restricted to the field of Fe-muscovite. These crystals are heterogeneous in composition and characterized by resorbed cores and overgrowths (Fig. 11b).

Large mica cores from the wall zone are enriched in Cs and depleted in Li-Ta with higher Nb/Ta values compared to larger crystals from the aplite border (Fig. 14b). A late mica rim from the wall zone and small crystal from the aplite border are depleted in Li and enriched in Cs compared to the earliest identified crystals. The Ta content can either be enriched (wall zone) or depleted (aplite border) in these particular generations. In the garnet-mica-rich replacement body, the mica has lower Li-Ta contents and higher Cs concentrations than in the large mica cores from the aplite border and wall zone of the pegmatite. Biotite from the less metasomatized granodioritic country rock is very poor in Ta and enriched in Li-Cs compared to (Fe-) muscovite from the aplite border and wall zone. Regarding the Black greisen in the metasomatized raft of country rock, the Ta content increases whereas Li-Cs contents and Nb/Ta ratio decrease from mica cores to rims. The Ta enrichment and Li-Cs depletion are even higher in (Fe-) muscovite from the Green greisen. Micas with high Li-Ta contents are mostly associated with the metasomatized rafts of granodioritic country rock.

#### ***4.2.4. Li-Ta-Be Kokerboomrand I pegmatite***

Mica crystals from the aplite border and the wall zone of the Li-Ta-Be Kokerboomrand I pegmatite have a comparable major element composition and fall in lower part of the field of Fe-muscovite (Fig. 12c). In the intermediate zone, the purple mica that replaces spodumene (Figs. 6a and 8b) is strongly heterogeneous in texture (Fig. 11c). A first skeletal core (core 1), with a Li-muscovite to zinnwaldite composition, is filled by zinnwaldite (core 2). Both core generations are overgrown by two generations of lepidolite (rim1 and rim 2). A fifth generation of mica (rim 3), with a Li-muscovite to muscovite composition, is locally replacing the earlier mica generations. The green mica from the greisenized intermediate zone, replacing both spodumene and lamellar albite (Figs. 8d and 11d), also has a variable composition, with a dominant first generation (mica 1) ranging from Fe-muscovite to zinnwaldite, and a second generation with a muscovite composition (mica 2) forming patches in mica 1. Dioctahedral mica such as Fe-muscovite replaces trioctahedral mica (e.g. Fe-biotite and siderophyllite) in the metasomatized granodioritic country rocks of the Kokerboomrand I pegmatite (Fig. 11e). Mica crystals from the country rock form an almost continuous evolution trend in the feal vs. mgli diagram (Fig. 12c) with Fe-biotite and Fe muscovite representing the end members.

The Ta and Cs contents of mica generally decrease from the aplite border to the wall zone, whereas Li is relatively constant (Fig. 14c). Regarding purple mica crystals from the intermediate zone, the Li and Cs contents are higher than in mica from the aplite border, typically increasing from core to rim. Mica rims are strongly depleted in Ta compared to the cores. Purple mica cores have the highest Ta content among the pegmatites whereas the opposite is true for the rims. Predominant green mica 1 and small patches of mica 2 from the greisenized intermediate zone could not be analyzed separately resulting in a highly variable rare metal composition. This 'average' composition is comparable to mica from the non-greisenized intermediate zone with

regards to Ta-Cs contents, and transitional between the aplite border and intermediate zone for Li. The rare metal content of mica from the metasomatized granodioritic country rock is also highly variable and generally higher in the strongly metasomatized portions. In the metasomatized rocks, the rare metal content of trioctahedral mica is generally higher than in dioctahedral mica. The compositions of mica from the metasomatized granodiorite show the same Cs-Ta variation as in the pegmatite; however, Li contents are lower compared to mica from the intermediate zone.

#### **4.2.5. *Li-Ta-Be Norabees I pegmatite***

In the Li-Ta-Be Norabees I pegmatite, the mica from the wall zone is commonly zoned with muscovite to Li-Fe-muscovite cores overgrown by Li-Fe-muscovite to zinnwaldite (rim 1). These cores and rims are locally replaced or overgrown by Fe-muscovite (rim 2, Figs. 11f and 12d). Similar to the Kokerboomrand I pegmatite, purple mica from the intermediate zone of the Norabees I pegmatite is characterized by a heterogeneous, locally skeletal, core with a muscovite to Li-muscovite composition overgrown by zinnwaldite and lepidolite (Figs. 11g and 12d). In the less metasomatized granodiorite, Mg-biotite occurs whereas in the strongly metasomatized granodiorite raft, mica cores have a Fe-biotite to Fe-muscovite compositions and are replaced by different varieties of Fe-muscovite (Figs. 11h and 12d). Mica crystals from the less and strongly metasomatized granodiorites form a continuous evolution trend in the  $\text{Fe}^{\text{II}}$  vs.  $\text{Mg}^{\text{II}}$  diagram.

In the Li-Ta-Be Norabees I pegmatite (Fig. 14d), the Li, Cs and Ta contents of mica cores generally increase from the wall zone toward the intermediate zone. In both of these zones, the mica rims are strongly enriched in Li-Cs and depleted in Ta compared to the cores. In the less metasomatized granodiorite, the Li and Cs contents of Mg-biotite are comparable to that of mica cores from the wall zone of the pegmatite. However, these Mg-biotite crystals are more depleted

in Ta. Mica cores in the strongly metasomatized granodioritic country rock raft are significantly enriched in Li, Cs and Ta compared to Mg-biotite from less metasomatized granodiorite. However, mica rims are generally depleted in Li and Cs compared to the cores, and Ta concentrations of the rims are even lower than in Mg-biotite from less metasomatized granodiorite. In general, the highest Cs contents of the Norabees I pegmatite are found in mica cores from the metasomatized granodioritic raft and the Li contents of these mica crystals exceed those of mica cores from the wall zone. Mica flakes from the metasomatized granodiorite are generally depleted in Ta compared to mica from the pegmatite.

#### **4.3. Oxide and rare metal-rich mineral petrography and compositions**

Representative BSE images of oxides and rare metal-rich minerals from the pegmatites and their country rocks are shown in Figure 15 and Supplementary File 5, Fig. S5.3. The chemical composition of columbite group minerals (CGM), pyrochlore group minerals (PGM) and rutile are provided in Supplementary File 9 and shown in Figure 16. A detailed petro-geochemical description of oxide minerals is provided in supplementary File 8 and summarized below. The nomenclature of PGM is from Atencio et al. (2010).

##### ***4.3.1. Weakly mineralized pegmatites***

The main oxide in weakly mineralized pegmatite is represented by texturally homogeneous columbite-Fe to columbite-Mn. CGM are commonly replaced by zero-valence-dominant pyrochlore with a spongy texture along the rims (Figs. 15a, 16a-b).

##### ***4.3.2. Nb-Ta-Be Witkop and Kokerboomrand II pegmatites***

Mn-columbite is the dominant oxide in the wall zone of the Kokerboomrand II pegmatite (Fig. 16a). The crystals are characterized by homogeneous to oscillatory textures and are

commonly replaced along cracks or rims by (fluor)calciomicrolite or zero-valence-dominant pyrochlore with a spongy texture (Fig. 16b).

Despite CGM having been mined from the Witkop pegmatite (Schutte, 1972), only PGM were found in our samples along with rare Bi and Mn oxide minerals. In the wall and intermediate zones, PGM were observed either as spongy crystals or micrometric veinlets in mica cleavages. In the greisenized intermediate zone, PGM is present either as homogeneous crystals of (fluor)calciomicrolite, found along cracks and mica cleavages, or as spongy zero-valence-dominant microlite (Figs. 16b and S5.3).

#### **4.3.3. *Li-Ta-Be-Bi Noumas I pegmatite***

CGM are abundant in the aplite border and wall zone of the Noumas I pegmatite. The crystals are characterized by either homogeneous textures (Fig. 15b), normal zoning with increase of Ta content from core to rim (Fig. 15c), inverse zoning, oscillatory zoning (Fig. 15d) or complex patchy zoning (Fig. 15e). CGM are commonly replaced along rims or cracks by spongy PGM (Figs. 15b-c). In the aplite border, CGM are columbite-Fe (Fig. 16a). However, CGM from the wall zone range in composition from columbite-Mn to tantalite-Mn and Ta-richer CGM, including one tapiolite-Fe (Fig. 16a), are complexly zoned. The composition of PGM from the aplite border and the wall zone, characterized by high A-site vacancy, ranges from zero-valence-dominant microlite and pyrochlore to calciomicrolite and calciopyrochlore (Fig. 16b). Micrometric veinlets of Mn oxide minerals crosscutting albite are locally found in the wall zone of the pegmatite (Fig. S5.3). Bi-minerals generally consisting of native Bi surrounded by Bi oxide minerals are abundant in garnet-mica-rich replacement bodies (Fig. 15f) and U ( $\pm$  Th, Pb, Cu)-rich phosphates, such as torbernite and plumbogummite, are rarely observed (Fig. S5.3).

Nb-Ta-rutile and microlite are common in the metasomatized granodioritic rafts and mostly restrained to an apatite-rich zone, occurring at the transition between the Green and Black greisens (Fig. 7c). These crystals are locally oscillatory zoned with Ta, Nb, and Ta/(Nb+Ta) values increasing from core to rims (Figs. 15g and 16c). Calciomicrolite or fluorcalciomicrolite are either replacing rutile or occur as homogeneous crystals in the Green greisen (Fig. 16b). Mn oxide minerals are rarely found along the cleavage of mica from the Green greisen.

#### ***4.3.4. Li-Ta-Be Kokerboomrand I pegmatite***

Only two CGM crystals, with a homogeneous texture, were found in the aplite border of the Kokerboomrand I pegmatite and have a columbite-Fe to columbite-Mn composition (Fig. 16a). Rare Nb-Ta-rutile crystals are characterized by a complex texture with Nb-Ta-rich rutile (Rt 1, Fig. 15h) partially replaced by an assemblage of Nb-Ta-poor rutile (Rt 2) and calciomicrolite (Figs. 16b-c). In the wall zone, CGM are characterized by a homogeneous or oscillatory texture and are columbite-Mn (Fig. 16a). These crystals are commonly replaced by homogeneous to spongy calciomicrolite or zero-valence-dominant microlite along the rims (Fig. 16b). Oxide minerals were not observed in the more pristine areas of the intermediate zone but PGM are abundant in the albitized and greisenized portions. In these strongly metasomatized zones, homogeneous (fluor)calciomicrolite is locally altered to PGM with a spongy texture and a (fluor)calciomicrolite to zero-valence-dominant microlite composition (Fig. 16b). PGM in the greisenized intermediate zone are commonly replaced by Li-mica and brecciated by native Bi and Bi oxide minerals that also occur along the cleavage planes of Li-mica (Fig. 15i). PGM with Nb>Ta were also observed in the cleavage of trioctahedral mica crystals from the strongly metasomatized granodiorite. In this zone, titanite is partially replaced by Nb-rich rutile and columbite-Mn (Figs. 16a, 16c and S5.3).

#### ***4.3.5. Li-Ta-Be Norabees I pegmatite***

In the Li-Ta-Be Norabees I pegmatite, CGM are rare and have a columbite-Mn composition. They are observed in the wall zone either as crystals partially replaced by PGM or as resorbed inclusions with albite inside PGM (Figs. 15j-k). PGM vary in texture from relatively homogeneous to spongy. Homogeneous PGM are fluorcalciomicrocline or calciomicrocline whereas spongy PGM range in composition from calciomicrocline to zero-valence-dominant microcline and pyrochlore (Fig. 16b). Nb-Ta-rutile crystals were rarely observed in the wall zone (Fig. 16c) and spodumene is locally crosscut by tens of micrometer-thick veinlets of fluorite and pollucite (Fig. S5.3). PGM also occur in the intermediate zone, and relatively homogeneous fluorcalciomicrocline or calciomicrocline are commonly altered into spongy calciomicrocline along the rims (Fig. 15l).

#### **4.4. Whole-rock geochemistry of country rocks**

The whole-rock major and trace element composition of the weakly to strongly metasomatized granodioritic country rocks of the Li-Ta-Be-(Bi) Noumas I, Kokerboomrand I and Norabees I pegmatites is reported in Supplementary File 10 and shown as log-log isocon diagrams (Grant, 1986; Baumgartner and Olsen, 1995) (Fig. 17). Mica and oxide mineral compositions (see Sections 4.2 and 4.3) suggest that a significant amount of Ta and Nb, commonly considered as fluid-immobile elements, were transferred into the country rocks. Therefore, it is difficult to precisely define the slope of the isocon and compensate for the effect of mass and volume changes that can be significant during, for example, greisenization processes (e.g. Launay et al., 2019). The main replacement reactions involved during greisenization and albitization are reported in Table 1. During these reactions, Al is expected to remain relatively immobile but it always shows an apparent enrichment in the metasomatized granodiorites.

Therefore, Al is used in Figure 17 to define the maximum slope of the isocon; elements that are significantly enriched during metasomatism are expected to plot above this line.

The Green and Black greisens from the Noumas I pegmatite as well as the metasomatized granodiorite from the Norabees I pegmatite, which experienced greisenization and tourmalinization, show significant K enrichment and Na depletion (Fig. 17a-c). This is in agreement with the fact that the pristine granodiorite consists dominantly of plagioclase and that the metasomatic agent introduced additional K to the system for the formation of muscovite (Table 1, R2-3). The depletion in Na can be explained by the breakdown of plagioclase. In contrast, the moderately metasomatized granodiorite from the Kokerboomrand I pegmatite is, as suggested by its plagioclase-rich character (Fig. 7d) and the high albite content of plagioclase (Ab<sub>73-82</sub>, Fig. 9c), significantly enriched in Na indicating albitization (Fig. 17d). Phosphorous is significantly enriched in the greisenized granodiorites from the Noumas I and Norabees I pegmatites, whereas the albitized granodiorite from the Kokerboomrand I pegmatites is P depleted. In the Noumas I pegmatite, the Green greisen (NOU-17-6b) is strongly enriched in Ta (164 ppm), Be (37 ppm), Cs (1149 ppm), Nb (116 ppm), Li (774 ppm) and Bi (7.2 ppm) compared to the less altered granodiorite (NOU-17-10; Ta = 1.4, Be = 1.7, Cs = 58, Nb = 12, Li = 380, Bi = 4.5 ppm). Beryllium, Nb and Ta are less enriched in the Black greisen compared to the Green greisen, but Li, Cs and Bi show higher concentrations (NOU-17-6a; Ta = 4.3, Be = 11, Cs = 2265, Nb = 16, Li = 1156, Bi = 6.3 ppm). Similarly, the greisenized granodioritic raft (NORA-17-4) from the Norabees I pegmatite is strongly enriched in Be (49 ppm), Cs (2165 ppm), Ta (11 ppm), Bi (84 ppm), Li (1783 ppm) and Nb (23 ppm) compared to the less metasomatized granodiorite (NORA-17-5, Be = 4, Cs = 166, Ta = 1, Bi = 17, Li = 589, Nb = 9 ppm). The albitized granodioritic country rock (KOK-17-12) of the Kokerboomrand I pegmatite also

contains a significant amount of Li (667 ppm), Ta (4 ppm), Nb (23 ppm) and Be (19 ppm) compared to less metasomatized granodiorites from the other localities.

## 4.5. Isotope analyses

### 4.5.1. *Monazite and zircon U-Pb geochronology*

A significant amount of monazite crystals was recovered from the aplite border of the Kokerboomrand I pegmatite. Monazite, with a size of 100 to 300  $\mu\text{m}$ , is generally anhedral and rounded in shape showing patchy zoning in BSE images, which reflects a higher Th concentration in bright zones. Monazite crystals commonly contains 1 to 10  $\mu\text{m}$  large apatite inclusions (Supplementary File 5, Fig. S5.4). Twenty crystals were analyzed by LA-MC-ICP-MS for their U/Pb systematics (one spot analysis per crystal; Supplementary File 11), avoiding inclusion-rich zones. A cluster of fifteen concordant analyses yields a concordia age of  $985.9 \pm 4.2$  Ma (MSWD = 1.7) whereas five analyses are slightly discordant (5-10 %) and most probably reflect common Pb contamination (Fig. 18a).

A significant amount of zircon crystals was found in the Kokerboomrand I, Noumas I and Norabees I pegmatites. The 100 to 300  $\mu\text{m}$ -large crystals are generally subhedral to euhedral and characterized by bright cores and dark rims, typically with oscillatory zoning in cathodoluminescence images (Fig. S5.4). The LA-MC-ICP-MS U-Pb results for zircon are provided in Supplementary File 11, and Wetherill concordia diagrams are shown in Supplementary File 5, Figure S5.5. In the aplite border of the Kokerboomrand I pegmatite, the 21 analyses on seventeen crystals plot in a concordant to strongly discordant position in the concordia diagram, defining  $^{207}\text{Pb}/^{206}\text{Pb}$  ages from  $1474 \pm 8$  to  $2286 \pm 8$  Ma. Twenty analyses from sixteen zircon crystals form a discordia line and yield an upper intercept age of  $1872 \pm 17$  Ma, with a lower intercept age of  $102 \pm 25$  Ma (MSWD = 22). One analysis with ~90% of

discordance ( $^{207}\text{Pb}/^{206}\text{Pb}$  age =  $2286 \pm 8$  Ma), potentially reflecting Pb loss and common Pb contamination, was excluded from the calculation. In the aplite border of the Noumas I pegmatite, the twelve spot analyses on twelve crystals are concordant to strongly discordant and have  $^{207}\text{Pb}/^{206}\text{Pb}$  ages ranging from  $1187 \pm 11$  to  $3021 \pm 8$  Ma. Ten analyses align along a discordia and yield lower and upper intercept ages of  $-28 \pm 3$  and  $1866 \pm 14$  Ma, respectively (MSWD = 4.7). Four out of these ten analyses yield a concordia age of  $1876 \pm 9$  Ma (MSWD = 0.5), which is identical within uncertainty to the upper intercept age. One concordant analysis has a  $^{207}\text{Pb}/^{206}\text{Pb}$  age of  $1187 \pm 11$  Ma whereas another has a  $^{207}\text{Pb}/^{206}\text{Pb}$  age of  $2104 \pm 7$  Ma but is strongly discordant ( $> 30\%$ ). Twenty analyses were done on seventeen zircon crystals from the wall zone of the Norabees I pegmatite and have  $^{207}\text{Pb}/^{206}\text{Pb}$  ages from  $167 \pm 40$  to  $1890 \pm 10$  Ma. The twenty analyses are concordant to strongly discordant and tend to align along a same discordia line that defines lower and upper intercept ages of  $148 \pm 13$  and  $1866 \pm 23$  Ma, respectively (MSWD = 8.5). Four out of these twenty analyses yield a concordia age of  $1862 \pm 21$  Ma (MSWD = 2.6) which is identical within uncertainty to the upper intercept age. The  $^{207}\text{Pb}/^{206}\text{Pb}$  zircon ages for all studied pegmatites ( $n = 17$ ), excluding age results with discordance  $> 5\%$  ( $n = 36$ ), are shown as a histogram and kernel density estimate (Fig. 18b). Fifteen analyses form one main population with a weighted average age of  $1871 \pm 8$  Ma (MSWD = 4.5). Two crystals fall outside this main population with ages of  $1187 \pm 11$  and  $1789 \pm 15$  Ma.

#### 4.5.2. *Monazite Sm-Nd isotope analyses*

Seventeen monazite crystals from the aplite border of the Kokerboomrand I pegmatite were analyzed for Sm-Nd isotopes by LA-MC-ICP-MS (Supplementary File 12). These spot analyses were performed close to the previously conducted U-Pb spot analyses (Supplementary File 5, Fig. S5.4). The  $^{147}\text{Sm}/^{144}\text{Nd}$  and  $^{143}\text{Nd}/^{144}\text{Nd}$  compositions, ranging from 0.071 to 0.102 and 0.510956

to 0.511370, respectively, correspond to initial  $\epsilon\text{Nd}(t)$  values of -17.3 to -11.7, recalculated at the age of 986 Ma (see Section 4.6.1). The average initial  $\epsilon\text{Nd}(t)$  value of  $-14.2 \pm 3.3$  ( $2\sigma$ ) is reported in a  $\epsilon\text{Nd}(t)$  versus age diagram (Fig. 18c).

## 5. Discussion

### 5.1. Ages, source(s) and emplacement of the Orange River pegmatites

Monazite from the Li-Ta-Be Kokerboomrand I pegmatite yields a concordia age of  $985.9 \pm 4.2$  Ma that is significantly younger than the mean  $^{207}\text{Pb}/^{206}\text{Pb}$  age of  $1871 \pm 8$  Ma obtained from the most concordant zircon crystals of the Li-Ta-Be-(Bi) pegmatites, including Kokerboomrand I (Figs. 18a and 18b). The mean  $^{207}\text{Pb}/^{206}\text{Pb}$  zircon age is identical within error to a zircon U-Pb concordia age of  $1879 \pm 7$  Ma obtained by Macey et al. (2017) for the Gaarseep granodiorite of the Vioolsdrif Suite, which represents the country rock of these pegmatites. Therefore, zircon crystals from the pegmatites are likely inherited and the monazite age of  $985.9 \pm 4.2$  Ma is interpreted here as the emplacement age of the Kokerboomrand I pegmatite. This new U-Pb monazite age is in agreement with previously obtained unpublished U-Pb monazite ages for other pegmatites from the Orange River belt, ranging from 960 to 1040 Ma (Lambert, 2013; Doggart, 2019). These younger emplacement ages also conform with the fact that most pegmatites in the study area crosscut the foliation of their metagranodioritic host rocks. In the western part of the belt, most pegmatites strike subvertically at 120 to 140° (Schutte, 1972) (Fig. 3) suggesting a strong tectonic control on their emplacement. On a regional scale, pegmatite emplacement is synchronous with D4 dextral deformation that occurred between 1005 and 960 Ma along subvertical faults such as the ~120° striking Pofadder Shear Zone (Lambert, 2013) (PSZ, Fig. 1). Along this fault, pegmatites were emplaced into ductile to brittle structural sites such as foliation planes, Riedel shears, dilatant jogs, extensional fractures and fold axial planes that developed

over 45 million years of PSZ evolution (Lambert, 2013). In the western part of the Orange River belt, 120-140° striking pegmatites were potentially emplaced in Riedel shears of D4-related strike slip faults. However, a detailed structural analysis is needed to better understand the geological conditions that controlled pegmatite magma emplacement.

As the U-Pb systematic of monazite is sensitive to interactions with fluids (e.g. Grand'Homme et al., 2016) or melts (Weinberg et al., in press), it is possible that monazite crystals from the Kokerboomrand I pegmatite are, similar to zircon, inherited but that their U-Pb ages are reset and reflect the crystallization of the pegmatite melt. If true, then the Sm-Nd system of monazite might have remained closed and could be inherited from the source or country rock. However, the Sm-Nd isotopic composition of monazite from the Li-Ta-Be Kokerboomrand I pegmatite is very similar to monazite from other LCT pegmatites of the western part of the Orange River pegmatite belt (Doggart, 2019) (Fig. 18c). Such homogeneity on a regional scale suggests that the composition of monazite is indeed representative of the pegmatite melts and that monazite was not inherited from the source or the country rocks.

The monazite Sm-Nd mantle extraction age of LCT pegmatites overlaps with that of ca. 1.9 Ga old igneous rocks from the Richtersveld magmatic arc, such as the plutonic Vioolsdrif Suite and the volcanic Orange River Group (Reid, 1997; Macey et al., 2017), which represent the host rocks of these pegmatites (Figs. 1, 3 and 18c). This suggests that the LCT pegmatites may have ultimately formed by partial melting of these Paleoproterozoic arc-related rocks. However, the average rare metal contents of the Orange River Group (Li = 20, Nb = 12, Ta = 1.0, Cs = 9.9 ppm) and Vioolsdrif Suite (Li = 22, Nb = 12, Ta = 1.0, Cs = 8.4 ppm), including the Gaarseep granodiorite hosting the pegmatites (Li = 27, Nb = 11, Ta = 1.2, Cs = 9.9 ppm, Macey et al., 2017), are similar to the mean values of the upper continental crust (Li = 24, Nb = 12, Ta = 0.9

ppm, Table 2, Rudnick and Gao, 2003), with the exception of Cs (4.9 ppm). In general, highly peraluminous rare metal granites and pegmatites are typically derived from crustal lithologies that are pre-enriched in rare metals (e.g. Romer and Kroner, 2016; Gourcerol et al., 2019). Therefore, an additional source material may be involved in the genesis of LCT pegmatites from the western part of the Orange River belt. We note that the amphibolite-grade metasedimentary rocks of the Bushmanland Group (Fig. 2), which were deposited to the north of the Bushmanland Subprovince between 1.6 and 1.1 Ga (Cornell et al., 2009), also have similar mantle extraction ages than monazite from the LCT pegmatites (Bailie et al., 2007) (Fig. 18c), which could provide a genetic link. In the study area, equivalents of these sedimentary rocks may have been underthrust beneath the Richtersveld magmatic arc during the main period of D2 accretion that is recorded in the Namaqualand Sector between 1.2 and 1.1 Ga (e.g. Macey et al., 2018). Partial melting of these metasedimentary rocks during D4 regional strike-slip deformation at ca. 1 Ga may also have led to pegmatite formation (Fig. 2). The U-Pb zircon data obtained for the pegmatites (Fig. 18b) are in good agreement with a contribution from a source that is younger than the Richtersveld magmatic arc. Indeed, most inherited zircon crystals found in the pegmatites are ca. 1.9 Ga old and may therefore be interpreted as either granodioritic country rock assimilation or inheritance from a Richtersveld igneous source. However, one zircon grain with a concordant  $^{207}\text{Pb}/^{206}\text{Pb}$  age of  $1187 \pm 11$  Ma may reflect the contribution of equivalents of the Bushmanland Group sediments, for which a detrital zircon age range from 1154 to 2865 Ma has been reported (Cornell et al., 2009). Lithium- and B-rich sedimentary successions are commonly proposed as fertile sources for LCT pegmatites (e.g. Simmons and Webber, 2008; Gourcerol et al., 2019). Unfortunately, rare element concentrations are generally lacking for the Bushmanland Group sedimentary rocks hampering an assessment of their fertility. The only exception is Nb for which an average concentration of 17 ppm (Bailie et al., 2007), slightly

higher than the mean upper crust value of 12 ppm (Table 2, Rudnick and Gao, 2003), is recorded. Importantly, tourmaline-, kornepine- and werdingite-bearing metasediments, commonly interpreted as B-rich meta-evaporites, are described locally from the Bushmanland Subprovince, including the Bushmanland Group (Waters and Moore, 1985; Moore, 1986; Moore et al., 1990; Cornell et al., 2006). This suggests that Bushmanland-derived sediments may represent a fertile source for the Orange River belt LCT pegmatites. In general, the Nd isotopic compositions of granitoids from the northern Bushmanland Subprovince (Clifford et al., 1995; Pettersson et al., 2009) do not overlap with those of monazite from the LCT pegmatites. Thus, these igneous rocks are unlikely to represent a significant source of the pegmatite magmas (Fig. 18c). This leads us to conclude that the LCT pegmatites from the western part of the Orange River belt may have been derived from two possible sources: (1) the Paleoproterozoic igneous rocks of the Richtersveld magmatic arc and/or (2) Bushmanland-derived Mesoproterozoic sediments that possibly contained evaporite units.

Pegmatite magma emplacement in Namaqualand from 1040 to 960 Ma (Lambert, 2013; Doggart, 2017) overlaps in age with the final stages of mainly A-type granitoid magmatism of the Spektakel Suite between 1100 and 1030 Ma, as well as with mafic magmatism of the Koperberg Suite between 1060 and 1010 Ma (Macey et al., 2018, and references therein) (Fig. 2). A crustal source with significant mantle input was suggested for the Spektakel Suite, whereas both lower crustal (Duchesne et al., 2007) and mantle (Maier et al., 2012) sources were proposed for the origin of the Koperberg Suite. Contemporaneous mafic and felsic magmatism from 1100 to 1010 Ma in the Namaqualand Sector was suggested to be the expression of mafic under- and intra-plating in a back-arc setting (Macey et al., 2018). This mechanism of efficient heat transfer into

the crust could have also triggered melting within the Richtersveld magmatic arc and the underthrust Bushmanland sedimentary rocks to form regionally widespread pegmatite magmas.

LCT pegmatites are commonly seen as residual liquids produced during the extreme differentiation of large peraluminous granitic intrusions (e.g. Černý et al., 2005; Černý and Ercit, 2005; London, 2018). Alternatively, they are interpreted as liquids formed during low degrees of partial melting of fluxing element- and rare metal-rich crustal lithologies that experienced limited differentiation during ascent in the crust (e.g. Černý et al., 2005 and references therein; Gourcerol et al., 2019). In the western part of the Orange River belt, pegmatite magma emplacement was contemporaneous with the ca. 1 Ga old peraluminous Warmbad Suite of granites (Macey et al., 2015) (Fig. 2) so that a residual pegmatite origin cannot be excluded.

## **5.2. Pegmatite fertility indicators and early-stage differentiation**

Differentiation markers based on mineral compositions, such as high Rb, Cs, Li, Ta contents and low K/Rb, K/Cs, Na/Li, Fe/Mn and Nb/Ta values of mica, K-feldspar, garnet, tourmaline, beryl or columbite group minerals are known to be useful exploration tools when searching for pegmatite-related rare metal deposits (e.g. Gordiyenko, 1971; Černý et al., 1985; Černý, 1989a; Černý, 1989b; Selway et al., 2005). During this study of LCT pegmatites from the western part of the Orange River belt, we use the major and trace element compositions of mica to document the petrogenesis of these intrusions, because the heterogeneous texture and coarse crystal size of the pegmatites would render whole-rock analyses meaningless. Mica represents a powerful petrogenetic recorder considering its large capacity for element substitutions and its widespread occurrence in almost all pegmatite zones and the granitoid country rocks. In contrast to feldspar and quartz, mica can incorporate much more significant amounts of Li, Ta, Nb and Cs, which are among the main elements of economic interest in these pegmatites.

In the study area, large dioctahedral mica cores from weakly mineralized pegmatites are generally characterized by higher Nb/Ta ( $>14$ ) and Nb but lower Ta, Li and Cs compared to the aplite borders and wall zones of mineralized pegmatites (Fig. 13). Similarly, the K/Rb values of dioctahedral mica crystals from the aplite borders and wall zones of the Li-Ta-Be pegmatites are also low relative to mica from weakly mineralized pegmatites and wall zones of Nb-Ta-Be pegmatites, with a threshold at around 40 (Supplementary File 5, Fig. S5.2). Assuming progressive crystallization of heterogeneous pegmatites from the aplite border toward the pegmatite core (e.g. London, 2014), the effect of internal evolution on mica cores from the aplite borders and wall zones likely remained limited and their composition can be used as a proxy for the evolution of the parental melt. In Figure 13, the negative correlation between Nb/Ta, K/Rb and the Li, Cs and Ta contents of dioctahedral mica of weakly and strongly mineralized pegmatites may reflect the concomitant crystallization of mica, feldspar and oxide minerals from the parental melts. In particular, the decrease of mica Nb/Ta ratios, reflecting an enrichment in Ta and a depletion in Nb (Fig. 13), may be attributed to the extraction of muscovite (Stepanov et al., 2014) and columbite (Linnen and Keppler, 1997). Accordingly, CGM from weakly mineralized pegmatites are also characterized by low Ta\* [ $\text{Ta}/(\text{Ta}+\text{Nb})$ ] and Mn\* [ $\text{Mn}/(\text{Mn}+\text{Fe})$ ] compared to the aplite borders and wall zones of mineralized pegmatites (Fig. 16a). In contrast, the Ab contents of plagioclase (Fig. 9) and K/Rb ratios of microcline (Supplementary File 5, Fig. S5.1) are similar for the weakly and strongly mineralized pegmatites. Overall, the compositional evolution of dioctahedral mica and CGM from weakly to strongly mineralized pegmatites potentially reflects a variable degree of fractional crystallization either in a granitic pluton belonging to the Warmbad Suite (Macey et al., 2015) or in dykes during magma ascent toward the surface (Yamato et al., 2015). However, it must be noted that the nature of the magma source

or the conditions of partial melting including melt extraction (Wolf et al., 2018) may lead to similar compositional differences.

### **5.3. Internal evolution of the pegmatites**

#### **5.3.1. Previous work**

The parental melts of LCT pegmatites are commonly regarded as undercooled liquids crystallizing down to 250°C below the wet granite solidus of ~650°C (London, 2014, 2018). Under these conditions, the decrease of crystal nucleation rate and increase of ionic diffusion can lead to the formation of large crystals. Moreover, the differences in chemical potential between different solid solutions in an undercooled melt can explain some of the typical zonation trends observed in pegmatites with sequential crystallization of plagioclase, K-feldspar and quartz from the borders to the core of the pegmatites. Undercooling and fast crystallization may also lead to the formation of a boundary layer at the crystallization front by constitutional zone refining, a process by which elements that are incompatible in feldspar and quartz become enriched in the residual liquid. Boundary pile-up of fluxing elements, such as F, H, Li, P and B at the crystal growth front can explain the giant size of crystals and the pronounced enrichment in rare metals in the intermediate zones of pegmatites (London, 2014, 2018).

Fluid and melt inclusion studies suggest that at least three immiscible phases can coexist during the crystallization of pegmatite magmas. This may include a highly viscous, silicate-rich, water- and flux-poor peraluminous melt (type-A), a low viscosity, water- and flux-rich, silicate-poor, peralkaline melt (type-B), and a lower salinity aqueous fluid (type-C) (e.g. Thomas et al., 2012). Melt-melt immiscibility can occur below the critical temperature of ~720°C and the proportion of hydrothermal fluids in the system increases during cooling. Such interpretation of melt and fluid inclusion data was challenged by London (2014, 2015) who suggested that type-B

melts may represent the formation of boundary layer liquids. However, boundary pile-up cannot, for example, explain the coexistence of type-A and type-B melt inclusions along a single solvus in a temperature versus water content diagram (Thomas and Davidson, 2015). The compositions of melt inclusions suggest that Li, F and Be will strongly partition into water-rich melts (type-B), whereas the behavior of Rb, Cs, Nb and Ta is unclear, because these elements do not appear to preferentially partition into any particular type of melt (Rickers et al., 2006; Thomas et al., 2011b, 2019; Thomas and Davidson, 2016). Moreover, the metal concentrations in the melts are correlated with temperature, where the highest contents are reached near the critical temperature of  $\sim 720$  °C and water contents of around 25 wt.% before melt-melt-immiscibility. Based on detailed mapping of trace elements in muscovite and CGM in a LCT pegmatite from Ireland, Kaeter et al. (2018) proposed a three-stage model for the magmatic-hydrothermal transition. Their stage I marks the end of purely magmatic crystallization from a peraluminous melt. During stage II, a hydrosaline melt coexists as an immiscible phase with a silicic melt, whereas stage III involves significant melt and crystal interaction with a hydrothermal fluid. Lithium, Cs, Rb and Be are generally considered as fluid-mobile elements (e.g. Förster et al., 1999) and partitioning experiments with granitic melts and aqueous fluids as well as fluid inclusion studies suggest that these elements can partition significantly into Cl-rich fluid phases (e.g. Webster et al., 1989; Harlaux et al., 2017; Iveson et al., 2019). Although Nb and Ta are generally poorly soluble in aqueous fluids, both elements can be mobilized at low temperature ( $<100$ °C) as polyoxometalates (Friis and Casey, 2018). Their solubility also increases at high temperatures ( $>100$ °C) in F-rich aqueous solutions and experimental studies suggest that Nb is more mobile than Ta under most conditions relevant to pegmatite formation (Zaraisky et al., 2010; Timofeev et al., 2015, 2017). However, experiments with F-rich fluids and aluminosilicate melts suggest that both Nb and Ta preferentially partition into the melt phase (Chevychelov et al., 2005).

### 5.3.2. *Paragenetic sequence of pegmatites*

Our petrographic observations of pegmatites and their metasomatized country rocks from the Orange River belt are summarized in the paragenetic sequence of Figure 19. As several episodes of replacement were identified, the relative timing of mineral crystallization in pegmatites is subdivided into a primary stage I, early metasomatic stage II and late metasomatic stage III (quartz crystallization potentially occurred during all stages but is not discussed here):

- *Stage I:* crystallization of K-feldspar, prismatic to sugary oligoclase and albite, spodumene, garnet, beryl, (Li-Fe-) muscovite, tourmaline, CGM, rutile, apatite, zircon and monazite.
- *Stage II:* replacement of early K-feldspar, primary plagioclase and spodumene by sugary to lamellar albite (cleavelandite variety) and Li-mica with a Li-muscovite to zinnwaldite composition (Figs. 6a-c and 8a-c, Table 1, R5-6); replacement of CGM, rutile and albite by a first generation of PGM (Figs. 15h, j, k).
- *Stage III.1:* overgrowth of mica cores by zinnwaldite and lepidolite (Figs. 11c, 11f and 11g); strong localized greisenization characterized by the replacement of spodumene, K-feldspar, albite and PGM by (Fe-) muscovite and zinnwaldite in the intermediate zones (Figs. 5d, 6c-d, 8d-e, 11d, Table 1, R1-3); crystallization of PGM along cleavage planes of metasomatic mica (Supplementary File 5, Fig. S5.3).
- *Stage III.2:* emplacement of garnet-mica-rich replacement bodies mineralized in Bi ( $\pm$ U and Th) in the wall zones (Figs. 5c and 15f); late mica overgrowth (Fig. 11a) and crystallization of small mica crystals in feldspar throughout the pegmatites; replacement of CGM and PGM by native Bi or Bi oxide minerals (Fig. 15i) and a second generation of spongy PGM (Figs. 15b-c, 15l and S5.3); emplacement of Mn

oxide mineral veinlets in lamellar albite and replacement of spodumene by fluorite and pollucite (Fig. S5.3); alteration of spodumene rims (Fig. 10).

### ***5.3.3. Stage I: supersaturation, isothermal fractional crystallization and constitutional zone refining***

In the western part of the Orange River belt, the typical internal zonation of pegmatites, with plagioclase-rich aplite borders, wall zones, intermediates zones and a K-feldspar-quartz core (Fig. 4), is in agreement with isothermal fractional crystallization (Fig. 20a). Boundary pile-up combined with fractional crystallization can explain the concentration of spodumene in the intermediate zone of the Noumas I and Kokerboomrand I pegmatites (Fig. 4, Fig. 5d) as well as the decrease of Fe from green spodumene of the wall zone to pink spodumene of the intermediate zone of the Norabees I pegmatite (Figs. 5e-f, 10 and 20a). Evidence for supersaturation processes is provided, for example, in the Noumas I pegmatite by the presence of garnet and apatite layering in the aplite border. This may reflect magma undercooling as also recorded by the graphic textures observed in the weakly mineralized and Nb-Ta-Be pegmatites (e.g. London, 2014).

Columbite group minerals found in mineralized pegmatites are either homogeneous (Fig. 15b) or show different types of compositional zoning, such as normal zoning (with increasing of Ta content from core to rim, Fig. 15c), inverse zoning, oscillatory zoning (Fig. 15d) or complex patchy zoning (Fig. 15e). Normal zoning is commonly interpreted as reflecting the lower solubility of columbite over tantalite in peraluminous melts and therefore progressive enrichment of Ta in the melt during CGM crystallization (Linnen and Keppler, 1997). Van Lichtervelde et al. (2007; 2018) interpreted oscillatory zoning in CGM as the result of fast disequilibrium crystallization in a supersaturated melt, with the lowest and highest Ta\* zones recording the

highest degrees of disequilibrium. Crystallization experiments also suggest that concomitant crystallization of tantalite and tapiolite reflects supersaturation-induced disequilibrium crystallization (Van Lichtervelde et al., 2018). Therefore, oscillatory zoning of CGM together with the coexistence of tapiolite and tantalite (Figs. 15e and 16a) in the studied mineralized pegmatites may record disequilibrium crystallization in a supersaturated melt. In the Noumas I and Kokerboomrand I pegmatites, the Ta\* and Mn\* values of CGM are higher in the wall zones compared to the aplite borders, which is in agreement with migration of a boundary layer liquid during progressive crystallization of the intrusion (Fig. 20a). Crystallization of Nb-Ta-rutile in the Kokerboomrand I and Norabees I pegmatites may suggest high  $fO_2$  conditions in the supersaturated melt (Van Lichtervelde et al., 2018). Indeed, melting and crystallization experiments indicate that the crystallization of complete solid solutions between a rutile-structured component and tantalite can be triggered by increasing the  $Fe^{3+}/Fe^{2+}$  ratio of the melt (Van Lichtervelde et al., 2018).

Evidence for constitutional zone refining is lacking from the evolution of the rare metal content of dioctahedral mica from the aplite border to the wall zone of the Noumas I and Kokerboomrand I pegmatites. If constitutional zone refining had been operational during mica crystallization, an increase of the mica rare metal content toward the pegmatite cores should be expected. However, mica crystals from the aplite border are enriched in Ta compared to those from the wall zone. Cesium is either enriched or depleted in the aplite border, and the Li contents are either similar in these two zones or higher in the aplite border (Figs. 14b-c). We therefore suggest that the dioctahedral mica compositions were affected by metasomatic processes during stage II or stage III.

#### ***5.3.4. Stage II: melt-melt immiscibility and melt-dominated metasomatism***

The impact of metasomatism on plagioclase composition is well expressed in the Witkop I pegmatite. Here, lamellar albite (cleavelandite) that replaces microcline in the greisenized intermediate zone is characterized by higher Ab content ( $Ab_{97-99}$ ) than prismatic oligoclase and albite from the wall and intermediate zones ( $Ab_{85-98}$ ; Fig. 9a). Similarly, lamellar plagioclase replacing K-feldspar in the wall zone of the Kokerboomrand II pegmatite also has a very high Ab content ( $Ab_{97-99}$ , Fig. 9a). In the Kokerboomrand I pegmatite, cleavelandite replacing spodumene in the intermediate zone (Figs. 6a, 8b, 9c) is also characterized by almost pure albite composition ( $Ab_{>98}$ ) and the same is true for lamellar plagioclase replacing spodumene in the greisenized intermediate zone (Figs. 6c and 9c). However, sugary or prismatic albite from the aplite border ( $Ab_{92-93}$ ) and wall zone ( $Ab_{92-98}$ ), respectively, show lower Ab contents and the composition of albite from the wall zone is variable and transitional between the aplite border and intermediate zone (Fig. 9c). Sugary and lamellar albite replacing K-feldspar in the aplite border and wall zone of the Noumas I pegmatite, respectively, as well as albite veinlets in spodumene have also a very high Ab content ( $Ab_{97-100}$ , Fig. 9b). In the Norabees I pegmatite, the composition of regular to lamellar plagioclase from the wall zone varies ( $Ab_{0.93-0.99}$ ) and lamellar albite from the intermediate zone ( $Ab_{0.98-0.99}$ ) plots at the end of this trend (Fig. 9d). Lamellar albite or cleavelandite is interpreted here as metasomatic in origin and generally has higher albite content than the earlier prismatic and sugary plagioclase also affected by a variable degree of albitization. As suggested by the relatively wide range of Ab values of prismatic plagioclase in the wall zones of pegmatites and the wide spatial distribution of lamellar albite, albitization was likely pervasive with a particularly strong impact on the intermediate zones. As lamellar albite is commonly replaced by mica in greisens (Figs. 8d-e), Na metasomatism probably preceded greisenization.

The replacement of CGM (Figs. 15j-k) and rutile (Fig. 15h) by PGM, with a high A-site occupancy and a dominant (fluor)calciomicrolite composition (Figs. 16b), which are themselves replaced by mica in greisens (Fig. 15i), likely occurred during or soon after albitization. This interpretation is also supported by the intimate association between albite and CGM occurring as resorbed inclusions in (fluor)calciomicrolite (Fig. 15k). Calcium may have been provided by the albitization of plagioclase while Na, F and Ta may have come from the metasomatic medium. Some of the Ta may have been provided by the breakdown of CGM and rutile. Significant Ta enrichment must have occurred during this early magmatic-hydrothermal phase, because stage II PGM from the mineralized pegmatites are enriched in Ta compared to the stage I simply zoned CGM (Fig. 21). However, rare complexly zoned CGM locally reach higher Ta contents than (fluor)calciomicrolite.

In the intermediate zones of the Kokerboomrand I and Norabees I pegmatites, purple Li-mica with a Li-muscovite to zinnwaldite core replaces spodumene (Figs. 6a and 8b) or locally forms mm-wide veinlets cutting albite. In Figure 6a, purple Li-mica can be observed to concentrate along the corroded rim of spodumene and, as seen in thin section (Fig. 8b), Li mica appears to partially replace lamellar albite. Thus, the Li-mica cores have crystallized after spodumene and during or soon after lamellar albite. The Li source may have been spodumene upon its breakdown, or the metasomatic medium, whereas a significant portion of the required K may have originated from K-feldspar breakdown. In addition to their high  $\text{Li}_2\text{O}$  contents (up to 4 wt.%), the mica cores from the intermediate pegmatite zones are strongly enriched in Cs and Ta reaching up to 6000 and 230 ppm, respectively (Fig. 14c-d). Such Ta enrichment is in agreement with the concomitant crystallization of (fluor)calciomicrolite.

Albitites are typically spatially associated with greisens in the cupola of highly evolved granites. Two stages of albitization, i.e. preceding and postdating greisenization, are commonly described (e.g. Štemprok, 1987; Schwartz and Surjono, 1990; Pirajno, 2013; Launay et al., 2019). The first stage of alkali-metasomatism is commonly ascribed to the circulation of a Na- (or K-) rich aqueous solution formed at the end of the crystallization of highly evolved Na-rich granitic melt. Albitization reactions typically lead to a decrease of the alkali/H<sup>+</sup> ratio of the system and this can in return induce the destabilization of K-feldspar, plagioclase and biotite and the replacement of these minerals by muscovite and quartz (i.e. greisenization). By liberating Na-K and re-increasing the alkali/H<sup>+</sup> ratio of the fluid, the greisenization reactions (Table 1) may induce a second stage of alkali-metasomatism including albitization. Albitization and especially greisenization induce an increase of porosity that will enhance the sustainability of such a magmatic-hydrothermal system (Launay et al., 2019). In the mineralized LCT pegmatites from the Orange River belt, albitization is much more widespread than greisenization and metasomatic lamellar albite (cleavelandite) is replaced by muscovite or Li-mica in greisen (Figs. 8d-e). Provided that the opposite textural relationship was not observed, it appears reasonable to conclude that albitization occurred early during the magmatic-hydrothermal evolution of the pegmatites. A similar paragenetic sequence was described for LCT pegmatites from the Gatumba area in Rwanda where albitization related to cleavelandite crystallization preceded greisenization (Dewaele et al., 2011). The metasomatic agent causing albitization in LCT pegmatites from the Orange River belt, and likely elsewhere, might be a Na-rich aqueous fluid or hydrosaline melt (described as type-B melt in Thomas et al., 2012). This second hypothesis is supported by the study of Müller et al. (2018) on albite zones of evolved NYF pegmatites from Evje-Iveland in Norway where hydrosaline melts with water contents  $\geq 34$  wt.% are found as primary inclusions in cleavelandite along with primary fluid inclusions. These authors argued that the formation of

albite-rich zones and cleavelandite is the result of melt-melt and additional melt-fluid immiscibility. Similar to LCT pegmatites from the Orange River belt, cleavelandite from the Evje-Iveland pegmatites also occurs outside albite zones suggesting that the highly mobile Na-rich melts and fluids migrated through the almost completely crystallized intrusion (Müller et al., 2018). In the Orange River pegmatite belt and Evje-Iveland area, the Na-metasomatic agents were probably strongly enriched in Ta (and Nb), which are elements that are generally considered as poorly mobile in aqueous fluids (e.g. Timofeev et al., 2017) with low fluid-melt partition coefficients (Chevychelov et al., 2005). Such Nb-Ta enrichment and mobility would be in agreement with the contribution of an alkali hydrosaline melt where high F concentrations also increase HFSE solubility (e.g. Linnen and Cuney, 2005; Zraisky et al., 2010). In conclusion, we suggest that stage II marks the immiscibility and pervasive circulation of a highly mobile Na-F and Li-Cs-Ta-rich hydrosaline melt with potential contribution from an early aqueous fluid (Fig. 20b).

#### ***5.3.5. Stage III.1: melt-fluid immiscibility and aqueous fluid-dominated metasomatism***

Strong and localized greisenization affected the intermediate zones of the Kokerboomrand I (Figs. 5d and 6c) and Witkop I (Fig. 6d) pegmatites. (Li-) Fe-muscovite to zinnwaldite (mica 1) replace spodumene, albite and (fluor)calciomicrocline in the Kokerboomrand I pegmatite (Figs. 8d, 11d, 12c) whereas muscovite replaces microcline and albite in the Witkop I pegmatite (Figs. 8e, 11a, 12a). Stage III.1 mica from the Kokerboomrand I pegmatite is strongly enriched in Cs containing up to 7000 ppm. The Ta and  $\text{Li}_2\text{O}$  contents are variable, and can reach high contents of up to 150 ppm and 2 wt.%, respectively (Fig. 14a). The Ta and Cs contents of these metasomatic mica crystals, together with stage II mica from the intermediate zone, are some of the highest detected among micas from the pegmatite. Muscovite cores from the greisenized

intermediate zone of the Witkop I pegmatite are strongly enriched in Cs and Ta but depleted in  $\text{Li}_2\text{O}$  compared to (Fe-) muscovite cores from the wall zone and intermediate zone. Therefore, the metasomatic agent involved in greisenization was generally enriched in K, Cs and Ta, but Li concentrations were low at the Witkop I pegmatite and high at the Kokerboomrand I pegmatite. As suggested for the Li-mica of stage II, part of the K component of the metasomatic agent may have originated from the breakdown of K-feldspar whereas Li may have been derived from the breakdown of spodumene. In the Kokerboomrand I pegmatite, a portion of the Ta may have originated from microlite breakdown. The transformation of feldspar to muscovite during greisenization is commonly interpreted as the result of interaction with acidic magmatic aqueous fluids (i.e. low alkali/ $\text{H}^+$  ratio) over a wide range of temperatures (250–450°C; Launay et al., 2019 and references therein) and salinities (10 to >40 wt.% NaCl equivalent; e.g. Pirajno, 2013). By progressively decreasing the alkali/ $\text{H}^+$  ratio of the system, stage I albitization might have triggered greisenization, i.e. the destabilization of plagioclase and K-feldspar and their replacement by muscovite or Li-mica (Table 1, R1-3). Stage III.1 may represent the progressive transition from a magmatic-hydrothermal system dominated by a Na-rich hydrosaline melt with relatively high alkali/ $\text{H}^+$  ratio toward a system involving an acidic aqueous fluid characterized by low alkali/ $\text{H}^+$  ratios. This aqueous fluid phase might have exsolved from the hydrosaline melt and both media likely mobilized a significant amount of Cs and Ta (Fig. 20c). Additional evidence of Ta mobility immediately after greisenization comes from the presence of small (fluor)calciomicrolite crystals along the cleavage planes of muscovite in the Witkop I pegmatite (Fig. S5.3).

In the wall zone of the Norabees I pegmatite, muscovite to Li-Fe-muscovite cores are partially resorbed and/or overgrown by Li-Fe-muscovite to zinnwaldite (Figs. 11f and 12d).

Similarly, at Norabees I and Kokerboomrand I, heterogeneous Li-muscovite to zinnwaldite cores from the intermediate pegmatite zones are overgrown by zinnwaldite and lepidolite (Figs. 11c, 11g, 12c-d). In all of these cases, strong enrichment in Li and Cs occurs from the cores to the rims of mica crystals, and the highest contents are found in the mica rims within the intermediate pegmatite zones reaching up to 6 wt.%  $\text{LiO}_2$  and 1 wt.% of Cs (Figs. 14c-d). However, the mica rims are strongly depleted in Ta compared to the cores, with contents not exceeding 50 ppm in the intermediate zone of the Kokerboomrand I pegmatite. The mica crystallization experiments performed on a pegmatitic melt by Pichavant et al. (2016) indicate that an increase of oxygen fugacity in the melt may lead to the formation of muscovite overgrowing trioctahedral micas of siderophyllite composition. By analogy, the opposite textural relationship for micas of the Kokerboomrand I and Norabees I pegmatites (i.e. a dioctahedral mica core followed by a trioctahedral mica rim) may reflect a decrease of the oxygen fugacity. The sharp decrease in Ta concentration between mica cores and rims, however, suggests that these zones did not crystallize from the same medium. Indeed, this contrasting behavior between Li-Cs and Ta may suggest that zinnwaldite and lepidolite rims crystallized dominantly from an aqueous fluid in which Ta is expected to be less soluble than Li and Cs.

#### **5.3.6. Stage III.2: late hydrothermal phase**

Garnet-mica-rich replacement bodies occur as fracture filling in the wall zone of the Noumas I pegmatite close to the contact with the intermediate zone (Fig. 5c). These replacement bodies commonly contain native Bi rimmed by Bi oxide minerals (Fig. 15f) along with scarce U ( $\pm$  Th, Pb, Cu)-rich phosphates, such as torbernite and plumbogummite (Fig. S5.3). Bismuth oxide minerals replace stage II (fluor)calciomicrocline and also occur in the cleavage planes of stage III.1 Li-mica in the greisenized intermediate zone of the Kokerboomrand I pegmatite (Fig. 15i). This suggests

that Bi-rich hydrothermal activity occurred after the metasomatic stages II and III.1. Large Fe-muscovite cores from the garnet-mica-rich replacement bodies are enriched in Cs (~1000 ppm) and depleted in  $\text{Li}_2\text{O}$  (< 0.1) and Ta (~50 ppm) compared to mica from the aplite border and wall zone of the Noumas I pegmatites. In all pegmatites, stage I, II and III.1 mica crystals are commonly overgrown or replaced along their rims by thin zones of muscovite and Fe-muscovite (Figs. 11a and 12), and such late dioctahedral micas also occur as small crystals in feldspar. However, due to their small crystal size, it was impossible to analyze their rare metal compositions, with the exception of four small crystals found inside feldspar in the wall zone of the Kokerboomrand II pegmatite (Fig. 14a) and two small crystals occurring inside feldspar in the aplite border and wall zone of the Noumas I pegmatite (Fig. 14b). Except for the mica rim from the Noumas I wall zone, which is strongly enriched in Ta (~190 ppm), the late mica crystals are enriched in Cs and depleted in Li and Ta compared to the larger mica cores from the same pegmatite. Therefore, these late mica rims and small crystals may have a similar origin as Fe-muscovite from the garnet-mica-rich replacement bodies of the Noumas I pegmatite. The alteration of pink spodumene rims with K-Cs enrichment in the intermediate zone of the Norabees I pegmatite potentially occurred during this stage.

Stage I CGM and stage II homogeneous PGM are commonly replaced by spongy PGM (Figs. 15a-c, 15l and S5.3) that are characterized by high A-site vacancies and relatively low  $\text{Ta}^*$  values (Fig. 16b). The (fluor)calciomicrolite that was replaced by stage III.1 Li-mica in the Kokerboomrand I pegmatite does not show significant alteration to spongy PGM (Fig. 15i), which suggests that the formation of zero-valence-dominant PGM probably occurred later. Cation vacancies in the A-site of PGM may reflect either actual site vacancies, or the presence of structurally bound water (Atencio et al., 2010). The later would be in agreement with the

formation of zero-valence-dominant PGM in a water-rich environment and therefore the increase of A-site vacancies in PGM during the interaction with an aqueous fluid phase. This leads us to suggest that zero-valence dominant pyrochlore and microlite have a late hydrothermal origin. Zero-valence-dominant PGM from the wall zone and aplite border of the Noumas I pegmatite are locally enriched in Bi with up to ~0.5 apfu (~30 wt.% Bi<sub>2</sub>O<sub>3</sub>, Supplementary File 9), suggesting that Bi minerals may have formed from the same hydrothermal fluid as the zero-valence-dominant PGM. Zero-valence-dominant PGM are generally characterized by lower Ta contents and higher Nb and Nb/Ta than PGM with a high A-site occupancy, but are depleted in both Nb and Ta compared to the CGM they replaced (Figs. 16b, 21 and S5.6).

In short, we suggest that stage III.2 marks the final stage of the magmatic-hydrothermal evolution of the pegmatites and involves an aqueous fluid that was enriched in Bi, Cs (and U) along with K to form muscovite, and perhaps Al to form garnet, but was relatively depleted in Li-Ta-Nb (Fig. 20d). This fluid might have been sourced partly from zones where stage III.1 greisenization occurred because breakdown of K-feldspar is the most obvious source of K (Table 1, R1).

#### **5.4. Interactions between pegmatites and country rocks**

Strong, pervasive and multi-pulse metasomatism of the granodioritic country rocks of mineralized pegmatites (Fig. 19) is expressed as:

- *Stage A*: transformation of Mg-biotite to Fe-biotite, siderophyllite and Fe-muscovite.
- *Stage B.1*: replacement or overgrowth of early metasomatic trioctahedral and dioctahedral mica by Fe-muscovite (Figs. 11e and 11h); formation of the Black greisen in the country rock of the Noumas I pegmatite (Figs. 7a-c).

- *Stage B.2:* replacement of early metasomatic by late metasomatic dioctahedral mica in the Black greisen of the Noumas I pegmatite (Fig. 11b); formation of the apatite-rich zone and Green greisen in the country rock of the Noumas I pegmatite and crystallization of PGM and Nb-Ta-rutile (Figs 7a-c and 15g).

Stages A and B must have been also associated with the destabilization of plagioclase and K-feldspar (Table 1, R1-3, R5-6). The relative timing of fluorite and tourmaline crystallization was not constrained due to the absence of clear textural criteria. Better textural and geochemical evidence allows the timing of albitization to be discussed below.

#### **5.4.1. Stage A: early magmatic-hydrothermal alteration**

Early magmatic-hydrothermal alteration of the granodioritic country rocks of the mineralized pegmatites is expressed by the transformation of primary Mg-biotite to Fe-biotite, siderophyllite and Fe-muscovite (Figs. 12b-d). In the strongly metasomatized country rocks of the Kokerboomrand I and Norabees I pegmatites, the early metasomatic mica crystals are strongly enriched in rare metals with up to 2 wt.%  $\text{Li}_2\text{O}$ , 2 wt.% Cs and 150 ppm Ta (Figs. 14c-d). Based on the magmatic-hydrothermal evolution defined in the mineralized pegmatites, stage A of country rock alteration was likely contemporaneous with the metasomatic stage II recorded in the pegmatites. Accordingly, early metasomatism/alteration of the pegmatites and their country rocks is characterized by high Li, Cs and Ta mobility. The metasomatic agent could be a hydrosaline melt or a related aqueous fluid phase that would be sufficiently mobile to percolate through the country rock (Fig. 20b). Albitization of the country rock, as implied for the Kokerboomrand I pegmatite based on whole-rock (Fig. 17) and plagioclase compositions (Fig. 9c), may have partly occurred at this stage, resulting from the interaction with a Na-rich aqueous medium exsolved from the pegmatite.

#### **5.4.2. Stage B.1: late magmatic-hydrothermal alteration**

Stage B.1 is marked by the replacement or overgrowth of early metasomatic (stage A) Fe-biotite, siderophyllite and Fe-muscovite by a new generation of Fe-muscovite (Figs. 11e, 11h, 12c and 12d, Table 1, R4). Formation of the Black greisens associated with the crystallization of Fe-muscovite cores (Fe-Ms 1) in the country rock rafts of the Noumas I pegmatite likely also occurred during this stage (Figs. 7a-c, 11b and 12b). In the strongly metasomatized granodiorite of the Kokerboomrand I pegmatite, Fe-muscovite from stage B.1 is depleted in Ta (1-60 ppm) but significantly enriched in Cs and Li<sub>2</sub>O with contents up to 2500 ppm and 1.5 wt.%, respectively. This greisenization event may correspond to the metasomatic stage III.1 recorded in the pegmatites that is characterized by important Li and Cs mobility but only moderate mobilization of Ta. Additional albitization may have occurred during stage B.1 as the breakdown of plagioclase during greisenization (Table 1, R2) likely produced Na-rich aqueous fluids (Fig. 20c).

Interestingly, primary Mg-biotite from the weakly metasomatized country rocks of the Noumas I (Fig. 14b) and Norabees I (Fig. 14c) pegmatites is depleted in Ta (< 4 ppm) and significantly enriched in Li<sub>2</sub>O (0.5-0.9 wt.%) and Cs (300-1200 ppm). This indicates that Mg-biotite underwent significant alteration caused by a metasomatic agent interpreted either as a stage III.1 or stage II hydrothermal fluid. These fluids appear to have interacted with the country rocks at distances several meters away from the pegmatite bodies.

#### **5.4.3. Stage B.2: late hydrothermal alteration**

Stage B.2 processes were identified only in the greisenized granodioritic rafts from the Noumas I pegmatite. This stage is characterized by the replacement and overgrowth of Fe-muscovite (Fe-Ms 1) by a second generation of Fe-muscovite (Fe-Ms 2, Fig. 11b) as well as the

formation of an apatite-rich transition zone and the Green greisen at the contact with the pegmatite (Figs. 7a-c and 12b). Fe-muscovite rims from the Black greisen are enriched in Ta but depleted in Li and Cs compared to the core (Fig. 14b). Muscovite from the Green greisen is even more depleted in Li ( $\text{Li}_2\text{O}$  ~0.2 wt.%) and more enriched in Ta (130-170 ppm) compared to Fe-muscovite rims from the Black greisen ( $\text{Li}_2\text{O}$  0.6-0.7 wt.%, Ta ~20 ppm). Strong metasomatic enrichment in Ta (and Nb) is evidenced by the presence of (fluor)calciomicrocline and Nb-Ta-rutile, with local oscillatory zoning showing a relative enrichment of Ta over Nb from core to rim (Figs. 15g, 16b-c). Such Ta enrichment of the country rocks potentially occurred in relation with the late hydrothermal stage III.2 recorded in the pegmatites (Fig. 20d). Indeed, stage III.2 is characterized by the replacement of CGM and (fluor)calciomicrocline by zero-valence-dominant pyrochlore, and such process is associated with a depletion in Ta (and Nb). Therefore, Ta (and Nb) must have been moved elsewhere, and a transfer into the country rocks is most likely. During this stage, Bi- and Mn oxide minerals crystallized probably within the country rocks of the pegmatites.

### **5.5. Metasomatism, rare metal mineralization and Nb-Ta geochemical fractionation**

This study of the western part of the Orange River belt demonstrates that strong but variable rare metal mobilization occurred during the multi-stage magmatic-hydrothermal evolution of LCT pegmatites. The rare metal compositions of mica formed during the various stages of pegmatite evolution are compared with metasomatic mica from the country rocks in terms of their Nb-Ta versus Ta, Nb, Li and Cs systematics (Fig. 22). The mica crystals with the highest rare metal contents are unequivocally metasomatic in origin. Maximum Li and Cs contents are reached during stage II and III.1, which are interpreted as progressive transitions from a magmatic-hydrothermal system dominated by a hydrosaline melt toward a system dominated by

an aqueous fluid. Mica with the highest Ta contents also formed during stage II, while the Ta contents of stage III.1 mica are highly variable. However, mica crystals that formed during the late hydrothermal stage III.2 are overall depleted in rare metals. Interestingly, all metasomatic mica crystals from the pegmatites are characterized by very low Nb contents (< 200 ppm) and generally low Nb/Ta values < 2, falling at the end of the evolutionary trend displayed by stage I magmatic mica in a Nb/Ta versus Nb diagram. The impact of metasomatism on Ta concentration and Nb-Ta geochemical fractionation is also shown in Figure 21, where it becomes clear that magmatic-hydrothermal stage II and III.1 (fluor)calciomicrocline with high A-site occupancy is generally enriched in Ta with lower Nb/Ta compared to stage I CGM, which are mostly simply zoned.

An ongoing debate exists regarding the role of magmatic-hydrothermal processes in the formation of Ta deposits and the geochemical fractionation of Nb and Ta, which are generally considered as geochemical “twins” (e.g. Ballouard et al., 2016a, 2016b; Stepanov et al., 2016; Van Lichtervelde et al., 2018). The evolution trend of highly peraluminous granites and pegmatites is marked by a more pronounced increase of Ta relative to Nb and, thus, a decrease of the Nb/Ta ratio (Linnen and Cuney, 2005; Stepanov et al., 2014; Ballouard et al., 2016a) (Fig. 23). Some studies have shown that fractional crystallization of Nb-Ta oxide minerals (Linnen and Keppler, 1997; Linnen and Cuney, 2005) and mica (Raimbault and Burnol, 1998; Stepanov et al., 2014; López-Moro et al., 2017) induces a decrease of the Nb/Ta ratio in the residual melt. However, an extreme degree of differentiation (>> 90 %) is required to significantly fractionate Nb from Ta, and to reach economic concentrations of Ta (Ballouard et al., 2016a). Van Lichtervelde et al. (2018) argued that such extreme enrichment and “twin” element geochemical decoupling must reflect supersaturation-induced disequilibrium crystallization in an undercooled

melt. However, rare metal-enriched MPG and LCT pegmatites associated with rare metal deposits, and generally characterized by whole-rock Nb/Ta ratios  $< 5$  (Ballouard et al., 2016a), commonly show strong evidence of metasomatism, such as greisenization and albitization. Several authors have argued that magmatic-hydrothermal processes do not contribute to the high Ta enrichment relative to Nb of these intrusions (e.g. Raimbault et al., 1995; Linnen and Cuney, 2005; Van Lichtenvelde et al., 2008, 2007; 2018; Anderson et al., 2013; Harlaux et al., 2017; Llorens González et al., 2017; López-moro et al., 2017). Nevertheless, numerous studies, including the new evidence presented here, have provided geochemical and textural constraints supporting the idea that Ta is being enriched over Nb to economic quantities during magmatic-hydrothermal processes (e.g. Ohnenstetter and Piantone, 1992; Dostal and Chatterjee, 2000; Thomas et al., 2011a, 2009; Badanina et al., 2010, 2015; Dostal et al., 2015; Zhu et al., 2015; Xie et al., 2016; Breiter et al., 2017; Wu et al., 2017, 2018; Alfonso et al., 2018; Fosso Tchunte et al., 2018; Kaeter et al., 2018).

The skepticism regarding a significant role of magmatic-hydrothermal processes for the transport and geochemical fractionation of Nb and Ta comes particularly from the fact that Ta- and Nb-rich haloes appear to be absent in the country rocks of rare metal granites and pegmatites such as the Beauvoir granite in France and the Tanco pegmatite in Canada (Cuney et al., 1992; Linnen and Cuney, 2005). However, whole-rock analyses of the country rocks of mineralized LCT pegmatites from the Orange River belt indicate strong Nb-Ta enrichment in the strongly metasomatized granodiorites with contents of up to ~120 and 160 ppm (Nb/Ta = 0.7-1), respectively, in a Green greisen from the Noumas I pegmatite (Fig. 23). Moreover, the greisenized granodiorites from the Noumas I and Norabees I pegmatites are characterized by Nb/Ta  $< 5$ , supporting the suggestion of Ballouard et al. (2016a) that this ‘cut-off’ value can be

used as a marker to identify granites that experienced significant magmatic-hydrothermal alteration. Overall, our metasomatized granodioritic country rock samples follow a similar evolution trend to highly peraluminous granites with an anticorrelation between Nb/Ta values and Ta, Nb, Li and Cs contents (Fig. 23). The rare metal content of the strongly greisenized granodiorites is two orders of magnitude higher than the pristine granodiorites (Gaarseep granodiorite, Macey et al., 2017). These observed enrichment levels are comparable to those of the bulk Tanco pegmatite (Stilling et al., 2006), which represents one of the world's largest Li-Cs-Ta deposits. A similar Ta enrichment of up to 250 ppm was measured in metasomatized schists occurring at the contact with LCT pegmatites in the Cape Cross–Uis belt of Namibia (Fuchsloch et al., 2019). These recent studies from several large pegmatite belts show that metasomatic enrichment of country rocks to LCT pegmatites is more common than previously thought. However, the Li and Cs contents of weakly to moderately metasomatized granodiorites from the Orange River belt are also high compared to unaltered equivalents, which may indicate that Li-Cs were more mobile than Nb-Ta (Figure 23). The metasomatized country rock geochemical compositions are in agreement with mica compositions, as metasomatic micas from the country rocks are commonly characterized by low Nb/Ta values, low Nb contents and high concentrations of Li-Cs-Ta, comparable to that of mica from the pegmatites (Fig. 22). The observed Ta-Nb enrichment of the country rocks is also associated with crystallization of Nb-Ta-rutile, PGM and CGM (Fig. 21).

In summary, this comprehensive geochronological-petrological-geochemical study of LCT pegmatites from the Orange River belt indicates that although magmatic processes, such as fractional crystallization, constitutional zone refining and disequilibrium crystallization, play a major role in the formation of pegmatite- and granite-related rare metal deposits, magmatic-

hydrothermal processes including melt-melt and melt-fluid immiscibility and subsequent metasomatism may just be as important for ore genesis. Metasomatic rocks such as greisens and albitites occurring in the pegmatites and their immediate country rocks have to be considered as favorable targets during the research of Li-Cs-Ta-Nb deposits. As suggested by Kaeter et al. (2018), the magmatic-hydrothermal transition is a complex multi-stage process where aqueous fluids become progressively dominant over hydrosaline melts, and the various aqueous media involved may have very different capacities for metal transport. The strong and pervasive metasomatism of mineralized LCT pegmatites from the Orange River belt and their country rocks is in agreement with Thomas and Davidson (2016) who suggested that the parental media of pegmatites could be interpreted as critical melt or fluid containing several tens wt.% of dissolved water.

## 6. Conclusions

- Low Nb/Ta (<14) and K/Rb (<40) values of mica appear as good geochemical tools for the research of Li-Ta-(Nb)-Be deposits in the Orange River pegmatite belt. Compositional differences of (Fe-) muscovite between weakly and strongly mineralized pegmatites may reflect either a variable degree of fractional crystallization of the parental melts or variation in partial melting conditions including source composition.
- The Li-Ta-Be mineralized Kokerboomrand I pegmatite was emplaced at ca. 985 Ma contemporaneously with the emplacement of other pegmatites in the Orange River belt and regional strike-slip deformation. The Kokerboomrand I pegmatite formed by the partial melting of either Paleoproterozoic igneous rocks from the Richtersveld

magmatic arc or Mesoproterozoic sedimentary rocks from the Bushmanland Subprovince that were underthrust beneath the Richtersveld magmatic arc.

- Spodumene and CGM crystallized during the magmatic-dominated stage of the internal evolution of mineralized pegmatites in potential relation with undercooling and constitutional zone refining.
- Lamellar albite (cleavelandite variety) and (fluor)calciomicrolite crystallized from an immiscible hydrosaline melt at the beginning of the magmatic-hydrothermal transition. In the pegmatite intermediate zones, the compositional evolution of mica from Li-muscovite to lepidolite marks the transition from a system dominated by a hydrosaline melt toward a system progressively involving an aqueous fluid. Greisens and Bi mineralization mostly formed from a hydrothermal fluid.
- Magmatic-hydrothermal alteration of the immediate granodioritic country rocks of the mineralized pegmatites led to strong Li-Cs-Ta enrichment close to economic grade and induced significant decrease of the whole-rock Nb/Ta ratios.

The fact that the most strongly rare metal enriched mica crystals and Nb-Ta oxide minerals in the pegmatites and immediate country rocks are metasomatic in origin points to a strong impact of magmatic-hydrothermal processes on the formation of rare metal deposits. Greisens and albitites have to be considered as favorable exploration targets for Li-Cs-Ta mineralization. The formation of pegmatite-related mineral deposits in the Orange River belt, and probably elsewhere, is the result of a complex interplay between various magmatic and magmatic-hydrothermal processes.

## **Acknowledgements**

We are grateful to P. Hibberd for granting us access to the Blesberg mine and for precious information about the LCT pegmatites from the Orange River belt. A. Van Der Heever also helped during the sampling in the Blesberg mine. We would like to thank P. Nex who provided GIS data for the pegmatites. We acknowledge P. Pieterse for performing the ICP-MS analyses of the whole-rock powders. S. Mpelane helped us during SEM imaging and EDS analyses. L. Mangwane, B. Tshivhahuvhi and T. Ramaliba are thanked for thin section preparation. C. Vorster helped with heavy liquid mineral separation. T. Owen-Smith and F. Humbert are thanked for providing additional samples. The post-doctoral fellowship of C. Ballouard is funded by the University of Johannesburg, Faculty of Science and DSI-NRF CIMERA. Additional funding was provided by a NRF-CPRR-2018 grant #113403 to M. Elburg. The LA-MC-ICPMS facility was funded by NRF-NEP grant #93208, and is supported by DSI-NRF CIMERA. S. Tappe acknowledges support within the NRF-IPRR funding framework. The constructive comments of E. Gloaguen significantly improved the quality of the manuscript and we thank Y. Chen for editorial handling.

## References

- Alfonso, P., Hamid, S.A., Garcia-Valles, M., Llorens, T., López Moro, F.J., Tomasa, O., Calvo, D., Guasch, E., Anticoi, H., Oliva, J., Parcerisa, D., García Polonio, F., 2018. Textural and mineral-chemistry constraints on columbite-group minerals in the Penouta deposit: evidence from magmatic and fluid-related processes. *Mineral. Mag.* 82, S199–S222. <https://doi.org/10.1180/minmag.2017.081.107>
- Anderson, M.O., Lentz, D.R., Mcfarlane, C.R.M., Falck, H., 2013. A geological, geochemical and textural study of a LCT pegmatite: Implications for the magmatic versus metasomatic origin of Nb-Ta mineralization in the Moose II pegmatite, Northwest Territories, Canada. *J. Geosci. (Czech Republic)* 58, 299–320. <https://doi.org/10.3190/jgeosci.149>
- Andreoli, M. a. G., Hart, R.J., Ashwal, L.D., Coetzee, H., 2006. Correlations between U, Th Content and Metamorphic Grade in the Western Namaqualand Belt, South Africa, with Implications for Radioactive Heating of the Crust. *J. Petrol.* 47, 1095–1118. <https://doi.org/10.1093/petrology/egl004>
- Atencio, D., Andrade, M.B., Christy, A.G., Gieré, R., Kartashov, P.M., 2010. The pyrochlore supergroup of minerals: nomenclature. *Can. Mineral.* 48, 673–698.
- Bachmann, K., Schulz, B., Bailie, R., Gutzmer, J., 2015. Monazite geochronology and

- geothermobarometry in polymetamorphic host rocks of volcanic-hosted massive sulphide mineralizations in the Mesoproterozoic Areachap Terrane, South Africa. *J. African Earth Sci.* 111, 258–272.
- Badanina, E. V., Sitnikova, M.A., Gordienko, V. V., Melcher, F., Gäbler, H.E., Lodziak, J., Siritso, L.F., 2015. Mineral chemistry of columbite-tantalite from spodumene pegmatites of Kolmozero, Kola Peninsula (Russia). *Ore Geol. Rev.* 64, 720–735. <https://doi.org/10.1016/j.oregeorev.2014.05.009>
- Badanina, E. V., Siritso, L.F., Volkova, E. V., Thomas, R., Trumbull, R.B., 2010. Composition of Li-F granite melt and its evolution during the formation of the ore-bearing Orlovka massif in Eastern Transbaikalia. *Petrology* 18, 131–157. <https://doi.org/10.1134/S0869591110020037>
- Bailie, R., Armstrong, R., Reid, D., 2007a. The Bushmanland Group supracrustal succession, Aggeneys, Bushmanland, South Africa: provenance, age of deposition and metamorphism. *South African J. Geol.* 110, 59–86.
- Bailie, R., Armstrong, R., Reid, D., 2007b. Composition and single zircon U-Pb emplacement and metamorphic ages of the Aggeneys Granite Suite, Bushmanland, South Africa. *South African J. Geol.* 110, 87–110.
- Bailie, R., Gutzmer, J., Rajesh, H.M., 2011. Petrography, geochemistry and geochronology of the metavolcanic rocks of the mesoproterozoic Leerkrans Formation, Wilgenhoutsdrif Group, South Africa-back-arc basin to the Areachap volcanic arc. *South African J. Geol.* 114, 167–194.
- Bailie, R., Macey, P.H., Nethenzheni, S., Frei, D., le Roux, P., 2017. The Keimoes Suite redefined: The geochronological and geochemical characteristics of the ferroan granites of the eastern Namaqua Sector, Mesoproterozoic Namaqua-Natal Metamorphic Province, southern Africa. *J. African Earth Sci.* 134, 737–765.
- Bailie, R., Abrahams, G., Bokana, R., van Bever Donker, J., Frei, D., le Roux, P., 2019. The geochemistry and geochronology of the upper granulite facies Kliprand dome: Comparison of the southern and northern parts of the Bushmanland Domain of the Namaqua Metamorphic Province, southern Africa and clues to its evolution. *Precambrian Res.* 330, 58–100.
- Baldwin, J.R., 1989. Replacement phenomena in tantalum minerals from rare-metal pegmatites in South Africa and Namibia. *Mineral. Mag.* 53, 571–581.
- Ballouard, C., Branquet, Y., Tartèse, R., Poujol, M., Boulvais, P., Vigneresse, J.-L., 2016b. Nb-Ta fractionation in peraluminous granites: A marker of the magmatic-hydrothermal transition: Reply. *Geology* 44, e395. <https://doi.org/10.1130/G38169Y.1>
- Ballouard, C., Poujol, M., Boulvais, P., Branquet, Y., Tartèse, R., Vigneresse, J.L., 2016a. Nb-Ta fractionation in peraluminous granites: A marker of the magmatic-hydrothermal transition. *Geology* 44, 231–234. <https://doi.org/10.1130/G37475.1>
- Barbarin, B., 1996. Genesis of the two main types of peraluminous granitoids. *Geology* 24, 295. [https://doi.org/10.1130/0091-7613\(1996\)024<0295:GOTTMT>2.3.CO;2](https://doi.org/10.1130/0091-7613(1996)024<0295:GOTTMT>2.3.CO;2)
- Baumgartner, L.P., Olsen, S.N., 1995. A least-squares approach to mass transport calculations using the isocon method. *Econ. Geol.* 90, 1261–1270.
- Bial, J., Büttner, S., Appel, P., 2016. Timing and conditions of regional metamorphism and crustal shearing in the granulite facies basement of south Namibia : Implications for the crustal evolution of the Namaqualand metamorphic basement in the Mesoproterozoic. *J. African Earth Sci.* 123, 145–176. <https://doi.org/10.1016/j.jafrearsci.2016.07.011>

- Bial, J., Büttner, S.H., Schenk, V., Appel, P., 2015a. The long-term high-temperature history of the central Namaqua Metamorphic Complex: Evidence for a Mesoproterozoic continental back-arc in southern Africa. *Precambrian Res.* 268, 243–278.
- Bial, J., Büttner, S.H., Frei, D., 2015b. Formation and emplacement of two contrasting late-Mesoproterozoic magma types in the central Namaqua Metamorphic Complex (South Africa, Namibia): evidence from geochemistry and geochronology. *Lithos* 224, 272–294.
- Blichert-Toft, J., Puchtel, I.S., 2010. Depleted mantle sources through time: Evidence from Lu–Hf and Sm–Nd isotope systematics of Archean komatiites. *Earth Planet. Sci. Lett.* 297, 598–606. <https://doi.org/10.1016/j.epsl.2010.07.012>
- Bouvier, A., Vervoort, J.D., Patchett, P.J., 2008. The Lu–Hf and Sm–Nd isotopic composition of CHUR: Constraints from unequilibrated chondrites and implications for the bulk composition of terrestrial planets. *Earth Planet. Sci. Lett.* 273, 48–57. <https://doi.org/10.1016/j.epsl.2008.06.010>
- Breiter, K., Korbelová, Z., Chládek, Š., Uher, P., Knesl, I., Rambousek, P., Honig, S., Šešulka, V., 2017. Diversity of Ti–Sn–W–Nb–Ta oxide minerals in the classic granite-related magmatic-hydrothermal Cínovec/Zinnwald Sn–W–Li deposit (Czech Republic). *Eur. J. Mineral.* 29, 727–738.
- Buick, I.S., Storkey, A., Williams, I.S., 2008. Timing relationships between pegmatite emplacement, metamorphism and deformation during the intra-plate Alice Springs Orogeny, central Australia. *J. Metamorph. Geol.* 26, 915–936. <https://doi.org/10.1111/j.1525-1314.2008.00794.x>
- Černý, P., 1989a. Exploration strategy and methods for pegmatite deposits of tantalum, in: *Lanthanides, Tantalum and Niobium*. Springer, pp. 274–302.
- Černý, P., 1989b. Characteristics of pegmatite deposits of tantalum, in: *Lanthanides, Tantalum and Niobium*. Springer, pp. 195–239.
- Černý, P., Ercit, T.S., 2005. The classification of granitic pegmatites revisited. *Can. Mineral.* 43, 2005–2026. <https://doi.org/10.2113/gscanmin.43.6.2005>
- Černý, P., Meintzer, R.E., Anderson, A.J., 1985. Extreme fractionation in rare-element granitic pegmatites; selected examples of data and mechanisms. *Can. Mineral.* 23, 381–421.
- Chevychelov, V.Y., Zaisky, G.P., Borisovskii, S.E., Borkov, D.A., 2005. Effect of melt composition and temperature on the partitioning of Ta, Nb, Mn, and F between granitic (alkaline) melt and fluorine-bearing aqueous fluid: fractionation of Ta and Nb and conditions of ore formation in rare-metal granites. *Petrol. c/c Petrol.* 13, 305.
- Clifford, T.O.M.N., Barton, E.S., Stern, R.A., Duchesne, J.-C., 2004. U–Pb Zircon Calendar for Namaquan (Grenville) Crustal Events in the Granulite-facies Terrane of the O’okiep Copper District of South Africa. *J. Petrol.* 45, 669–691. <https://doi.org/10.1093/petrology/egg097>
- Clifford, T.O.M.N., Barton, E.S., Retied, E.A., Rex, D.C., Fanning, C.M., 1995. A Crustal Progenitor for the Intrusive Anorthosite—Charnockite Kindred of the Cupriferous Koperberg Suite, O’okiep District, Namaqualand, South Africa; New Isotope Data for the Country Rocks and the Intrusives. *J. Petrol.* 36, 231–258.
- Cornell, D.H., Humphreys, H., Theart, H.F.J., Scheepers, D.J., 1992. A collision-related pressure-temperature-time path for Prieska Copper Mine, Namaqua-Natal tectonic province, South Africa. *Precambrian Res.* 59, 43–71.
- Cornell, D.H., Pettersson, Å., 2007a. Ion probe zircon dating of metasediments from the Areachap and Kakamas Terranes, Namaqua-Natal Province and the stratigraphic integrity of the Areachap Group.

- South African J. Geol. 110, 575–584.
- Cornell, D.H., Pettersson, Å., 2007b. Ion probe dating of the Achab Gneiss, a young basement to the central Bushmanland ore district? *J. African Earth Sci.* 47, 112–116.
- Cornell, D.H., Pettersson, Å., Whitehouse, M.J., Scherstén, A., 2009. A New Chronostratigraphic Paradigm for the Age and Tectonic History of the Mesoproterozoic Bushmanland Ore District, South Africa. *Econ. Geol.* 104, 385–404. <https://doi.org/10.2113/gsecongeo.104.3.385>
- Cornell, D.H., Thomas, R.J., Gibson, R., Moen, H.F.G., Reid, D.L., Moore, J.M., Gibson, R.L., 2006. The Namaqua-Natal Province.
- Cuney, M., Barbey, P., 2014. Uranium, rare metals, and granulite-facies metamorphism. *Geosci. Front.* 5, 729–745. <https://doi.org/10.1016/j.gsf.2014.03.011>
- Cuney, M., Marignac, C., Weisbrod, A., 1992. The Beauvoir topaz-lepidolite albite granite (Massif Central, France); the disseminated magmatic Sn-Li-Ta-Nb-Be mineralization. *Econ. Geol.* 87, 1766–1794.
- Deveaud, S., Gumiaux, C., Gloaguen, E., Branquet, Y., 2013. Spatial statistical analysis applied to rare-element LCT-type pegmatite fields: An original approach to constrain faults-pegmatites-granites relationships. *J. Geosci. (Czech Republic)* 58, 163–182. <https://doi.org/10.3190/jgeosci.141>
- Deveaud, S., Millot, R., Villaros, A., 2015. The genesis of LCT-type granitic pegmatites, as illustrated by lithium isotopes in micas. *Chem. Geol.* 411, 97–111. <https://doi.org/10.1016/j.chemgeo.2015.06.029>
- Dewaele, S., Henjes-Kunst, F., Melcher, F., Sitnikova, M., Burgess, R., Gerdes, A., Fernandez, M.A., De Clercq, F., Muchez, P., Lehmann, B., 2011. Late Neoproterozoic overprinting of the cassiterite and columbite-tantalite bearing pegmatites of the Gatumba area, Rwanda (Central Africa). *J. African Earth Sci.* 61, 10–26.
- Dewey, J.F., Robb, L., Van Schalkwyk, L., 2006. Did Bushmanland extensionally unroof Namaqualand? *Precambrian Res.* 150, 173–182. <https://doi.org/10.1016/j.precamres.2006.07.007>
- Diener, J.F.A., White, R.W., Link, K., Dreyer, T.S., Moodley, A., 2013. Clockwise, low- metamorphism of the Aus granulite terrain, southern Namibia, during the Mesoproterozoic Namaqua Orogeny. *Precambrian Res.* 224, 629–652. <https://doi.org/10.1016/j.precamres.2012.11.009>
- Dill, H.G., 2015a. The Hagedorf-Pleystein Province: the Center of Pegmatites in an Ensialic Orogen, *Modern Approaches in Solid Earth Sciences*. Springer International Publishing, Cham (475 pp.).
- Dill, H.G., 2015b. Pegmatites and aplites: Their genetic and applied ore geology. *Ore Geol. Rev.* 69, 417–561. <https://doi.org/10.1016/j.oregeorev.2015.02.022>
- Doggart, S.W., 2019. Geochronology and isotopic characterisation of LCT pegmatites from the Orange River Pegmatite Province. (Thesis, Stellenbosch University) (134 pp.). <http://scholar.sun.ac.za/handle/10019.1/105944>
- Dostal, J., Chatterjee, A.K., 2000. Contrasting behaviour of Nb/Ta and Zr/Hf ratios in a peraluminous granitic pluton (Nova Scotia, Canada). *Chem. Geol.* 163, 207–218. [https://doi.org/10.1016/S0009-2541\(99\)00113-8](https://doi.org/10.1016/S0009-2541(99)00113-8)
- Dostal, J., Kontak, D.J., Gerel, O., Gregory Shellnutt, J., Fayek, M., 2015. Cretaceous ongonites (topaz-bearing albite-rich microleucogranites) from Ongon Khairkhan, Central Mongolia: Products of extreme magmatic fractionation and pervasive metasomatic fluid: rock interaction. *Lithos* 236–237, 173–189. <https://doi.org/10.1016/j.lithos.2015.08.003>

- Duchesne, J.-C., Auwera, J. Vander, Liégeois, J.-P., Barton, E.S., Clifford, T.N., 2007. Geochemical constraints of the petrogenesis of the O'okiep Koperberg Suite and granitic plutons in Namaqualand, South Africa: A crustal source in Namaquan (Grenville) times. *Precambrian Res.* 153, 116–142. <https://doi.org/10.1016/j.precamres.2006.11.005>
- Dufek, J., Bachmann, O., 2010. Quantum magmatism: Magmatic compositional gaps generated by melt-crystal dynamics. *Geology* 38, 687–690. <https://doi.org/10.1130/G30831.1>
- Fisher, D.J., 1968. Albite, variety cleavelandite, and the signs of its optic directions. *Am. Mineral. J. Earth Planet. Mater.* 53, 1568–1578.
- Förster, H.-J., Tischendorf, G., Trumbull, R.B., Gottesmann, B., 1999. Late-Collisional Granites in the Variscan Erzgebirge, Germany. *J. Petrol.* 40, 1613–1645. <https://doi.org/10.1093/etroj/40.11.1613>
- Fosso Tchunte, P., Tchameni, R., André-Mayer, A.-S., Dakoure, H., Turlin, F., Poujol, M., Nomo, E., Saha Fouotsa, A., Rouer, O., 2018. Evidence for Nb-Ta Occurrences in the Syn-Tectonic Pan-African Mayo Salah Leucogranite (Northern Cameroon): Constraints from Nb-Ta Oxide Mineralogy, Geochemistry and U-Pb LA-ICP-MS Geochronology on Columbite and Monazite. *Minerals* 8, 188.
- Friis, H., Casey, W.H., 2018. Niobium Is Highly Mobile As a Polyoxometalate Ion During Natural Weathering. *Can. Mineral.* 56, 905–912.
- Fuchsloch, W.C., Nex, P.A.M., Kinnaird, J.A., 2019. The geochemical evolution of Nb-Ta-Sn oxides from pegmatites of the Cape Cross-Uis pegmatite belt, Namibia. *Mineral. Mag.* 83, 161–179.
- Fuchsloch, W.C., Nex, P.A.M., Kinnaird, J.A., 2018. Classification, mineralogical and geochemical variations in pegmatites of the Cape Cross-Uis pegmatite belt, Namibia. *Lithos* 296–299, 79–95. <https://doi.org/10.1016/j.lithos.2017.09.030>
- Geringer, G.J., Schoch, A.E., Sukhanov, M., Zhuravlev, D., 1998. Geochemical and isotopic characteristics of different types of anorthosite in the Namaqua mobile belt, South Africa. *Chem. Geol.* 145, 17–46.
- Gordiyenko, V. V., 1971. Concentrations of Li, Rb, and Cs in potash feldspar and muscovite as criteria for assessing the rare-metal mineralization in granite pegmatites. *Int. Geol. Rev.* 13, 134–142.
- Gourcerol, B., Gloaguen, E., Melleton, J., Tuduri, J., Galiegue, X., 2019. Re-assessing the European lithium resource potential – A review of hard-rock resources and metallogeny. *Ore Geol. Rev.* 109, 494–519. <https://doi.org/10.1016/j.oregeorev.2019.04.015>
- Grand'Homme, A., Janots, E., Seydoux-Guillaume, A.-M., Guillaume, D., Bosse, V., Magnin, V., 2016. Partial resetting of the U-Th-Pb systems in experimentally altered monazite: Nanoscale evidence of incomplete replacement. *Geology* 44, 431–434.
- Grant, J.A., 1986. The isocon diagram; a simple solution to Gresens' equation for metasomatic alteration. *Econ. Geol.* 81, 1976–1982.
- Gunn, G., 2014. *Critical metals handbook*. John Wiley & Sons. (439 pp.).
- Harlaux, M., Mercadier, J., Bonzi, W.M.-E., Kremer, V., Marignac, C., Cuney, M., 2017. Geochemical signature of magmatic-hydrothermal fluids exsolved from the Beauvoir Rare-Metal Granite (Massif Central, France): insights from LA-ICPMS analysis of primary fluid inclusions. *Geofluids* 2017.
- Hugo, P.J., 1970. The pegmatites of the Kenhardt and Gordonia districts. *Memoir of Geological Survey of South Africa* 58. (93 pp.).
- Hulsbosch, N., Hertogen, J., Dewaele, S., André, L., Muchez, P., 2014. Alkali metal and rare earth

- element evolution of rock-forming minerals from the Gatumba area pegmatites (Rwanda): Quantitative assessment of crystal-melt fractionation in the regional zonation of pegmatite groups. *Geochim. Cosmochim. Acta* 132, 349–374. <https://doi.org/10.1016/j.gca.2014.02.006>
- Iveson, A.A., Webster, J.D., Rowe, M.C., Neill, O.K., 2019. Fluid-melt trace-element partitioning behaviour between evolved melts and aqueous fluids: Experimental constraints on the magmatic-hydrothermal transport of metals. *Chem. Geol.* 516, 18–41.
- Kaeter, D., Barros, R., Menuge, J.F., Chew, D.M., 2018. The magmatic–hydrothermal transition in rare-element pegmatites from southeast Ireland: LA-ICP-MS chemical mapping of muscovite and columbite–tantalite. *Geochim. Cosmochim. Acta* 240, 98–130. <https://doi.org/10.1016/j.gca.2018.08.024>
- Knoll, T., Schuster, R., Huet, B., Mali, H., Onuk, P., Horschinegg, M., Ertl, A., Giester, G., 2018. Spodumene pegmatites and related leucogranites from the austroalpine unit (eastern alps, central europe): Field relations, petrography, geochemistry, and geochronology. *Can. Mineral.* 56, 489–528. <https://doi.org/10.3749/canmin.1700092>
- Kontak, D.J., Creaser, R.A., Heaman, L.M., Archibald, D.A., 2005. U-Pb tantalite, Re-Os molybdenite, and  $^{40}\text{Ar}/^{39}\text{Ar}$  muscovite dating of the Brazil Lake Pegmatite, Nova Scotia; a possible shear-zone related origin for an LCT-type pegmatite. *Atl. Geol.* 41, 17–29.
- Konzett, J., Hauzenberger, C., Ludwig, T., Stalder, R., 2018a. Anatectic granitic pegmatites from the eastern alps: A case of variable rare metal enrichment during high-grade regional metamorphism. II: Pegmatite staurolite as an indicator of anatectic pegmatite parent melt formation - a field and experimental study. *Can. Mineral.* 56, 603–624. <https://doi.org/10.3749/canmin.1800011>
- Konzett, J., Schneider, T., Nedyalkova, L., Hauzenberger, C., Melcher, F., Gerdes, A., Whitehouse, M., 2018b. Anatectic granitic pegmatites from the eastern alps: A case of variable rare-metal enrichment during high-grade regional metamorphism - I: Mineral assemblages, geochemical characteristics, and emplacement ages. *Can. Mineral.* 56, 555–602. <https://doi.org/10.3749/canmin.1800008>
- Lambert, C.W., 2013. Granitic melt transport and emplacement along transcurrent shear zones: Case study of the Pofadder Shear Zone in South Africa and Namibia. (Thesis, Stellenbosch University) (128 pp.). <http://scholar.sun.ac.za/handle/10019.1/85682>
- Launay, G., Sizaret, S., Guillou-Frottier, L., Fauguerolles, C., Champallier, R., Gloaguen, E., 2019. Dynamic permeability related to greisenization reactions in Sn-W ore deposits: Quantitative petrophysical and experimental evidence. *Geofluids* 2019, 16–20. <https://doi.org/10.1155/2019/5976545>
- Linnen, R.L., Cuney, M., 2005. Granite-related rare-element deposits and experimental constraints on Ta-Nb-W-Sn-Zr-Hf mineralization, in Linnen RL and Samson IM, eds., rare-element geochemistry and mineral deposits., in: Geological Association of Canada, GAC, Short Course.
- Linnen, R.L., Keppler, H., 1997. Columbite solubility in granitic melts: consequences for the enrichment and fractionation of Nb and Ta in the Earth's crust. *Contrib. to Mineral. Petrol.* 128, 213–227. <https://doi.org/10.1007/s004100050304>
- Linnen, R.L., Lichtervelde, M. Van, Černý, P., 2012. Granitic Pegmatites as Sources of Strategic Metals. *Elements* 8, 275–280. <https://doi.org/10.2113/gselements.8.4.275>
- Llorens González, T., García Polonio, F., López Moro, F.J., Fernández Fernández, A., Sanz Contreras, J.L., Moro Benito, M.C., 2017. Tin-tantalum-niobium mineralization in the Penouta deposit (NW Spain): Textural features and mineral chemistry to unravel the genesis and evolution of cassiterite

- and columbite group minerals in a peraluminous system. *Ore Geol. Rev.* 81, 79–95. <https://doi.org/10.1016/j.oregeorev.2016.10.034>
- London, D., 2018. Ore-forming processes within granitic pegmatites. *Ore Geol. Rev.* 101, 349–383.
- London, D., 2015. Reply to Thomas and Davidson on “A petrologic assessment of internal zonation in granitic pegmatites”. *Lithos.* <https://doi.org/10.1016/j.lithos.2014.11.025>
- London, D., 2014. A petrologic assessment of internal zonation in granitic pegmatites. *Lithos* 184–187, 74–104. <https://doi.org/10.1016/j.lithos.2013.10.025>
- López-moro, F.J., García, F., Llorens, T., Luis, J., Contreras, S., Fernández, A., Candelas, M., Benito, M., 2017. Ta and Sn concentration by muscovite fractionation and degassing in a lens-like granite body : The case study of the Penouta rare-metal albite granite (NW Spain). *Ore Geol. Rev.* 82, 10–30. <https://doi.org/10.1016/j.oregeorev.2016.11.027>
- MacDonald, N., 2013. Mineralogical study and melt-fluid evolution of the Noumas I pegmatite, Northern Cape, South Africa. (Thesis, University of the Free State) (145 pp.). <https://scholar.ufs.ac.za/bitstream/handle/11660/775/MacDonaldN.pdf?sequence=1&isAllowed=y>
- Macey, P.H., Bailie, R.H., Miller, J.A., Thomas, R.J., de Beer, C., Frei, D., le Roux, P.J., 2018. Implications of the distribution, age and origins of the granites of the Mesoproterozoic Spektakel Suite for the timing of the Namaqua Orogeny in the Bushmanland Subprovince of the Namaqua-Natal Metamorphic Province, South Africa. *Precambrian Res.* 312, 68–98.
- Macey, P.H., Thomas, R.J., Minnaar, H.M., Gresse, P.G., Lambert, C.W., Groenewald, C.A., Miller, J.A., Indongo, J., Angombe, M., Shifotoka, G., Frei, D., Diener, J.F.A., Kisters, A.F.M., Dhansay, T., Smith, H., Doggart, S., Le Roux, P., Hartnady, M.I., Tinguely, C., 2017. Origin and evolution of the ~1.9 Ga Richtersveld Magmatic Arc, SW Africa. *Precambrian Res.* 292, 417–451. <https://doi.org/10.1016/j.precamres.2017.01.013>
- Macey, P.H., Minnaar, H., Miller, J.A., Lambert, C., Kisters, A.F.M., Diener, J., Thomas, R.J., Groenewald, C., Indongo, J., Angombe, M., Smith, H., Shifatoka, G., Le Roux, P., Frei, D., 2015. The Precambrian geology of the Warmbad region, southern Namibia. An interim explanation to 1: 50 000 geological map sheets of the 1: 250 000 2818 Warmbad sheet, in: Accompanied by Twenty-Four 1: 50,000 Geological Maps. *Geol. Surv. Namibia and Council for Geoscience of South Africa.*
- Matheis, G., 1987. Nigerian rare-metal pegmatites and their lithological framework. *Geol. J.* 22, 271–291.
- Maier, W.D., Andreoli, M. a. G., Groves, D.I., Barnes, S.-J., 2012. Petrogenesis of Cu-Ni Sulphide Ores from O’okiep and Kliprand, Namaqualand, South Africa: Constraints from Chalcophile Metal Contents. *South African J. Geol.* 115, 499–514. <https://doi.org/10.2113/gssajg.115.4.499>
- Melleton, J., Gloaguen, E., Frei, D., Novák, M., Breiter, K., 2012. How are the emplacement of rare-element pegmatites, regional metamorphism and magmatism interrelated in the Moldanubian domain of the Variscan Bohemian Massif, Czech Republic? *Can. Mineral.* 50, 1751–1773. <https://doi.org/10.3749/canmin.50.6.1751>
- Minnaar, H., Theart, H.F.J., 2006. The exploitability of pegmatite deposits in the lower Orange River area (Vioolsdrif – Henkries – Steinkopf). *South African J. Geol.* 109, 341–352. <https://doi.org/10.2113/gssajg.109.3.341>
- Moen, H.F.G., Armstrong, R.A., 2008. New age constraints on the tectogenesis of the Kheis Subprovince and the evolution of the eastern Namaqua Province. *South African J. Geol.* 111, 79–88.
- Moore, J.M., Waters, D.J., Niven, M.L., 1990. Werdingite, a new borosilicate mineral from the granulite

- facies of the western Namaqualand metamorphic complex, South Africa. *Am. Mineral.* 75, 415–420.
- Moore, J.M., 1986. A comparative study of metamorphosed supracrustal rocks from the western Namaqualand Metamorphic Complex. (Thesis, University of Cape Town) (421 pp.). <https://open.uct.ac.za/handle/11427/22585>
- Müller, A., Spratt, J., Thomas, R., Williamson, B.J., Seltmann, R., 2018. Alkali-F-rich albite zones in evolved NYF pegmatites: The product of melt-melt immiscibility. *Can. Mineral.* 56, 657–687. <https://doi.org/10.3749/canmin.1700087>
- Müller, A., Romer, R.L., Pedersen, R.B., 2017. The sveconorwegian pegmatite province -thousands of pegmatites without parental granites. *Can. Mineral.* 55, 283–315. <https://doi.org/10.3749/canmin.1600075>
- Norton, J.J., 1973. Lithium, Cesium, and Rubidium - the rare alkali metals. *Geol. Surv. Prof. Pap.* 365.
- Ohnenstetter, D., Piantone, P., 1992. Pyrochlore-group minerals in the Beauvoir peraluminous leucogranite, Massif Central, France. *Can. Mineral.* 30, 771–784.
- Pettersson, Å., 2008. Mesoproterozoic crustal evolution in Southern Africa. (Thesis, University of Gothenburg). <https://gupea.ub.gu.se/handle/2077/17269>
- Pettersson, Å., Cornell, D.H., Moen, H.F.G., Reddy, S., Evans, D., 2007. Ion-probe dating of 1.2 Ga collision and crustal architecture in the Namaqua-Natal Province of southern Africa. *Precambrian Res.* 158, 79–92.
- Pettersson, Å., Cornell, D.H., Yuhara, M., Hirahara, Y., 2009. Sm-Nd data for granitoids across the Namaqua sector of the Namaqua-Natal Province, South Africa. *Geol. Soc. London, Spec. Publ.* 323, 219–230.
- Pichavant, M., Villaros, A., Deveaud, S., Scaillet, B., Lahlafi, M., 2016. The influence of redox state on mica crystallization in leucogranitic and pegmatitic liquids. *Can. Mineral.* 54, 559–581. <https://doi.org/10.3749/canmin.1500079>
- Pirajno, F., 2013. Effects of Metasomatism on Mineral Systems and Their Host Rocks: Alkali Metasomatism, Skarns, Greisens, Tourmalinites, Rodingites, Black-Wall Alteration and Listvenites, in: *Metasomatism and the Chemical Transformation of Rock*. Springer Berlin Heidelberg, pp. 203–251.
- Raimbault, L., Burnol, L., 1998. The Richemont rhyolite dyke, Massif Central, France; a subvolcanic equivalent of rare-metal granites. *Can. Mineral.* 36, 265–282.
- Raimbault, L., Cuney, M., Azencott, C., Duthou, J.-L., Joron, J.L., 1995. Geochemical evidence for a multistage magmatic genesis of Ta-Sn-Li mineralization in the granite at Beauvoir, French Massif Central. *Econ. Geol.* 90, 548–576.
- Raith, J.G., 1995. Petrogenesis of the Concordia Granite Gneiss and its relation to W-Mo mineralization in western Namaqualand, South Africa. *Precambrian Res.* 70, 303–335.
- Raith, J.G., Cornell, D.H., Frimmel, H.E., De Beer, C.H., 2003. New insights into the geology of the Namaqua tectonic province, South Africa, from ion probe dating of detrital and metamorphic zircon. *J. Geol.* 111, 347–366.
- Reid, D.L., 1997. Sm-Nd age and REE geochemistry of Proterozoic arc-related igneous rocks in the Richtersveld subprovince, Namaqua Mobile Belt, Southern Africa. *J. African Earth Sci.* 24, 621–633.

- Rickers, K., Thomas, R., Heinrich, W., 2006. The behavior of trace elements during the chemical evolution of the H<sub>2</sub>O-, B-, and F-rich granite--pegmatite--hydrothermal system at Ehrenfriedersdorf, Germany: a SXRF study of melt and fluid inclusions. *Miner. Depos.* 41, 229–245.
- Robb, L.J., Armstrong, R.A., Waters, D.J., 1999. The History of Granulite-Facies Metamorphism and Crustal Growth from Single Zircon U–Pb Geochronology: Namaqualand, South Africa. *J. Petrol.* 40, 1747–1770. <https://doi.org/10.1093/petroj/40.12.1747>
- Roda-Robles, E., Villaseca, C., Pesquera, A., Gil-Crespo, P.P., Vieira, R., Lima, A., Garate-Olave, I., 2018. Petrogenetic relationships between Variscan granitoids and Li-(F-P)-rich aplite-pegmatites in the Central Iberian Zone: Geological and geochemical constraints and implications for other regions from the European Variscides. *Ore Geol. Rev.* 95, 408–430. <https://doi.org/10.1016/j.oregeorev.2018.02.027>
- Romer, R.L., Kroner, U., 2016. Phanerozoic tin and tungsten mineralization—Tectonic controls on the distribution of enriched protoliths and heat sources for crustal melting. *Gondwana Res.* 31, 60–95. <https://doi.org/10.1016/j.j.gr.2015.11.002>
- Rudnick, R.L., Gao, S., 2003. Composition of the Continental Crust. *Treatise on Geochemistry* 3, 659. <https://doi.org/10.1016/B0-08-043751-6/03016-4>
- Schutte, I.C., 1972. The main pegmatites of the area between Steinkopf, Violsdrif and Goodhouse, Namaqualand. *Memoir of Geological Survey of South Africa* 60 (19 pp.).
- Schwartz, M.O., Surjono, 1990. Greisenization and albitization at the Tikus tin-tungsten deposit, Belitung, Indonesia. *Econ. Geol.* 85, 691–713. <https://doi.org/10.2113/gsecongeo.85.4.691>
- Selway, J.B., Breaks, F.W., Tindle, A.G., 2005. A review of rare-element (Li-Cs-Ta) pegmatite exploration techniques for the Superior Province, Canada, and large worldwide tantalum deposits. *Explor. Min. Geol.* 14, 1–30.
- Shaw, R.A., Goodenough, K.M., Roberts, N.M.W., Horstwood, M.S.A., Chenery, S.R., Gunn, A.G., 2016. Petrogenesis of rare-metal pegmatites in high-grade metamorphic terranes: A case study from the Lewisian Gneiss Complex of north-west Scotland. *Precambrian Res.* 281, 338–362. <https://doi.org/10.1016/j.precamres.2016.06.008>
- Shmakin, B.M., 1983. Geochemistry and origin of granitic pegmatites. *Geochemistry Int.* 20, 1–8.
- Simmons, W.B.S., Webber, K.L., 2008. Pegmatite genesis: state of the art. *Eur. J. Mineral.* 20, 421–438. <https://doi.org/10.1127/0935-1221/2008/0020-1833>
- Štemprok, M., 1987. Greisenization (a review). *Geol. Rundschau* 76, 169–175. <https://doi.org/10.1007/BF01820580>
- Stepanov, A., Mavrogenes, J.A., Meffre, S., Davidson, P., 2014. The key role of mica during igneous concentration of tantalum. *Contrib. to Mineral. Petrol.* 167, 1–8. <https://doi.org/10.1007/s00410-014-1009-3>
- Stepanov, A.S., Meffre, S., Mavrogenes, J., Steadman, J., 2016. Nb-Ta fractionation in peraluminous granites: A marker of the magmatic-hydrothermal transition: COMMENT. *Geology* 44, e394–e394. <https://doi.org/10.1130/G38086C.1>
- Stewart, D.B., 1978. Petrogenesis of lithium-rich pegmatites. *Am. Mineral.* 63, 970–980.
- Stilling, A., Černý, P., Vanstone, P.J., 2006. The Tanco pegmatite at Bernic Lake, Manitoba. XVI. Zonal and bulk compositions and their petrogenetic significance. *Can. Mineral.* 44, 599–623.

<https://doi.org/10.2113/gscanmin.44.3.599>

- Thomas, R., Davidson, P., 2016. Revisiting complete miscibility between silicate melts and hydrous fluids, and the extreme enrichment of some elements in the supercritical state—consequences for the formation of pegmatites and ore deposits. *Ore Geol. Rev.* 72, 1088–1101.
- Thomas, R., Davidson, P., 2015. Comment on “A petrologic assessment of internal zonation in granitic pegmatites” by David London (2014). *Lithos* 212–215, 462–468. <https://doi.org/10.1016/j.lithos.2014.08.028>
- Thomas, R., Davidson, P., 2012. Water in granite and pegmatite-forming melts. *Ore Geol. Rev.* 46, 32–46. <https://doi.org/10.1016/j.oregeorev.2012.02.006>
- Thomas, R., Davidson, P., Appel, K., 2019. The enhanced element enrichment in the supercritical states of granite-pegmatite systems. *Acta Geochim.* 38, 335–349. <https://doi.org/10.1007/s11631-019-00319-z>
- Thomas, R., Davidson, P., Badanina, E., 2009. A melt and fluid inclusion assemblage in beryl from pegmatite in the Orlovka amazonite granite, East Transbaikalia, Russia: implications for pegmatite-forming melt systems. *Mineral. Petrol.* 96, 129–140. <https://doi.org/10.1007/s00710-009-0053-6>
- Thomas, R., Davidson, P., Beurlen, H., 2012. The competing models for the origin and internal evolution of granitic pegmatites in the light of melt and fluid inclusion research. *Mineral. Petrol.* 106, 55–73. <https://doi.org/10.1007/s00710-012-0212-z>
- Thomas, R., Davidson, P., Beurlen, H., 2011a. Tantalite- (Mn) from the Borborema Pegmatite Province, northeastern Brazil: conditions of formation and melt- and fluid-inclusion constraints on experimental studies 749–759. <https://doi.org/10.1007/s00126-011-0344-9>
- Thomas, R., Förster, H.-J., Rickers, K., Webster, J.D., 2005. Formation of extremely F-rich hydrous melt fractions and hydrothermal fluids during differentiation of highly evolved tin-granite magmas: a melt/fluid-inclusion study. *Contrib. to Mineral. Petrol.* 148, 582–601.
- Thomas, R., Webster, J.D., Davidson, P., 2011b. Be-daughter minerals in fluid and melt inclusions: implications for the enrichment of Be in granite-pegmatite systems. *Contrib. to Mineral. Petrol.* 161, 483–495. <https://doi.org/10.1007/s00410-010-0544-9>
- Thomas, R.J., Agenbacht, A.L.D., Cornell, D.H., Moore, J.M., 1994. The Kibaran of southern Africa: Tectonic evolution and metallogeny. *Ore Geol. Rev.* 9, 131–160. [https://doi.org/10.1016/0169-1368\(94\)90025-6](https://doi.org/10.1016/0169-1368(94)90025-6)
- Timofeev, A., Migdisov, A.A., Williams-Jones, A.E., 2017. An experimental study of the solubility and speciation of tantalum in fluoride-bearing aqueous solutions at elevated temperature. *Geochim. Cosmochim. Acta* 197, 294–304.
- Timofeev, A., Migdisov, A.A., Williams-Jones, A.E., 2015. An experimental study of the solubility and speciation of niobium in fluoride-bearing aqueous solutions at elevated temperature. *Geochim. Cosmochim. Acta.* <https://doi.org/10.1016/j.gca.2015.02.015>
- Tischendorf, G., Förster, H.-J., Gottesmann, B., 2001. Minor and trace-element composition of trioctahedral micas: a review. *Mineral. Mag.* 65, 249–276.
- Tischendorf, G., Gottesmann, B., Förster, H.-J., Trumbull, R.B., 1997. On Li-bearing micas: estimating Li from electron microprobe analyses and an improved diagram for graphical representation. *Mineral. Mag.* 61, 809–834.
- Van Lichtervelde, M., Grégoire, M., Linnen, R.L., Béziat, D., Salvi, S., 2008. Trace element geochemistry

- by laser ablation ICP-MS of micas associated with Ta mineralization in the Tanco pegmatite, Manitoba, Canada. *Contrib. to Mineral. Petrol.* 155, 791–806. <https://doi.org/10.1007/s00410-007-0271-z>
- Van Lichtervelde, M., Holtz, F., Melcher, F., 2018. The effect of disequilibrium crystallization on Nb-Ta fractionation in pegmatites: Constraints from crystallization experiments of tantalite-tapiolite. *Am. Mineral.* 103, 1401–1416.
- Van Lichtervelde, M., Salvi, S., Beziat, D., Linnen, R.L., 2007. Textural features and chemical evolution in tantalum oxides: Magmatic versus hydrothermal origins for Ta mineralization in the Tanco Lower pegmatite, Manitoba, Canada. *Econ. Geol.* 102, 257–276. <https://doi.org/10.2113/gsecongeo.102.2.257>
- Van Niekerk, H.S., 2006. The origin of the Kheis Terrane and its relationship with the Archean Kaapvaal Craton and the Grenvillian Namaqua Province in southern Africa. University of Johannesburg.
- Van Niekerk, H.S., Beukes, N.J., 2019. Revised definition/outline of the Kheis Terrane along the western margin of the Kaapvaal Craton and lithostratigraphy of the newly proposed Keis Supergroup. *South African J. Geol.* 122, 187–220.
- Van Schijndel, V., Cornell, D., Anczkiewicz, R., Scherstén, A., in press. Evidence for Mesoproterozoic collision, deep burial and rapid exhumation of garbenschiefer in the Namaqua Front, South Africa. *Geosci. Front.* <https://doi.org/10.1016/j.gsf.2019.06.004>
- Waters, D.J., 1989. Metamorphic evidence for the heating and cooling path of Namaqualand granulites. *Geol. Soc. London, Spec. Publ.* 43, 357–363.
- Waters, D.J., Moore, J.M., 1985. Kernerupine in Mg-Al-rich gneisses from Namaqualand, South Africa: mineralogy and evidence for late-metamorphic fluid activity. *Contrib. to Mineral. Petrol.* 91, 369–382.
- Webster, J.D., Holloway, J.R., Hervig, R.L., 1989. Partitioning of lithophile trace elements between H<sub>2</sub>O and H<sub>2</sub>O+CO<sub>2</sub> fluids and topaz rhyolite melt. *Econ. Geol.* 84, 116–134.
- Weinberg, R.F., Wolfram, L.C., Nebel, O., Hasalová, P., Závada, P., Kylander-Clark, A.R.C., Becchio, R., in press. Decoupled U-Pb date and chemical zonation of monazite in migmatites: The case for disturbance of isotopic systematics by coupled dissolution-reprecipitation. *Geochim. Cosmochim. Acta.* <https://doi.org/10.1016/j.gca.2019.10.024>
- Whitney, D.L., Evans, B.W., 2010. Abbreviations for names of rock-forming minerals. *Am. Mineral.* 95, 185–187.
- Wolf, M., Romer, R.L., Franz, L., López-moro, F.J., 2018. Tin in granitic melts: The role of melting temperature and protolith composition. *Lithos* 310–311, 20–30. <https://doi.org/10.1016/j.lithos.2018.04.004>
- Wu, M., Samson, I.M., Zhang, D., 2018. Textural Features and Chemical Evolution in Ta-Nb Oxides: Implications for Deuteric Rare-Metal Mineralization in the Yichun Granite-Marginal pegmatite, Southeastern China. *Econ. Geol.* 113, 937–960. <https://doi.org/10.5382/econgeo.2018.4577>
- Wu, M., Samson, I.M., Zhang, D., 2017. Textural and chemical constraints on the formation of disseminated granite-hosted W-Ta-Nb mineralization at the Dajishan Deposit, Nanling Range, Southeastern China. *Econ. Geol.* 112, 855–887.
- Xie, L., Wang, R.-C., Che, X.-D., Huang, F.-F., Erdmann, S., Zhang, W.-L., 2016. Tracking magmatic and hydrothermal Nb-Ta-W-Sn fractionation using mineral textures and composition: A case study

- from the late Cretaceous Jiepailing ore district in the Nanling Range in South China. *Ore Geol. Rev.* 78, 300–321. <https://doi.org/10.1016/j.oregeorev.2016.04.003>
- Yamato, P., Duret, T., May, D.A., Tartèse, R., 2015. Quantifying magma segregation in dykes. *Tectonophysics* 660, 132–147. <https://doi.org/10.1016/j.tecto.2015.08.030>
- Zaraisky, G.P., Korzhinskaya, V., Kotova, N., 2010. Experimental studies of Ta<sub>2</sub>O<sub>5</sub> and columbite–tantalite solubility in fluoride solutions from 300 to 550°C and 50 to 100 MPa. *Mineral. Petrol.* 99, 287–300. <https://doi.org/10.1007/s00710-010-0112-z>
- Zasedatelev, A.M., 1977. Quantitative of metamorphic generation of rare-metal pegmatites with lithium mineralization. *Dokl. Acad. Sci. USSR, Earth Sci. Ser.* 236, 219–221.
- Zasedatelev, A.M., 1974. Possible accumulation of lithium in host rocks of lithium pegmatite veins during old sedimentation processes. *Dokl. Acad. Sci. USSR, Earth Sci. Ser.* 218, 196–198.
- Zhu, Z.-Y., Wang, R.-C., Che, X.-D., Zhu, J.-C., Wei, X.-L., Huang, X., 2015. Magmatic–hydrothermal rare-element mineralization in the Songshugang granite (northeastern Jiangxi, China): Insights from an electron-microprobe study of Nb–Ta–Zr minerals. *Ore Geol. Rev.* 65, Part 4, 749–760. <https://doi.org/10.1016/j.oregeorev.2014.07.02>

## Captions

**Fig. 1.** Tectonostratigraphic map of the Namaqua Sector of the Namaqua-Natal metamorphic province of southern Africa, modified after Macey et al. (2018), showing the locations of rare element pegmatites. Pegmatite typology after Hugo (1970) and Schutte (1972). SZ: shear zone.

**Fig. 2.** Summary of geologic events in the Namaqua Sector from 1900 to 950 Ma. The Aus region, Namibia (Diener et al. 2013), located at the north-western extremity of the Kakamas terrane, is not shown in Fig. 1. LFROT: Lower Fish-River Onseepkans Thrust Zone. Data sources: 1, Robb et al. (1999); 2, Clifford et al. (2004); 3, Cornell et al. (2009); 4, Lambert (2013); 5, Doggart (2019); 6, Macey et al. (2018) and references therein; 7, Macey et al. (2017); 8, Raith et al. (2003); 9, Cornell and Pettersson (2007a); 10, Bial et al. (2015b); 11, Cornell and Pettersson (2007b); 12, Diener et al. (2013); 13, Bial et al. (2015a); 14, Pettersson et al. (2007); 15, Bailie et al. (2017); 16, Bailie et al. (2011); 17, Bachmann et al. (2015); 18, Cornell et al. (1992); 19, Waters (1989); 20, Moen and Armstrong (2008); 21, Pettersson (2008); 22, Macey et al. (2015); 23, Van Niekerk (2006); 24, Van Schijndel et al. (in press); 25, Bailie et al. (2019); 26, Bial et al. (2016). greens.: greenschist facies, amp.: amphibolite facies, gran.: granulite facies, gr: granite, D.: deformation.

**Fig. 3.** Simplified geological map of the western part of the Orange River pegmatite belt (Macey et al., 2017) showing the different types of LCT pegmatites and indicating the locations of pegmatites sampled during this study. Pegmatite locations, typology and associated mineralization after Schutte (1972).

**Fig. 4.** Simplified geological map of the heterogeneous-Li-Ta-Be Kokerboomrand I pegmatite modified after Schutte (1972).

**Fig. 5.** Selected field photographs of mineralized LCT pegmatites. Contact zone of the Noumas I pegmatite showing the transition from the aplite border toward the wall zone. (b) skeletal beryl from the wall zone of the Noumas I pegmatite. (c) Garnet-mica-rich replacement body occurring in the wall zone, close to the contact with the intermediate zone, of the Noumas I pegmatite. (d) Li-mica greisen replacing spodumene from the intermediate zone of the Kokerboomrand I pegmatite. (e) Green spodumene (G Spd)-bearing wall zone of the Norabees I pegmatite. (f) Pink spodumene (P Spd)-bearing intermediate zone of the Norabees I pegmatite. Mineral abbreviations following Whitney and Evans (2010).

**Fig. 6.** Selected hand sample photographs of metasomatized pegmatites. (a) Intermediate zone of the Kokerboomrand I pegmatite with pink spodumene partially replaced by albite and purple Li-mica. The three minerals are crosscut by quartz. (b) Albitized intermediate zone of the Kokerboomrand I pegmatite where pink spodumene is partially replaced by albite (Mic: microlite). (c) Greisenized intermediate zone of the Kokerboomrand I pegmatite where white spodumene is partially replaced by green Li-mica and albite. (d) Greisen consisting of muscovite, garnet and albite that occurs at the contact between intermediate zone and quartz core of the Witkop pegmatite. Mineral abbreviations following Whitney and Evans (2010).

**Fig. 7.** Representative field and hand sample photographs of the metasomatized granodioritic country rocks of the mineralized pegmatites. (a-b-c) Greisenized rafts of country rock occurring in the Noumas I pegmatite. In (c), the white arrow indicates the direction of the contact with the pegmatite (Peg.). A 1 to 4 mm thick white zone consisting of apatite and Ta-Nb-rich rutile occurs at the transition between the Green greisen, consisting of Fe-muscovite and muscovite, and Black greisen, consisting of Fe-muscovite. (d) Partially albitized granodiorite occurring close to the contact with the Kokerboomrand I pegmatite. In the main text, this sample (KOK-17-12) is referred to as moderately metasomatized granodiorite. (e) Strongly

metasomatized granodiorite, consisting of Fe-biotite, siderophyllite (Sid), Fe-muscovite, albite and quartz, partially assimilated in the wall zone of the Kokerboomrand I pegmatite. (f) Tourmalinized and greisenized raft of metagranodiorite occurring in the wall zone of the Norabees I pegmatite. The foliation (S) is indicated. Mineral abbreviations follow Whitney and Evans (2010).

**Fig. 8.** Images showing the textural relationship between plagioclase, microcline, spodumene and mica in mineralized LCT pegmatites. (a) Photomicrograph [crossed polars (XPL)] of a relic of microcline inside lamellar albite (cleavelandite) in the wall zone of the Noumas I pegmatite. (b) XPL image of lamellar albite and Li-mica replacing pink spodumene in the intermediate zone of the Kokerboomrand I pegmatite. Albite is also corroded by Li-mica. (c) XPL image of spodumene partially replaced by lamellar albite in the albitized intermediate zone of the Kokerboomrand I pegmatite. Both minerals are also partially replaced by very fine-grained mica. (d) Backscattered electron (BSE) image of lamellar albite partially replaced by Li-mica in the greisenized intermediate zone of the Kokerboomrand I pegmatite. (e) XPL image of anhedral microcline partially replaced by lamellar albite and muscovite in the greisenized intermediate zone of the Witkop pegmatite. Mineral abbreviations from Whitney and Evans (2010).

**Fig. 9.** Composition of plagioclase from (a) weakly mineralized and Nb-Ta-Be pegmatites as well as (b-d) Li-Ta-Be-(Bi) mineralized pegmatites and associated granodioritic country rock in an orthoclase-anorthite-albite ternary diagram. The dominant shape of plagioclase (prismatic, sugary, lamellar - cleavelandite) is indicated.

**Fig. 10.** Composition of spodumene (Spd) from mineralized LCT pegmatites in an Al versus Fe diagram (apfu). The slope  $a = -1$  is indicated.

**Fig. 11.** Selected backscattered electron (BSE) images (a, b, c, e, g) and chemical maps of F and calculated  $\text{Li}_2\text{O}$  (d,f) of mica from LCT pegmatites and their country rocks. (a) Mica from the greisenized intermediate zone of the Witkop pegmatite. Dark muscovite cores are overgrown by light rims with a muscovite to Fe-muscovite composition. (b) Mica from the metasomatized granodioritic country rock (Black greisen) of the Noumas I pegmatite. A first generation of light colored and Li-rich Fe-muscovite (Fe-Ms1) with numerous inclusions of ilmenite is partially replaced by a second generation of dark colored and Ta-rich Fe-muscovite (Fe-Ms2). (c) Li-mica from the intermediate zone of the Kokerboomrand I pegmatite. A heterogeneous core, constituted by skeletal zones with a Li-muscovite to zinnwaldite composition (core 1) and zinnwaldite infill (core 2), is overgrown by two different rims of lepidolite. (d) Spodumene and albite partially replaced by Li-mica (Mica 1: Fe-muscovite – Li-Fe-muscovite - zinnwaldite) in the greisenized intermediate zone of the Kokerboomrand I pegmatite. Li-mica is locally replaced by muscovite (Mica 2: dark color). (e) Mica from the strongly metasomatized granodioritic country rock of the Kokerboomrand I pegmatite. Trioctahedral mica (Fe-biotite and siderophyllite-Sid) is partially replaced by dioctahedral mica (Fe-Ms). (f) Mica from the wall zone of the Norabees I pegmatite. A mica core with a muscovite to Li-Fe-muscovite composition is overgrown by zinnwaldite (rim 1). The rim of zinnwaldite is locally replaced or overgrown by Fe-muscovite (rim 2). (g) Li-mica from the intermediate zone of the Norabees I pegmatite. A heterogeneous core with a muscovite, Li-muscovite to zinnwaldite composition is overgrown by zinnwaldite and lepidolite. (h) Mica from the metasomatized granodioritic country rock of the Norabees I pegmatite. Fe-biotite is partially replaced by Fe-muscovite. Mineral abbreviations from Whitney and Evans (2010).

**Fig. 12.**  $\text{Fe}_{\text{tot}} + \text{Mn} + \text{Ti} - \text{Al}^{\text{VI}}$  versus  $\text{Mg} - \text{Li}$  (atom per formula unit) classification (Tischendorf et al., 1997, 2001) showing the composition of mica from the Orange River LCT pegmatites and associated granodioritic country rocks. The Li composition was measured by LA-ICP-MS or calculated using the F contents measured by EPMA and equations of Supplementary File 3, Figure S3.2. Other elements were measured by EPMA.

**Fig. 12.** (ctd.)

**Fig. 13.** Nb/Ta versus (a) Ta, (b) Nb, (c) Li<sub>2</sub>O and (d) Cs diagrams comparing the composition of large dioctahedral mica cores from homogeneous weakly mineralized pegmatites with that from aplite borders and wall zones of heterogeneous and strongly mineralized pegmatites.

**Fig. 14.** Nb/Ta versus Li<sub>2</sub>O, Cs and Ta diagrams for mica from the (a) Noumas I, (b) Kokerboomrand I, (c) Norabees I and (d) Witkop mineralized pegmatites and associated granodioritic country rocks. Metasom.: metasomatized.

**Fig. 14.** (ctd.)

**Fig. 15.** Selected BSE images of Nb-Ta and Bi oxide minerals from pegmatites and their country rocks (CGM: columbite group mineral; Mic: microlite; Bi ox: Bi oxide mineral). (a) Columbite-Fe from a weakly mineralized pegmatite of the area of Kokerboomrand. The rim of the crystal is replaced by spongy zero-valence-dominant pyrochlore. (b) Homogeneous columbite-Mn from the wall zone of the Noumas I pegmatite partially replaced by spongy calciomicrolite along a crack. (c) Normally zoned columbite-Fe from the aplite border of the Li-Ta-Be-Bi Noumas I pegmatite, with increase of Ta content from core (medium grey) to rim (light grey), replaced along the rim by spongy zero-valence-dominant PGM (dark grey). (d) Oscillatory zoned columbite-tantalite-Mn from the wall zone of the Noumas I pegmatite. (e) complex columbite group mineral from the wall zone of the Noumas I pegmatite. The white zones (tantalite-Mn to tapiolite) are enriched in Ta compared to grey zones (tantalite-Mn). (f) Native Bi rimmed by Bi oxide minerals in a garnet-mica-rich replacement body of the Noumas I pegmatite. (g) Ta-(Nb-) rutile from the metasomatized granodioritic country rock of the Noumas I pegmatite. The Ta (and Nb)

content of the rutile increases significantly from core to rim. (h) Ta-Nb-rutile from the aplite border of the Li-Ta-Be Kokerboomrand I pegmatite. Along the bottom left edge, rutile 1 (medium grey) is replaced by rutile 2 (dark grey) and fluorcalciomicrolite (white). (i) Fluorcalciomicrolite from the greisenized intermediate zone of the Kokerboomrand I pegmatite. The crystal is corroded by Li-mica and brecciated by Bi oxide minerals (white phase) that also occur in the cleavage planes of Li-mica. (j) Columbite-Mn (light and dark grey zones) from the wall zone of the Li-Ta-Be Norabees I pegmatite partially replaced by calciomicrolite (white zone). A reaction zone depleted in Ta and enriched in Nb (CGM 2, dark grey) occurs at the contact between primary columbite-Mn (CGM1, light grey) and calciomicrolite. (k) Calciomicrolite from the wall zone of the Norabees I pegmatite with inclusions of resorbed columbite-Mn and albite. (l) (Fluor)calciomicrolite from the intermediate zone of the Norabees I pegmatite. Alteration along the rims (dark color and strong spongy texture) is associated with an increase of the A-site vacancy and a decrease of the F content.

**Fig. 16.** Chemical composition of Nb-Ta oxide minerals from LCT pegmatites and metasomatized granodioritic country rocks. (a) Ta / (Ta + Nb) versus Mn / (Mn + Fe) diagram (apfu) showing the composition of columbite group minerals. The dashed lines join the analyses made on one crystal containing tapiolite (Fig. 15e). The tantalite-tapiolite miscibility gap is from Van Lichtervelde et al. (2018). (b) Ta / (Ta + Nb) versus A-site vacancy diagram (apfu) for pyrochlore group minerals. (c) Ti-Nb-Ta ternary diagram (apfu) showing the composition of Nb-Ta-rutile. The texture of CGM (simply or complexly zoned) and PGM (homogeneous or spongy) is indicated. Simply zoned CGM included crystals with homogeneous textures as well as normal, inverse and oscillatory zoning.

**Fig. 17.** Log-log isocon diagram (Grant, 1986; Baumgartner and Olsen, 1995) evaluating the chemical change during metasomatism of the granodiorite country rock of the Noumas I (a-b), Norabees I (c) and Kokerboomrand I (d) pegmatites. In (a-b) the Green greisen (b) is located just at the contact with the

pegmatites whereas the Black greisen (a) is located ~20-30 cm away from the contact. In (d), the average composition of weakly metasomatized granodioritic country rocks from the Noumas I and Norabees I pegmatites is used as an initial composition due to poor outcropping conditions near the Kokerboomrand I pegmatite. Major elements are plotted in wt.% and trace elements in ppm. The grey dashed line ( $C=C_0$ ) represents the zero-mass-change isocon and the black isocon is based on constant alumina.

**Fig. 18.** Isotopic data on monazite and zircon from mineralized LCT pegmatites. (a) Tera-Wasserburg diagram for monazite from the aplite border of the Kokerboomrand I pegmatite (KOK-17-8). Ellipses shown with dashed outlines represent common Pb affected analyses that were not used for the calculation of the concordia age ( $2\sigma$ ). Error ellipses are reported at  $2\sigma$ . (b) Histogram and kernel density estimates for  $^{207}\text{Pb}/^{206}\text{Pb}$  ages of inherited zircon crystals (discordance < 5%) from the aplite borders and wall zones of Kokerboomrand I, Norabees I and Noumas I mineralized LCT pegmatites. (c) initial  $\epsilon\text{Nd}(t)$  versus age diagram reporting the average composition ( $2\sigma$ ) of monazite from the aplite border of the Kokerboomrand I pegmatite (KOK-17-8) calculated at 986 Ma. The average monazite Nd isotopic composition of other LCT pegmatites emplaced in the Richtersveld magmatic arc (Doggart, 2019) is indicated for comparison along with whole-rock Nd isotopic compositions of igneous rocks from the Richtersveld magmatic arc (Reid, 1997; Macey et al., 2017) as well as granitoids (Clifford et al., 1995; Geringer et al., 1998; Pettersson et al., 2009) and sedimentary rocks (Bailie et al., 2007a) from the northern part of Bushmanland Subprovince. The  $^{147}\text{Sm}/^{144}\text{Nd}$  value of 0.09 corresponds to the average value of monazite from the sample KOK-17-8. Present day  $^{147}\text{Sm}/^{144}\text{Nd}$  and  $^{143}\text{Nd}/^{144}\text{Nd}$  values of 0.2135 and 0.513151, respectively, were used for Depleted Mantle (Blichert-Toft and Puchtel, 2010). Present day  $^{147}\text{Sm}/^{144}\text{Nd}$  and  $^{143}\text{Nd}/^{144}\text{Nd}$  values of 0.196 and 0.51263, respectively, were used for CHUR (Bouvier et al., 2008).

**Fig. 19.** Paragenetic sequence for LCT pegmatites and metasomatized granodioritic country-rocks. CGM: columbite group mineral. Li-mica includes Li- (Fe-) muscovite, zinnwaldite and lepidolite.

**Fig. 20.** Schematic illustration of the magmatic-hydrothermal evolution of mineralized LCT pegmatites from the Orange River belt. (a) Stage I represents the magmatic-dominated crystallization of the pegmatite for border to core. Fractional crystallization and migration of a boundary layer liquid is suggested by the increase of Ta\* values of columbite group mineral (CGM) from the aplite border to wall zone as well as decrease of Fe contents of spodumene getting closer to the core. (b) stage II marks the immiscibility between a highly viscous silicic melt and low viscosity hydrosaline melt along with additional melt-fluid immiscibility. The alkaline aqueous media induced the pervasive albitization of the pegmatite and its country rock, crystallization of (fluor)calciomicrocline and Li-mica (i.e. Li-Ms and Znw) in the pegmatite and replacement of Mg-biotite by Fe-biotite in the granodiorite. (c) A silicic melt, alkaline hydrosaline melt and mainly acidic aqueous fluid were coexisting during stage III.1 that is expressed by crystallization of lepidolite in the pegmatite and localized greisenization of both the pegmatite and granodiorite. Greisenization of the pegmatite might have been triggered by a decrease of pH during albitization while plagioclase breakdown during greisenization of the granodiorite potentially led to albitization elsewhere in the country rock (albitite II). (d) During stage III.2, a late hydrothermal fluid induced the formation of Bi-mineralization, crystallization of (Fe-) muscovite as well as alteration of CGM and (fluor)calciomicrocline to zero-valence-dominant pyrochlore. Greisenization perdured in the granodiorite where a significant amount of Ta was transferred from the pegmatite.

**Fig. 21.** Comparison of the chemical composition of columbite group minerals (CGM), pyrochlore group minerals (PGM) and Nb-Ta-rutile in a Nb/Ta versus Ta<sub>2</sub>O<sub>5</sub> (wt.%) diagram.

**Fig. 22.** Nb/Ta versus (a) Ta, (b) Nb, (c) Li<sub>2</sub>O and (d) Cs diagrams comparing the composition of mica characteristic of the different evolutionary stages of the pegmatites as well as metasomatic mica from the metasomatized country rocks.

**Fig. 23.** Nb/Ta versus (a) Ta, (b) Nb, (c) Li and (d) Cs content diagrams showing the whole-rock composition of strongly metasomatized granodioritic country rocks of the LCT pegmatites from the western part of Orange River belt as well as less, moderately and non-metasomatized equivalents (Gaarseep granodiorite). The composition of highly peraluminous granites (Ballouard et al., 2016a), the Tanco LCT pegmatite (Stilling et al., 2006) and the upper continental crust (Rudnick and Gao, 2003) is shown for comparison. The composition of the unaltered Gaarseep granodiorite (Violsdrif Suite) is from Macey et al. (2017).

**Table 1.** Summary of the main replacement reactions related to greisenization and albitization as observed in the Orange River pegmatite belt, southern Africa.

**Table 2.** Li, Nb, Ta and Cs compositions of the main potential sources for LCT pegmatites of the western part of the Orange River belt, including igneous rocks from the Richtersveld magmatic arc (Violsdrif Suite and Orange River Group, Macey et al. 2017 and reference therein) as well as sedimentary rocks (Bushmanland Group, Bailie et al., 2007) and granitoids (Little Namaqualand Suite, Spektakel Suite, Concordia granite, Raith, 1995; Andreoli et al., 2006; Bailie et al., 2007b; Duchesne et al., 2007; Macey et al., 2018) from the Bushmanland Subprovince compared to the mean upper crust (Rudnick and Gao, 2003). The Gaarseep granodiorite belongs to the Violsdrif Suite and represents the main country rock of studied LCT pegmatites.

#### **Declaration of interests**

The authors declare that they have no known competing financial interests or personal relationships that could have appeared to influence the work reported in this paper.

The authors declare the following financial interests/personal relationships which may be considered as potential competing interests:

## Highlights

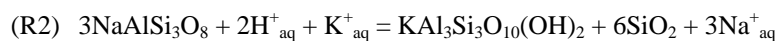
- Orange River LCT pegmatites formed at 1 Ga during regional strike-slip tectonics
- Pegmatites formed by melting of Richtersveld magmatic arc or Bushmanland sediments
- Spodumene and coltan are magmatic. Lepidolite and microlite are metasomatic
- Metasomatism led to strong Ta enrichment and low Nb/Ta in country rocks
- Magmatic-hydrothermal processes are crucial for rare metal deposit formation

## Greisenization

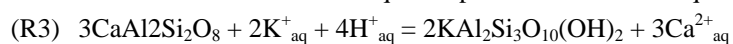
---



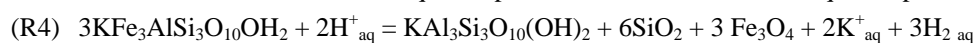
K-feldspar + acidic aqueous phase = muscovite + quartz + K-rich aqueous phase



Albite + acidic and K-rich aqueous phase = muscovite + quartz + Na-rich aqueous phase



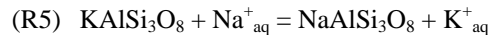
Anorthite + acidic and K-rich aqueous phase = muscovite + Ca-rich aqueous phase



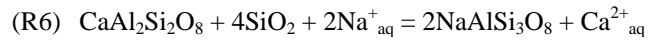
Biotite + acidic aqueous phase = muscovite + quartz + Fe oxide mineral + K-rich aqueous phase

**Albitization**

	Li (ppm)				Nb (ppm)				Ta (ppm)				Cs (ppm)			
	Min	Max	Average	n	Min	Max	Average	n	Min	Max	Average	n	Min	Max	Average	n
<b>Richterveld arc</b>																
Vioolsdrif Suite	1	71	22	55	0.7	44.0	10.5	308	0.1	5.4	1.0	55	0.1	5.4	8.4	61
<i>Gaarseep granodiorite</i>	19	41	27	5	2.2	44.0	11.2	86	0.8	1.4	1.2	5	5.2	13.0	7.7	20
Orange River Group	6	43	20	17	2.6	98.0	11.6	288	0.5	1.8	1.0	24	0.5	1.8	9.9	9
<b>Bushmanland Subprovince</b>																
Bushmanland Group					1.8	40.0	15.7	35								
Little Namaqualand Suite					6.0	24.0	16.8	34	0.5	1.1	0.8	2				
Concordia granite					4.0	27	11.2	15	0.5	0.9	0.7	4	1.2	2.7	2.0	4
Spektakel Suite					5.0	95.9	25.7	8	0.3	3.9	1.7	9	0.7	3.9	2.4	7
<b>Upper crust</b>			<b>24</b>				<b>12</b>				<b>0.9</b>				<b>4.9</b>	

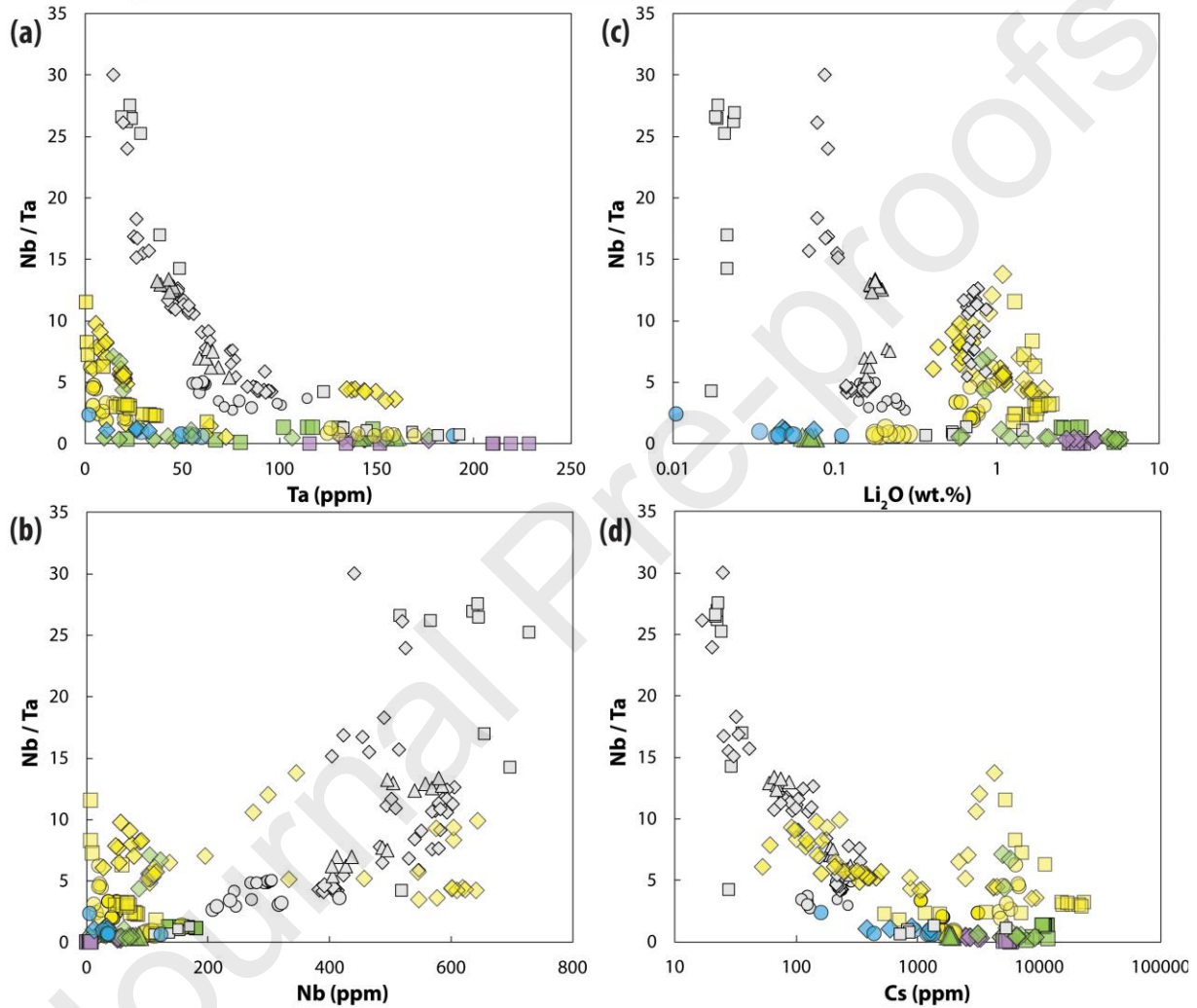
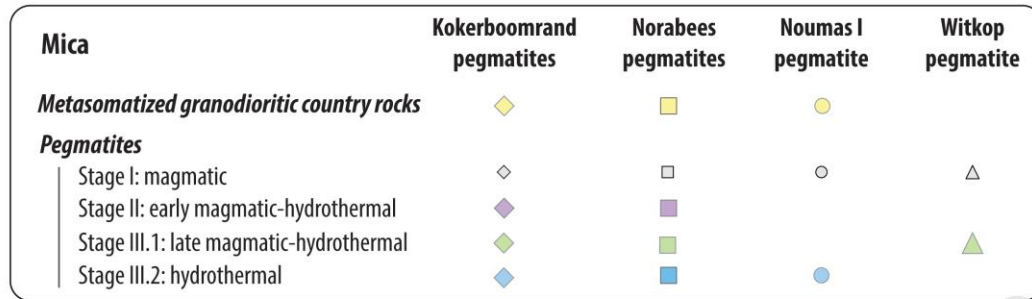


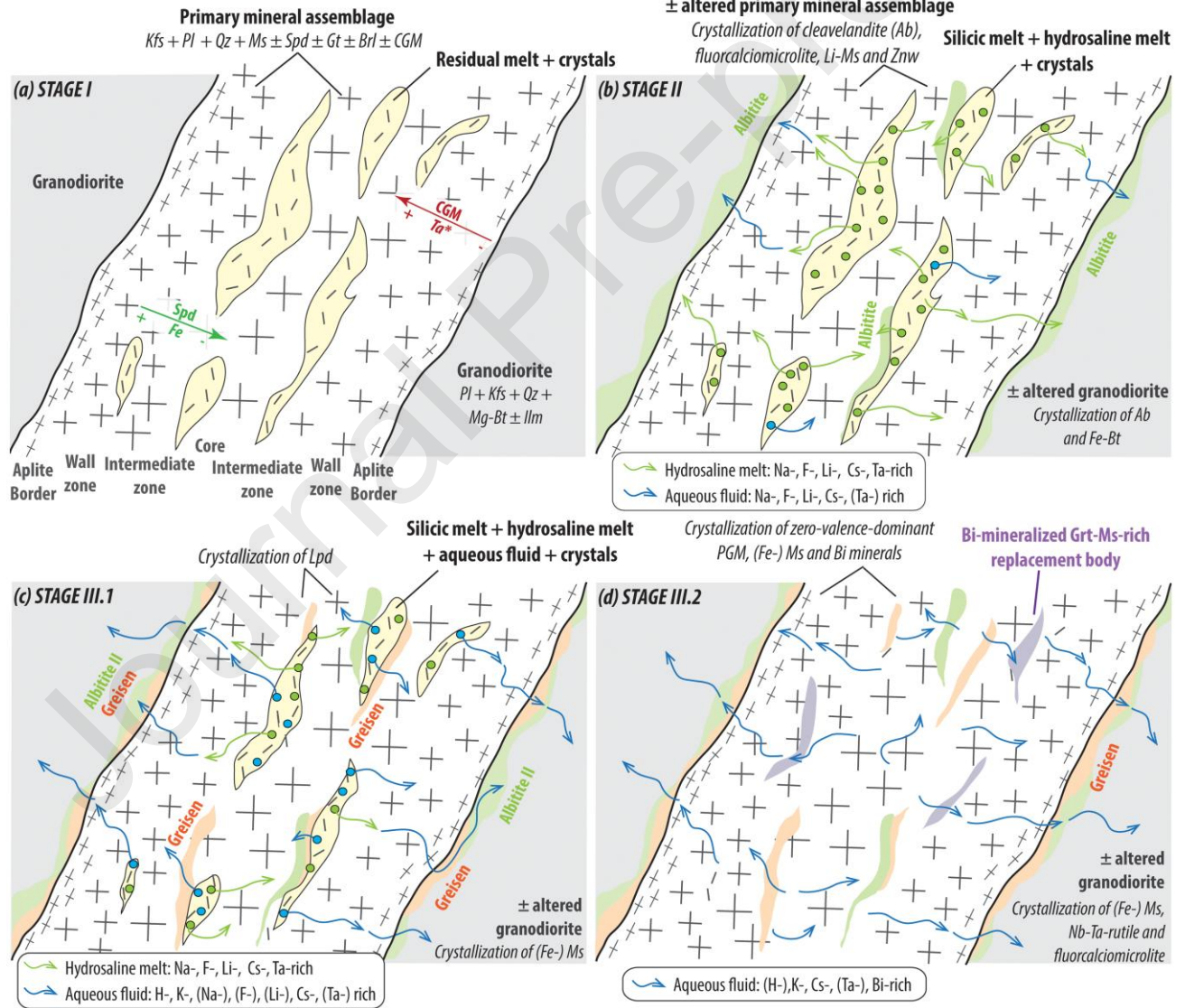
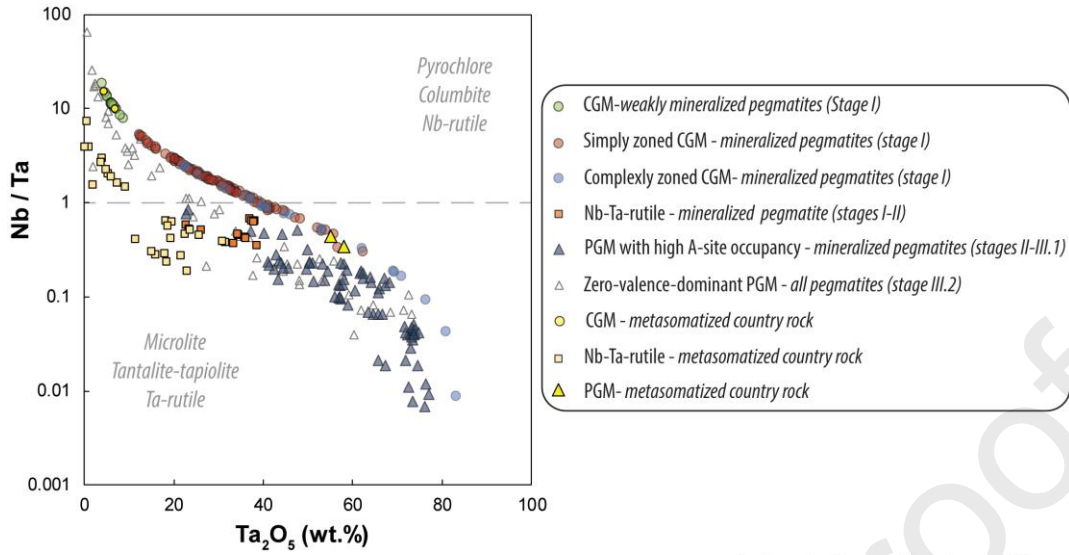
K-feldspar + Na-rich aqueous phase = albite + K-rich aqueous phase



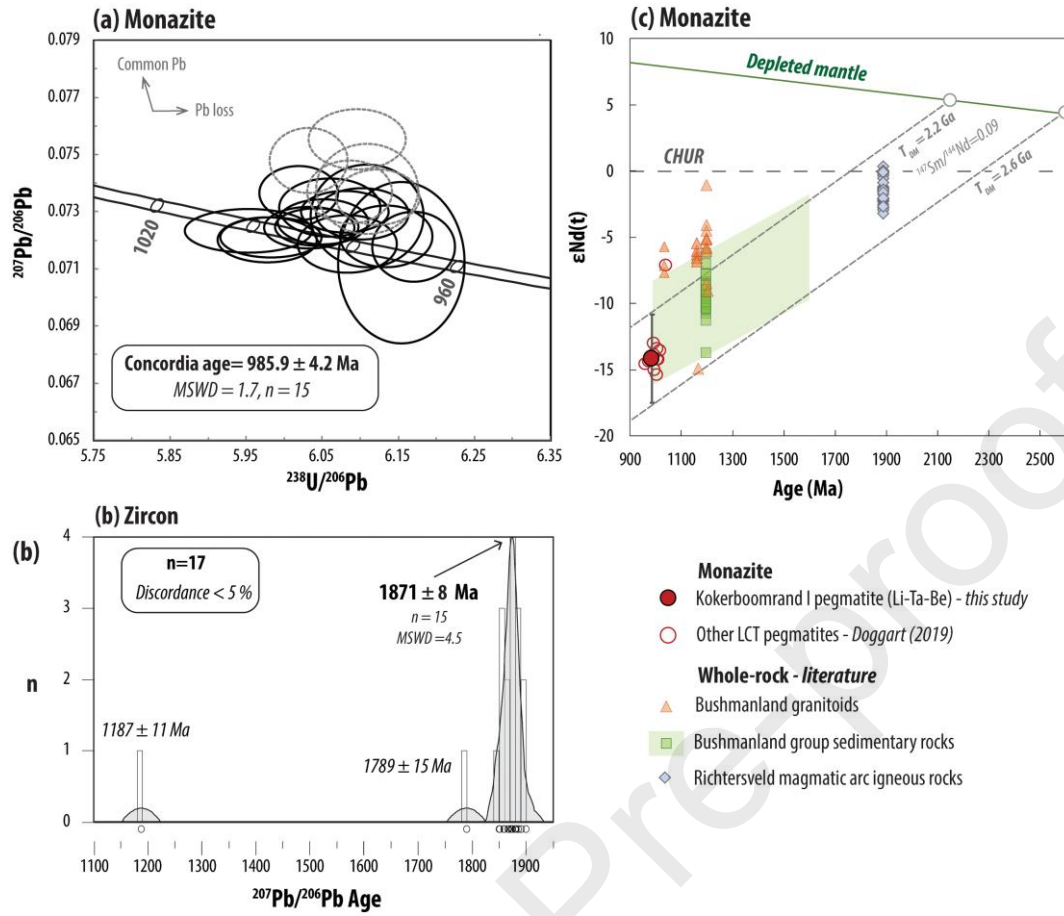
Anorthite + quartz + Na-rich aqueous phase = albite + Ca-rich aqueous phase

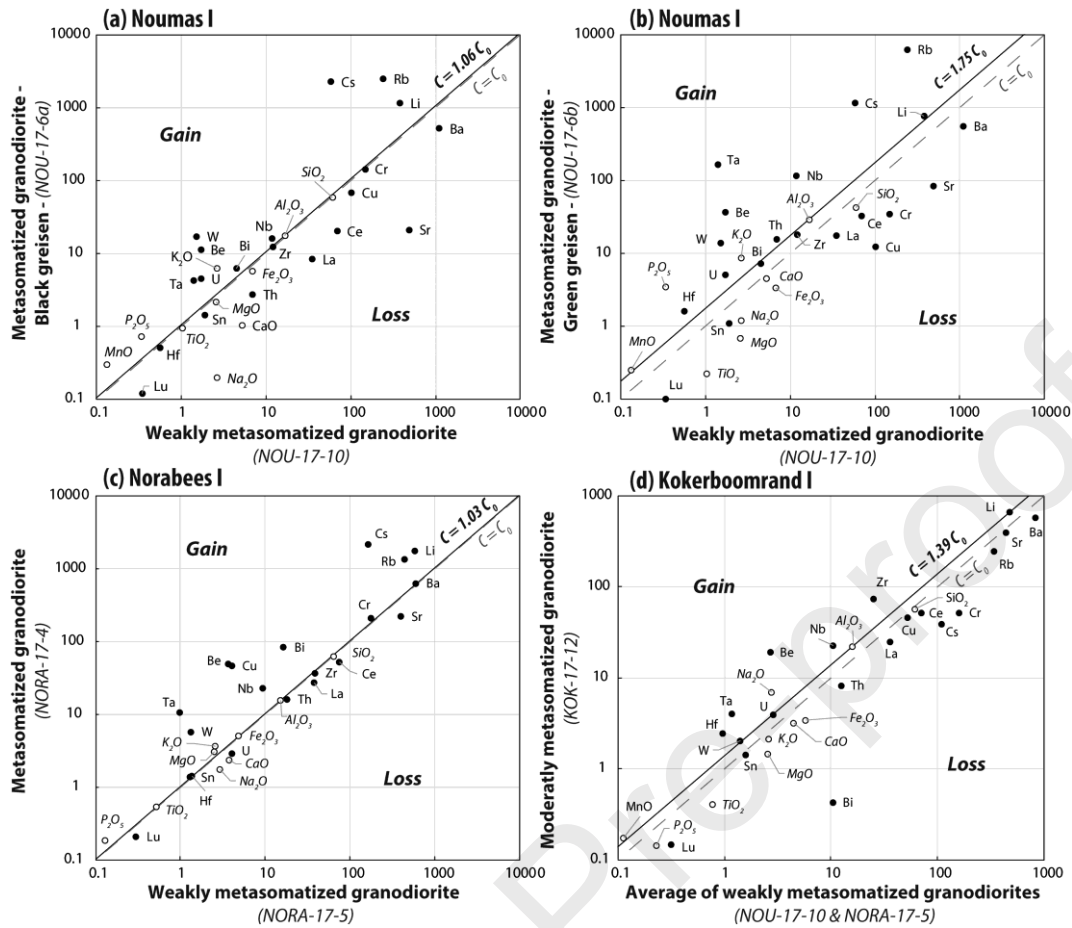
*aq*: aqueous

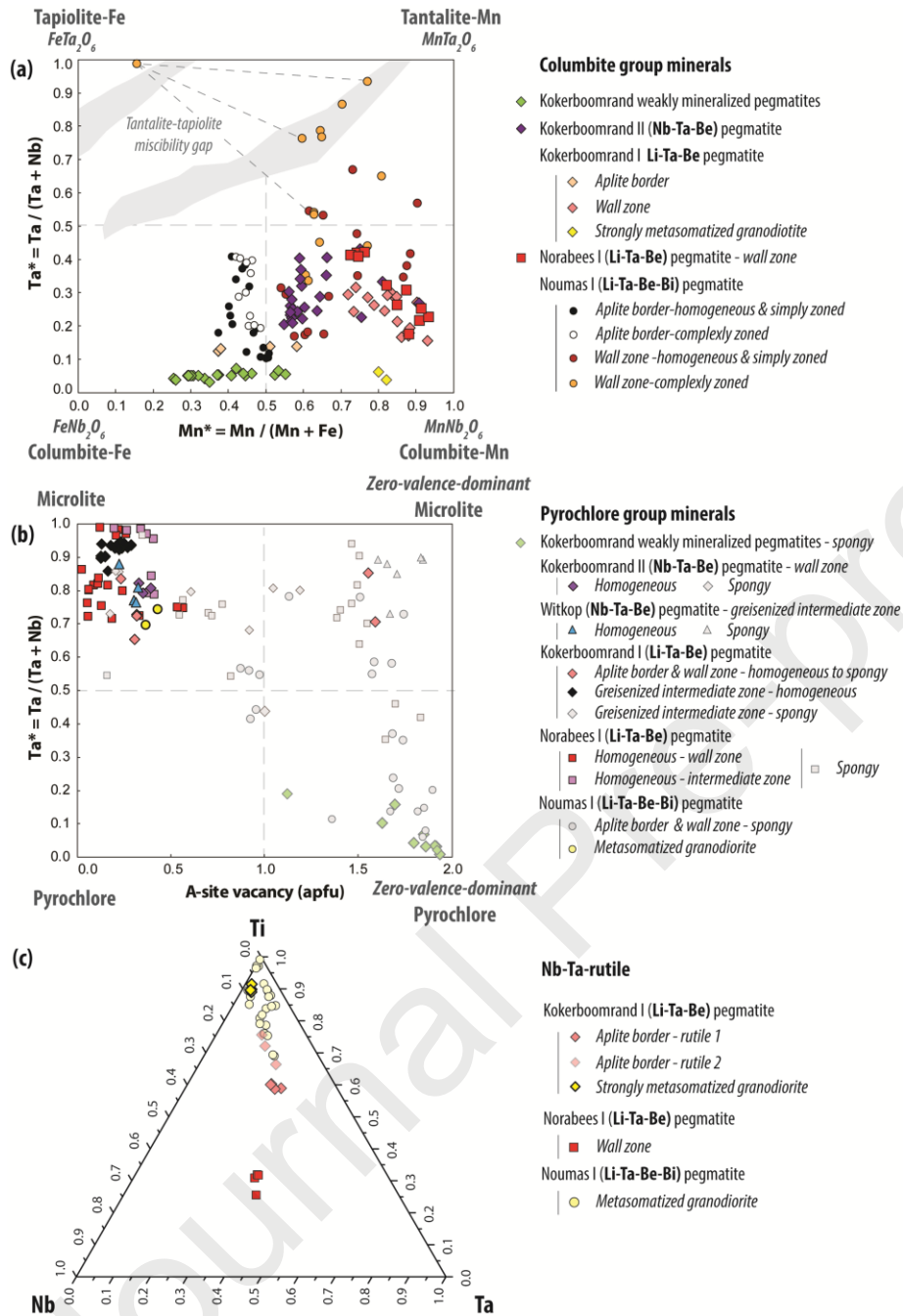


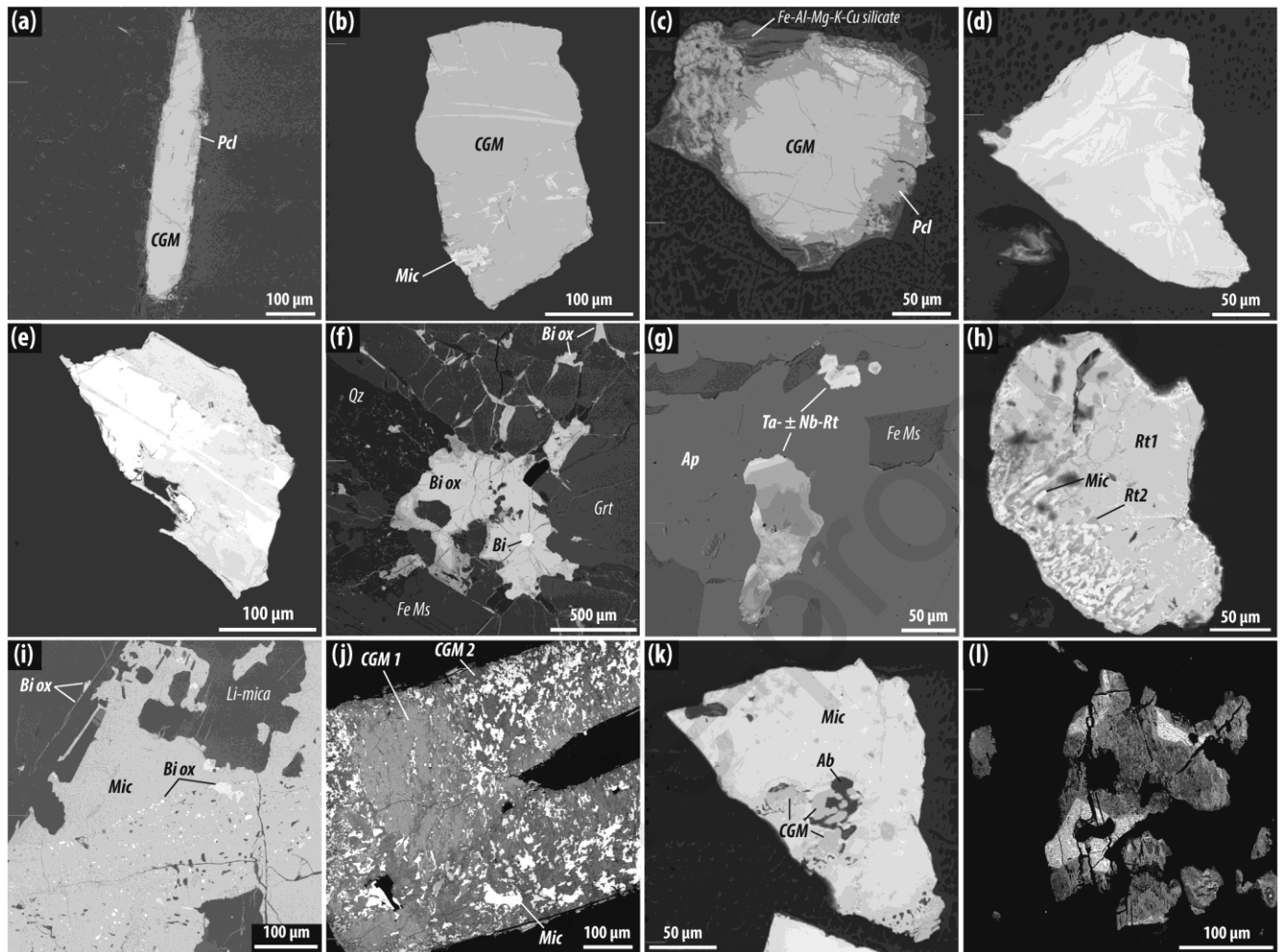


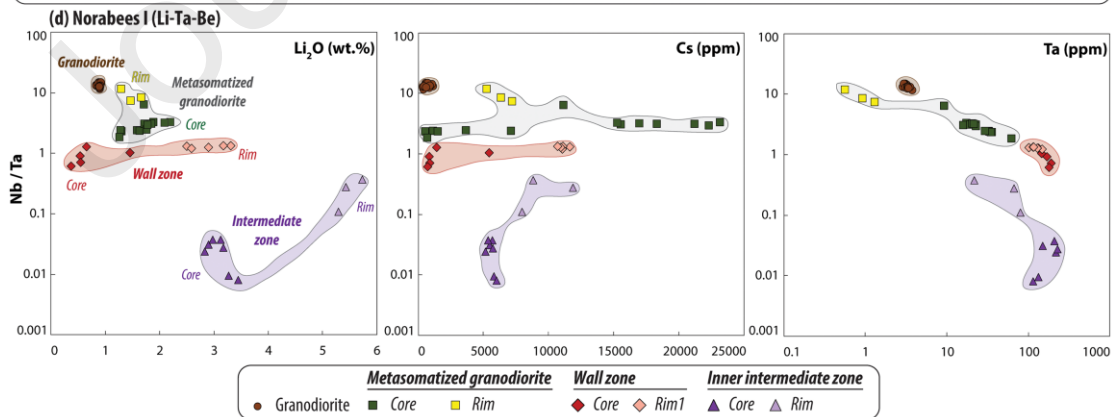
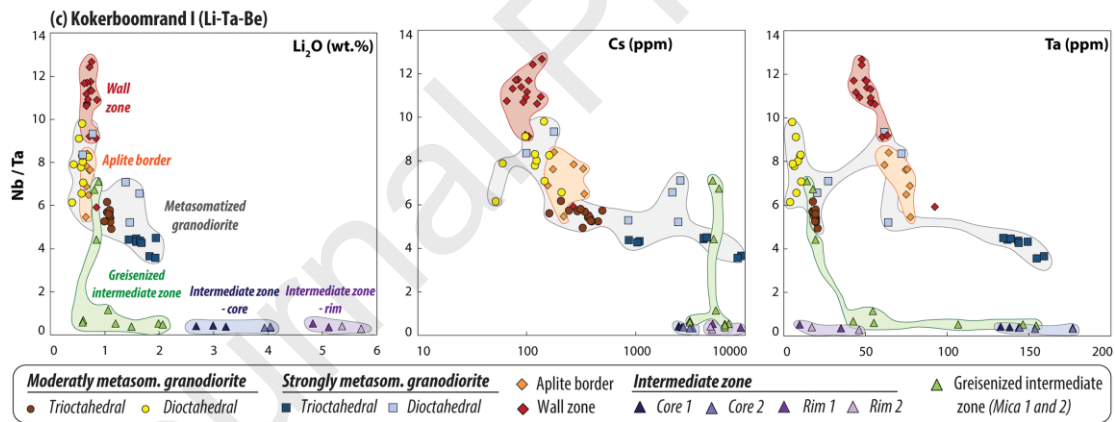
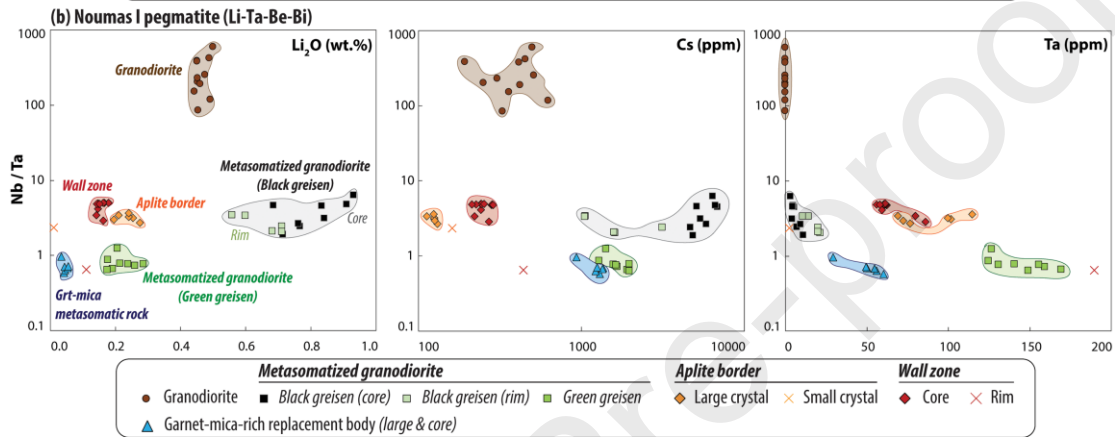
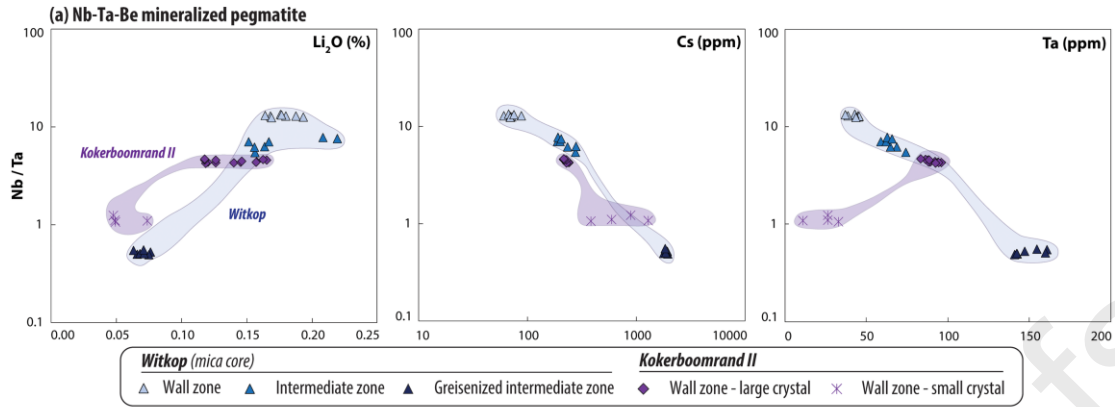
	Mineral	Magmatic	Magmatic-hydrothermal		Hydrothermal
		Stage I (985 Ma)	Stage II (985 Ma)	Stage III.1 (985 Ma)	Stage III.2 (985 Ma)
<b>Pegmatite</b>	Quartz	-----	-----	-----	-----
	K-feldspar	-----	Lamellar - cleavelandite	-----	-----
	Plagioclase	Ab > 0.85	Ab > 0.95	-----	-----
	(Fe-) muscovite	-----	Li-Cs-Ta-rich	Li-Cs-(Ta)-rich	Cs-rich
	Li-mica	-----	Li-Cs-Ta-rich	Li-Cs-rich	-----
	Spodumene	-----	-----	-----	-----
	Garnet (Sps)	-----	-----	-----	-----
	Beryl	-----	-----	-----	-----
	Tourmaline	-----	-----	-----	-----
	Apatite	-----	-----	-----	-----
	Zircon	-----	-----	-----	-----
	Monazite	-----	-----	-----	-----
	CGM	-----	-----	-----	-----
	Nb-Ta rutile	-----	-----	-----	-----
	Pyrochlore	-----	-----	-----	Zero-valence-dominant
	Microlite	-----	(Fluor)calcio	-----	-----
	Native Bi / Bi oxide	-----	-----	-----	-----
	Mn oxide	-----	-----	-----	-----
	Fluorite	-----	-----	-----	-----
	Pollucite	-----	-----	-----	-----
	Torbernite	-----	-----	-----	-----
	Pb gummite	-----	-----	-----	-----
	Barite	-----	-----	-----	-----
<b>Metasomatized granodiorite</b>	Quartz	Stage 0 (1870 Ma)	Stage A (985 Ma)	Stage B.1 (985 Ma)	Stage B.2 (985 Ma)
	Plagioclase	Andesine	Ab	Ab	-----
	K feldspar	-----	-----	-----	-----
	Mg-Biotite (Bt)	-----	-----	-----	-----
	Fe-Bt + Siderophyllite	-----	Li-Cs-Ta-rich	-----	-----
	(Fe-) muscovite	-----	-----	Li-Cs-(Ta)-rich	Cs-Ta-rich
	Tourmaline	-----	-----	-----	-----
	Garnet (Sps)	-----	-----	-----	-----
	Epidote	-----	-----	-----	-----
	Titanite	-----	-----	-----	-----
	Apatite	-----	-----	-----	-----
	Zircon	-----	-----	-----	-----
	Monazite	-----	-----	-----	-----
	Ilm-Mag	-----	-----	-----	-----
	Nb-Ta-rutile	-----	-----	-----	-----
	CGM	-----	-----	-----	-----
	Microlite	-----	-----	-----	-----
	Pyrochlore	-----	-----	-----	-----
	Fluorite	-----	-----	-----	-----
	Bi oxide	-----	-----	-----	-----
(Ba-rich) Mn oxide	-----	-----	-----	-----	

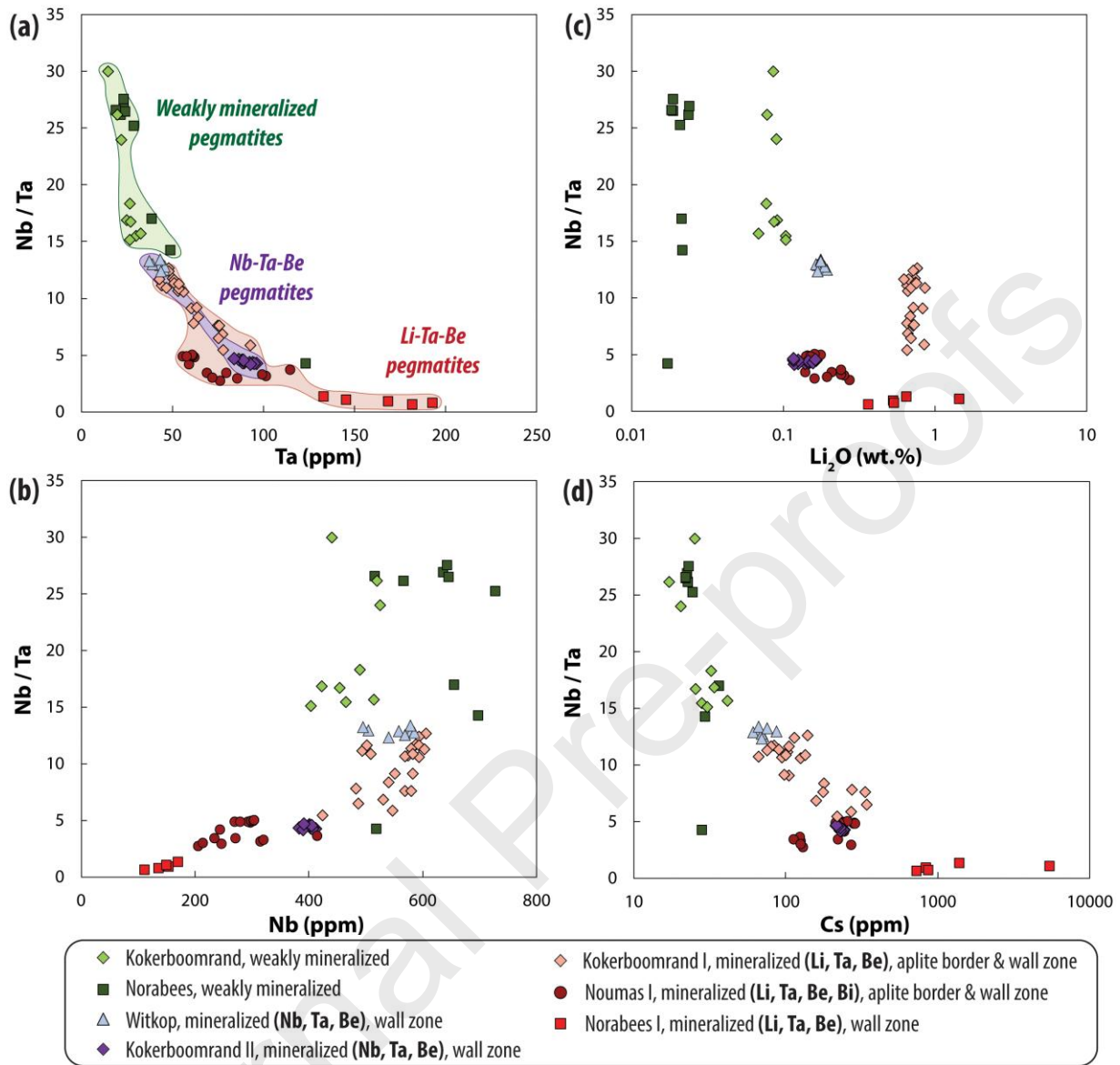


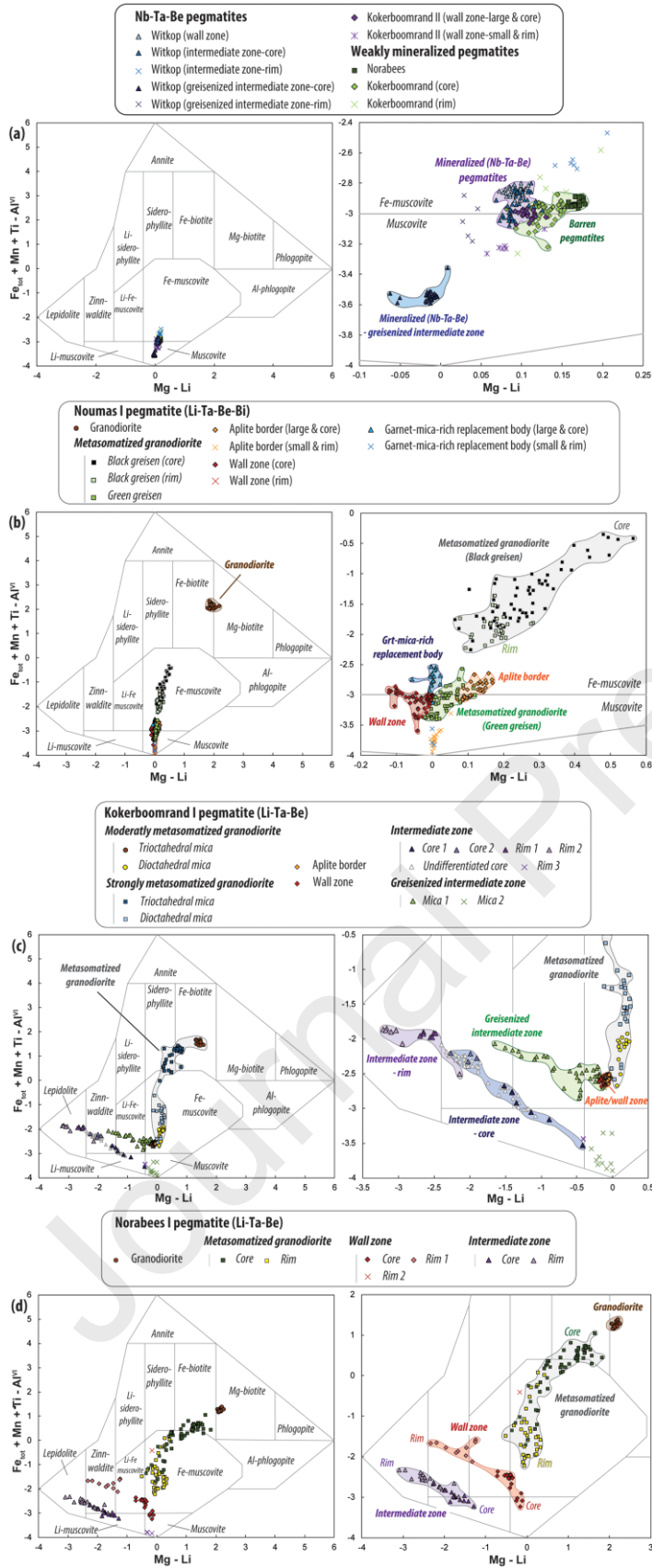


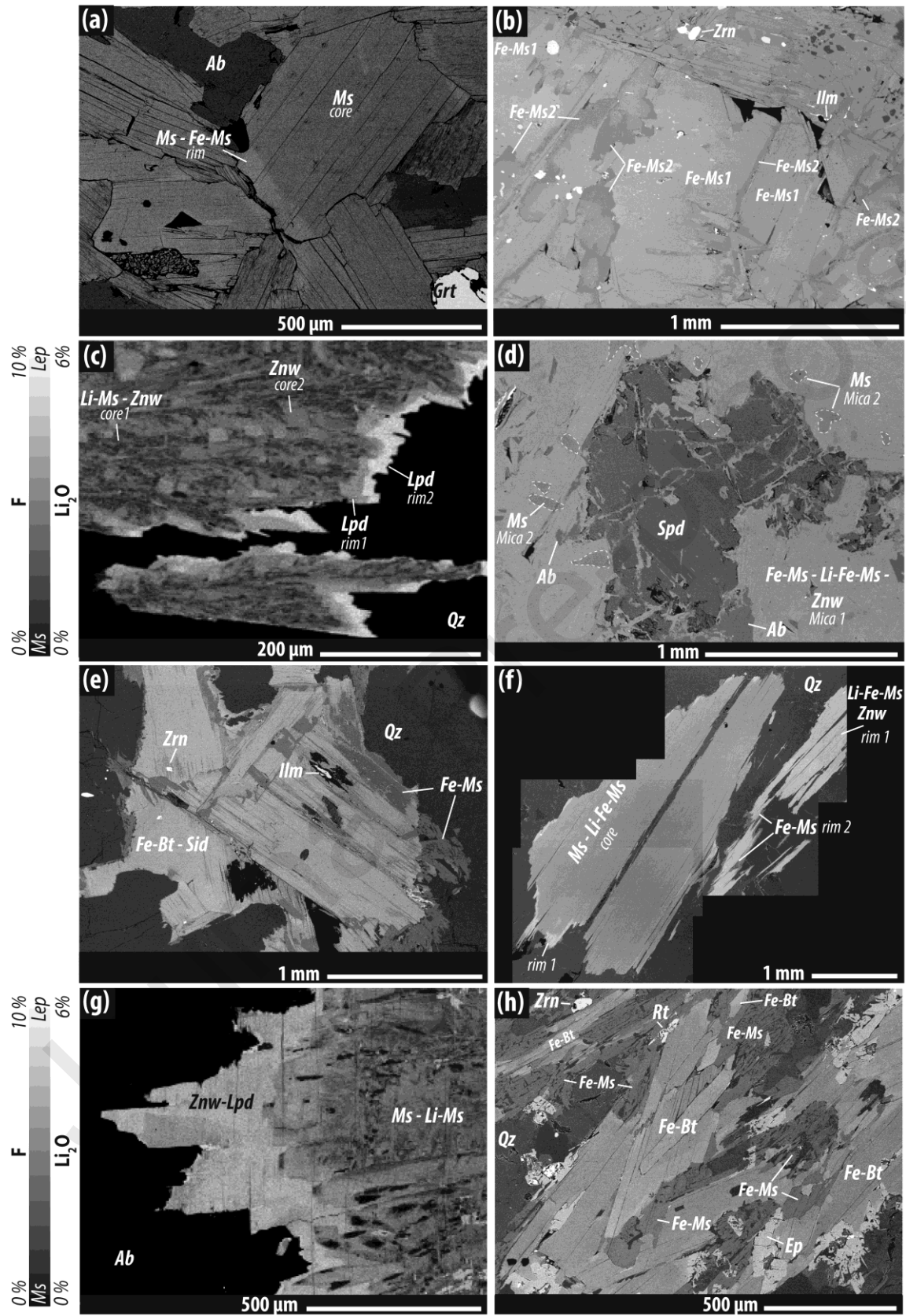


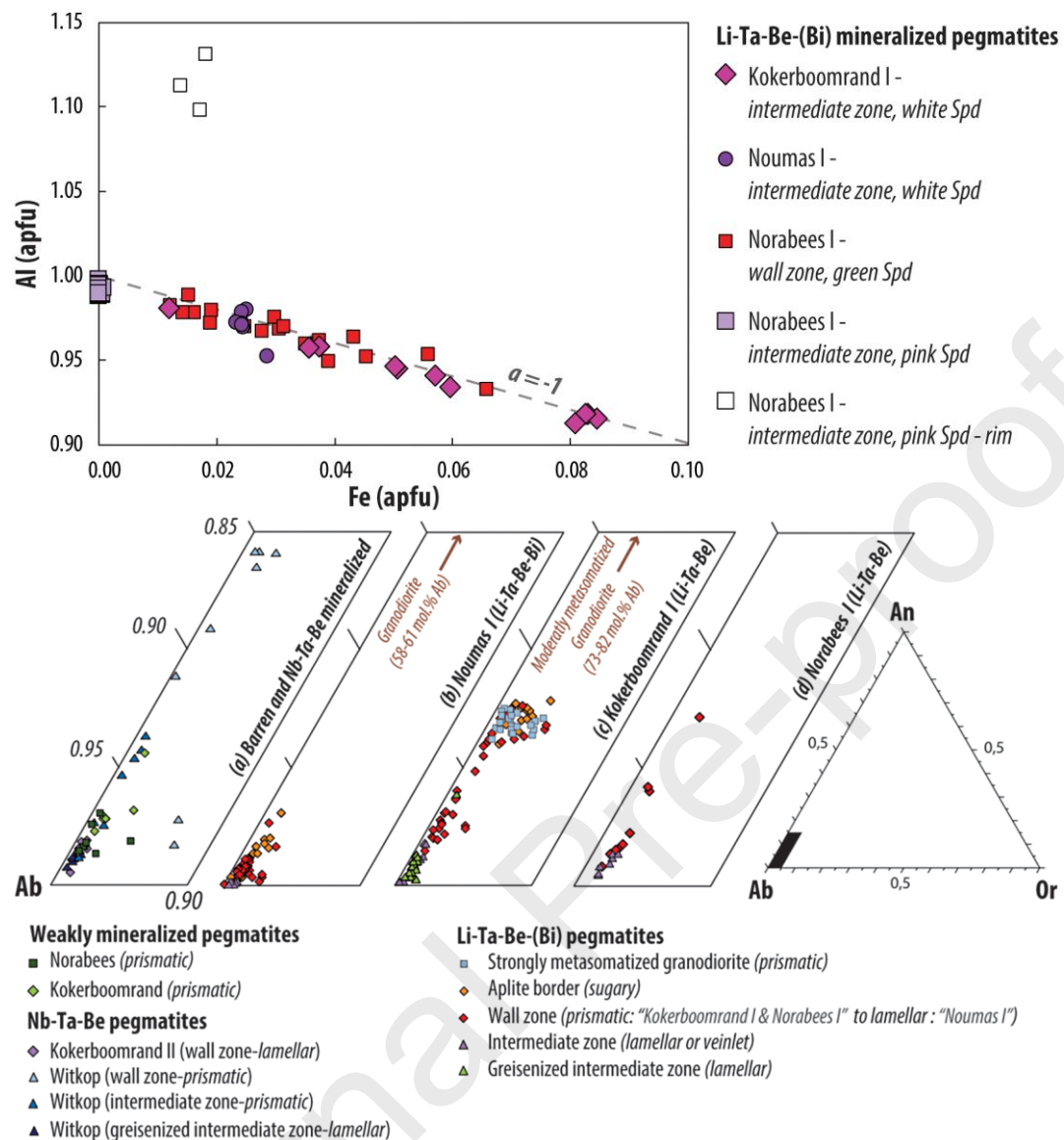


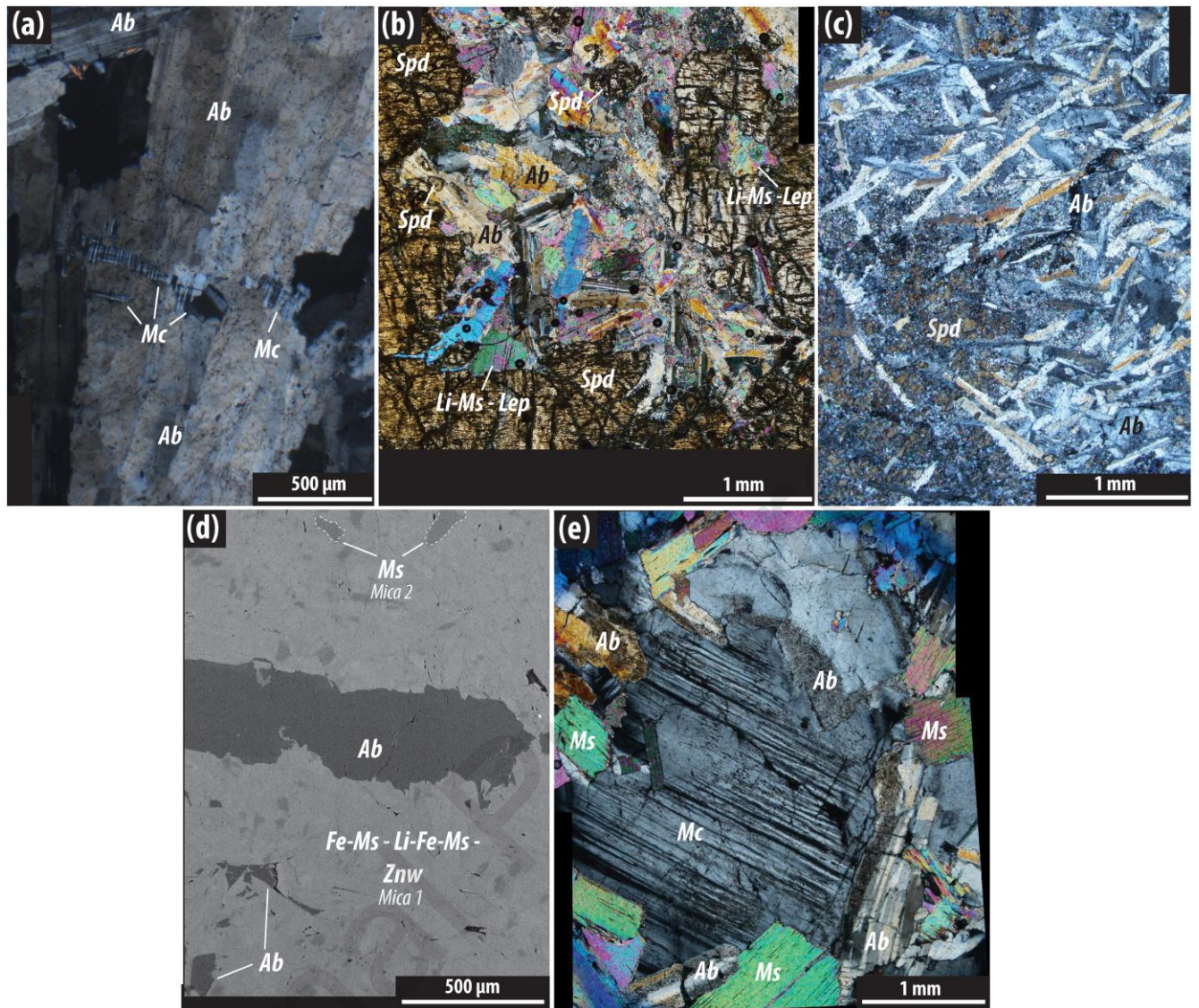


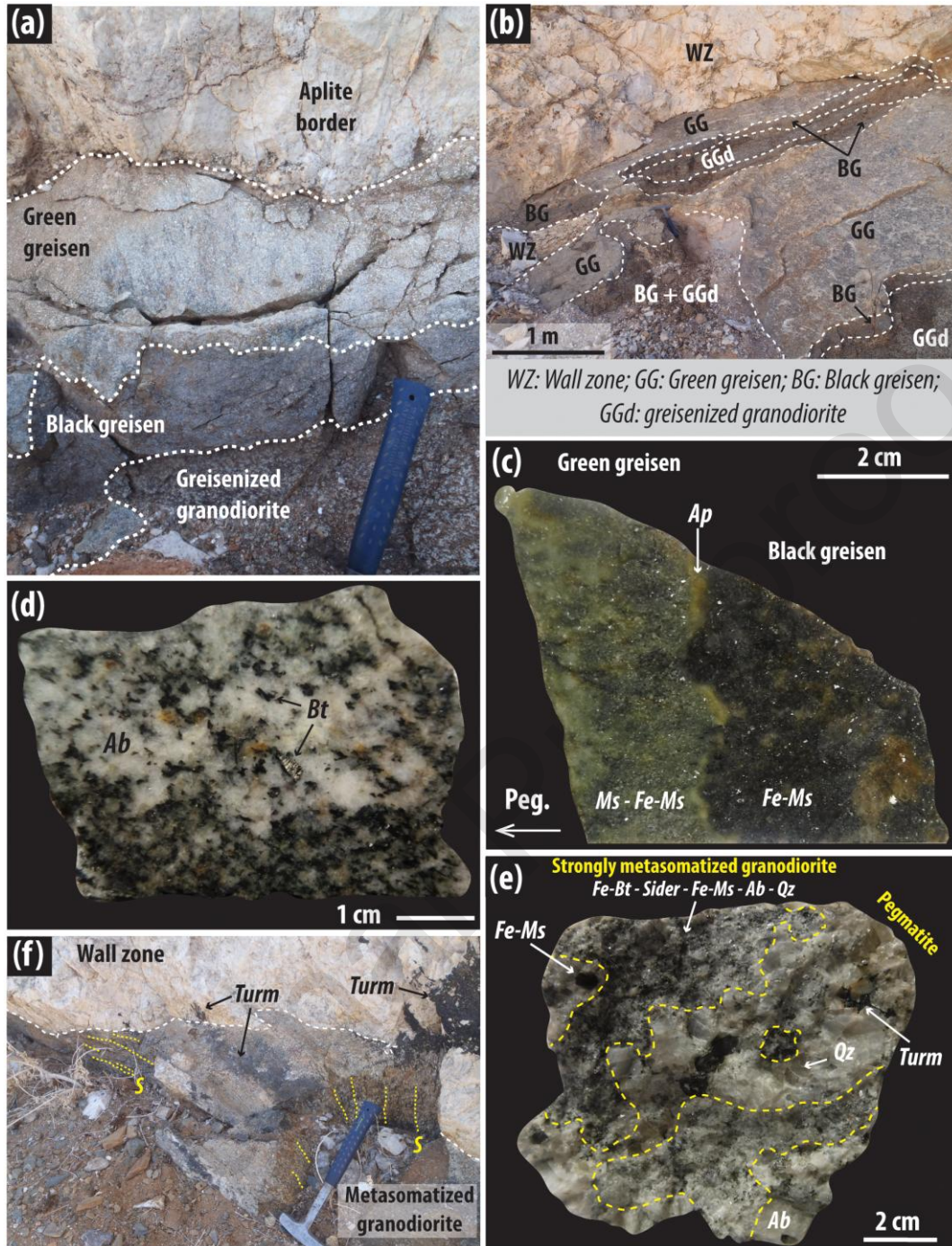


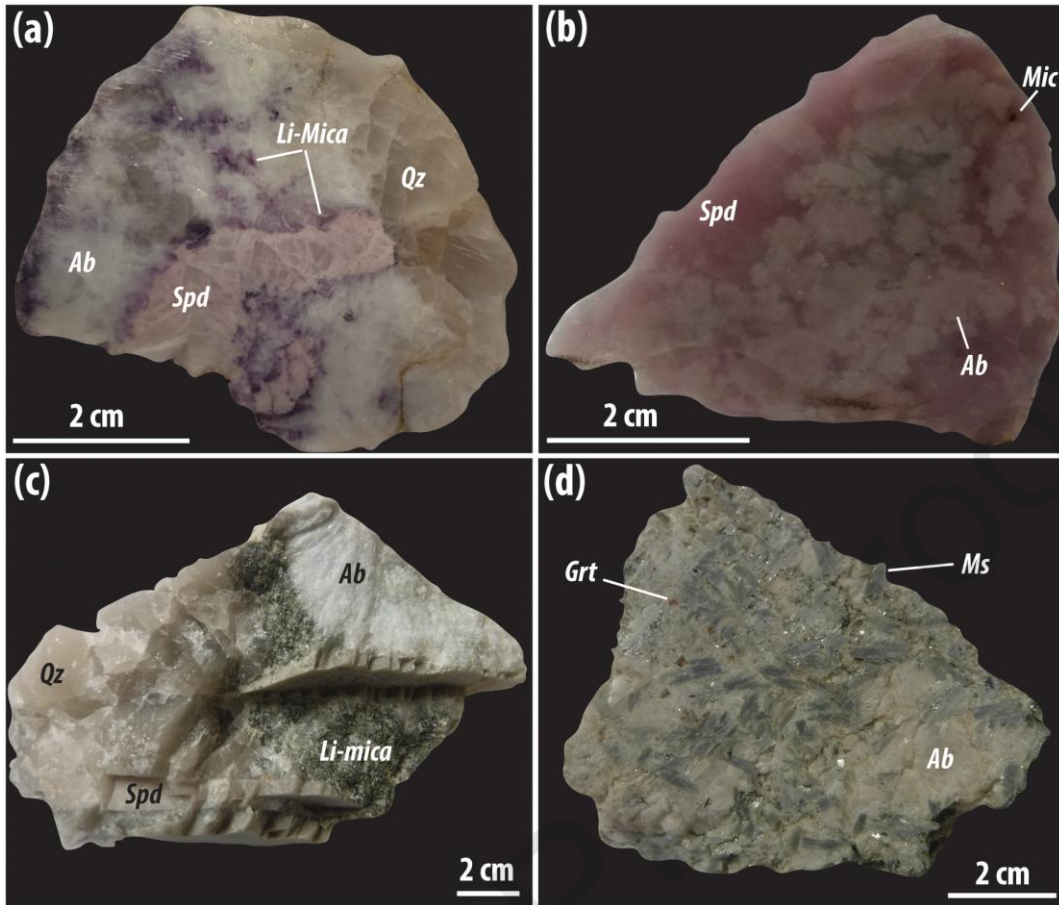


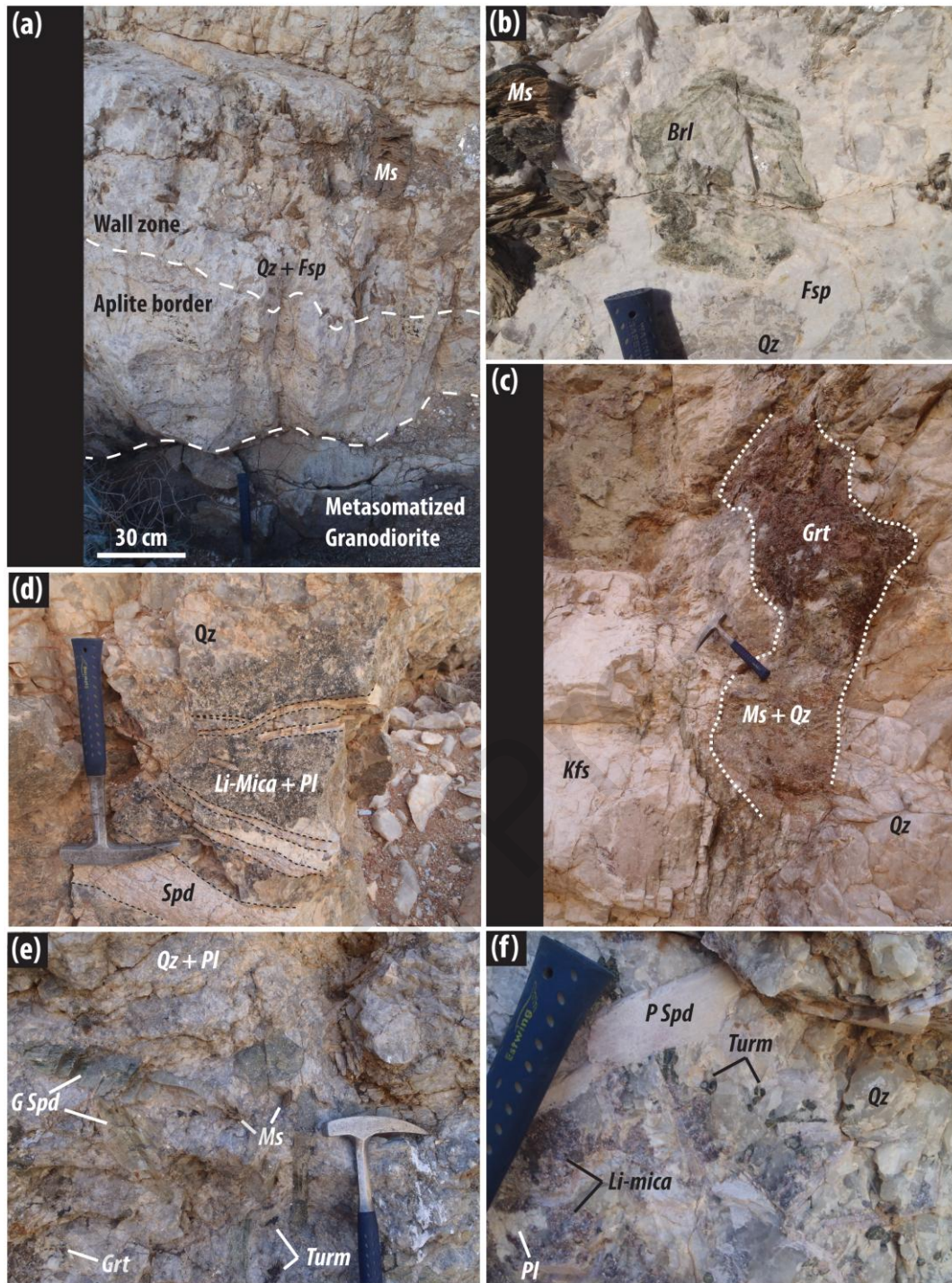


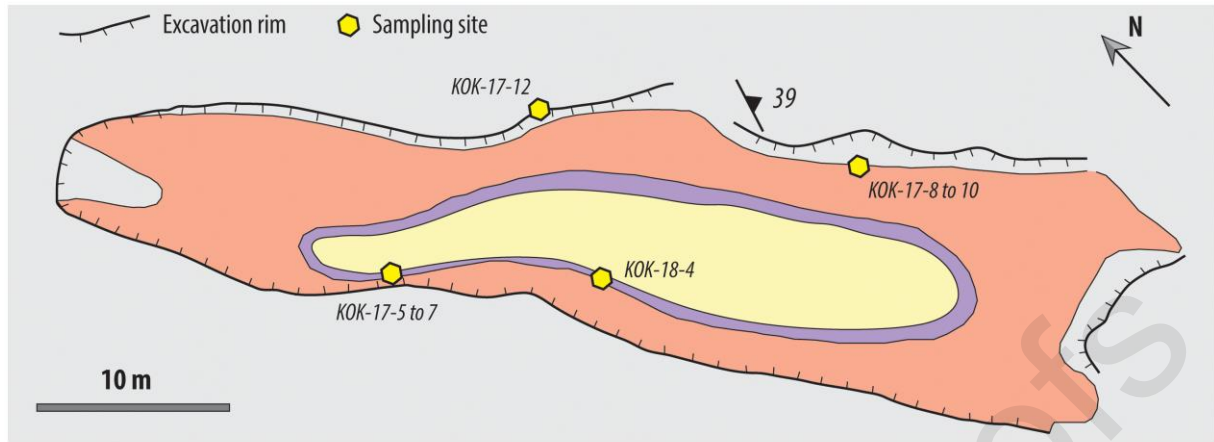




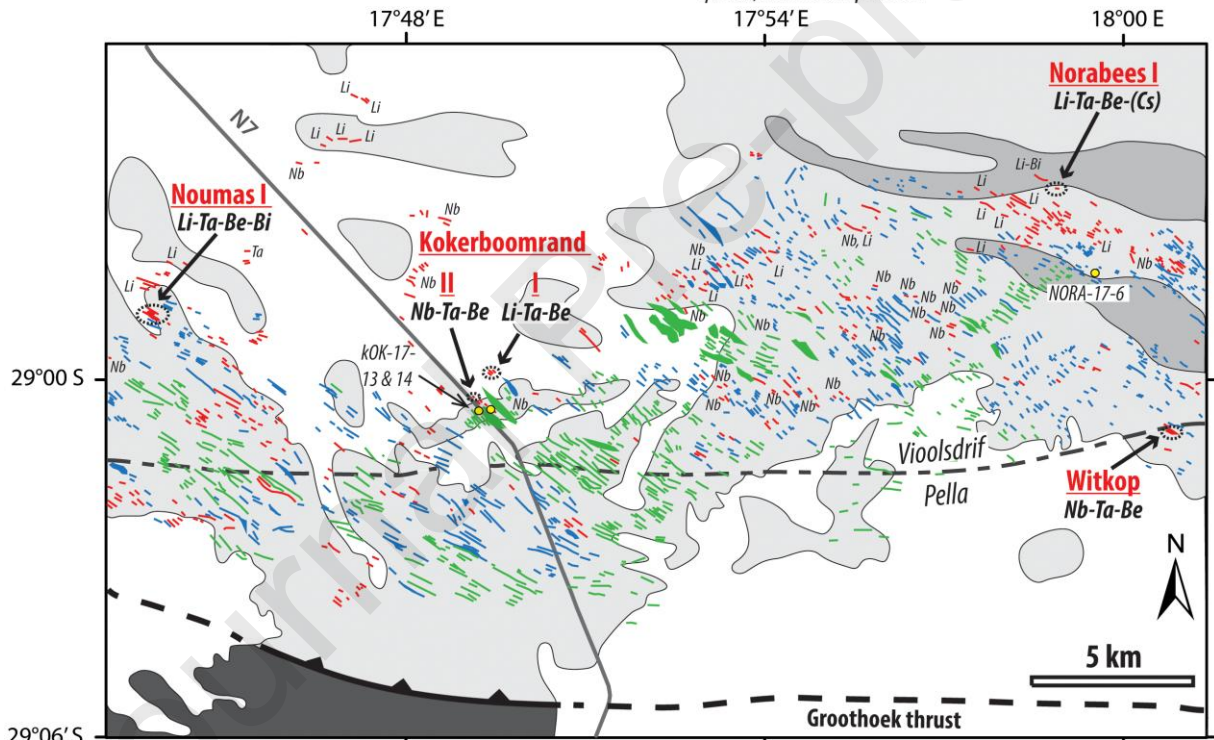








- |  |   |
|--|---|
| Metagranodiorite   | Intermediate zone:<br>quartz, plagioclase, spodumene, Li-mica |
| Aplite border and wall zone<br>quartz, plagioclase, microcline, muscovite, garnet, beryl | Core:<br>quartz, microcline-perthite                          |



- |   |   |  |
|---|---|--|
| Richtersveld Arc<br>Orange River (meta)volcano-sedimentary rocks (1.91-1.87 Ma) | Superficial deposit                                     | Heterogeneous-mineralized pegmatite              |
| Violsdrif Suite (meta)granitoids (1.91-1.87 Ma)                                 | Violsdrif / Pella Domains gradational metamorphic front | Homogeneous-mineralized pegmatite                |
| Bushmanland Subprovince   | National road   | Homogeneous-weakly mineralized pegmatite         |
|   |   | Sampled homogeneous-weakly mineralized pegmatite |

